Politecnico di Torino

Politecnico di Torino

Master's Degree in Automotive Engineering

2025/2026

Session of March 2026

Development and Control of an Electro-Hydraulic Actuator for Motorcycle Rider Assistance System

Supervisor:
Massimo Rundo

Candidate:
Alberto Vincenti
S322627

Abstract

The following study investigates the feasibility of development for an Electro-Hydraulic Actuator (EHA), to be implemented as rider assistance system for motorcycle purposes. It is an undisputed fact that the motorcycle is one of the most dangerous road vehicles, so it becomes of great relevance finding a way to improve the safety of the rider.

In this case the focus is posed on the riding quality, having the efforts of the actuator ensuring the vehicle body to lean on one side and exploit the cambering effect to correct the trajectory on the road. The aim is to obtain an automated manoeuvre that can be reproduced every time is needed.

The initial objective is to recreate an adequate model of the vehicle to estimate the possible range of forces, that the actuator will deal with; so that, in a second moment, it can be actuated the preliminary design of the hydraulic circuit. It is defined the most suitable choice for each component, and, in addition, it is created a controlling technique to automate the operations.

Once the system is ready, it is tested on virtual scenarios to examinate the responses of both the controller and the hydraulic unit. Further tests are done directly on the system components, inside a dedicated software environment.

The attended results will tell if this kind of system can be suitable for motorcycle purposes, although the outcomes must be interpreted at virtual level, leaving space to comparisons with real-world situations.

Contents

List of figures

List of Tables

Nomenclature

x: longitudinal direction,
y: lateral direction,
z: vertical direction,
φ: roll motion,
ψ: yaw motion,
δ: steering rotation,
ω: (wheel) rotation,
V: vehicle velocity,
a_i: vehicle acceleration,
F_i: force,
T_i: torque,
R_i: radius,
m_i: mass,
J_i: moment of inertia,
p: pressure,
Q: flow rate,
t_i: time instant,
SC_i: safety coefficient,
$\dot{x}$: time derivative,
$\ddot{x}$: time double derivative,
x_f: front pedix,
x_r: rear pedix,

CHAPTER I

Introduction

It is well proven that the motorcycle is one of the most dangerous road vehicles, a danger that comes either from the surrounding environment or from just a single wrong move of the rider. Though, beginner and expert riders should know very well the risks involved, when riding a motorcycle, it is imperative to search for solutions to lower them down, as much as possible.

Likewise for the automotive Advanced Driver Assistance Systems (ADAS), a motorcycle Advanced Rider Assistance System (ARAS) aims to improve riding safety. Hardware and software systems, like Anti-Lock Braking (ABS) or Traction Control, are already developed and largely implemented; the purpose of this works consists in the design of an ARAS that assists the rider in leaning the motorcycle, so that it is possible to control the trajectory when needed.

1. About motorcycles

Under a kinematic point of view, it is necessary to define the motorcycle as an assembly of four rigid elements: the chassis and everything that could be attached on (engine, tank, battery, ...), the steering system (handlebar, front suspension, ...), the front and the rear wheels.

The mechanical links among these elements work as kinematic constraints, reducing one or more degrees of freedom. Assuming rigid suspensions both at front and rear, i.e. neglecting the vertical movement of the sprung mass and the pitching rotation, the chassis is able to move along four out of six degrees of freedom: longitudinal and lateral motion, yaw and roll.

For the same assumption, the wheels can only rotate around their axes, without any relative motions. The steering system rotates around a joint hinged in the chassis; it is the rider, managing the handlebar, that gives the steering input to the front wheel.

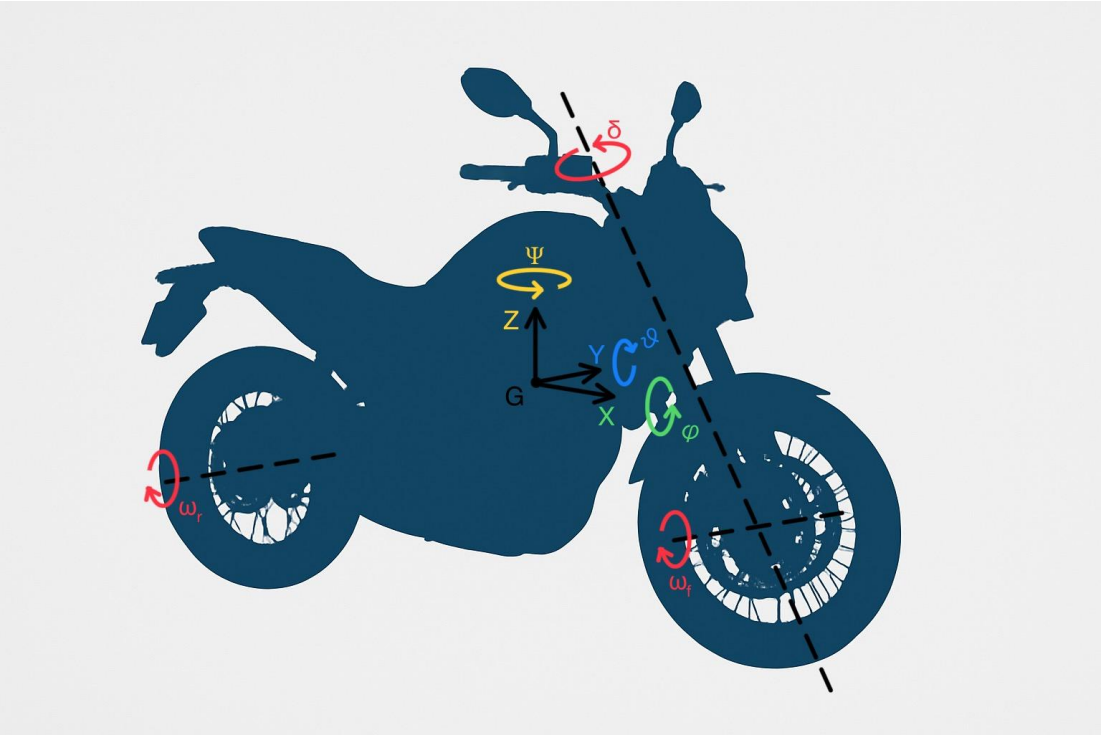

Figure 1.1: *six degrees of freedom of a motorcycle, assuming rigid suspensions; pitch (ϑ), roll (φ), yaw (ψ) and wheel rotations (ω).*

Secondly, motorcycle dynamics involve load transfers during acceleration and braking, but also when cornering. The assumption made on the suspensions does not change the fact that a certain amount of load would shift onto the rear or the front wheel, whether the vehicle is accelerating or braking. Every longitudinal load transfer is thought to occur exactly on the longitudinal axis and, therefore, having the only effect of loading or unloading the relative tire.
Tires are also subjected to lateral forces when taking a corner, in particular, motorcycles develop these forces by lateral slipping and cambering. The latter contribution is only centripetal; it is direct consequence of leaning the vehicle to contrast its centrifugal acceleration. As for the slip force, it can be centrifugal for low lateral acceleration and it becomes centripetal for higher values, anyway, it usually has a lower importance with respect to cambering.
Finally, it is possible to say that a motorcycle turns by leaning it towards the inside, laterally transferring a certain amount of weight. By doing so, the centre of gravity moves over a transversal plane and, more important, by rider input choice, deciding the leaning angle.

2. Countersteering

Countersteering is the base for most of riding techniques; counterintuitively, it consists in actuating the handlebar to the opposite direction of the turn. By doing so, the centrifugal acceleration, initially pointing inside the corner and opposite to the steered handlebar, initiates to lean the motorcycle by pushing its body to the wanted side. Therefore, still in the early stages of the curve, the rider gains a certain roll angle, that can control more easily for the rest of the manoeuvre. This method is very effective, but it requires a minimum velocity to help stabilizing

the drive, it usually depends on the type of vehicle and its geometrical features. For this reason, the context for the simulations conducted for this study, will only regard medium to high speed conditions.
At low speed, on the other hand, manoeuvres are actuated by steering the handlebar coincidently with the direction of the turn: here, the centrifugal acceleration is too low and cannot interfere with the steering dynamics.

Figure 1.2: *example of corner entrance with countersteering technique. Credits: Instagram, tutti_pazzi_per_la_pista.*

A study on the effects of the rider posture is off purpose for this work; nevertheless, it is worth mentioning that correctly moving the rider body inside the curve, hence shifting the centre of mass of the whole system, has an aiding influence. Meaning that this technique improves safety when cornering by reducing the lean angle for the same turning radius, relying on tires in less stressed conditions. That said, from now on, the rider will be considered rigidly linked to the motorcycle, excluding voluntary or involuntary relative movements.

3. Introduction to the actuator

The physical result, that this study is willing to lead to, concerns an electro-hydraulic linear actuator, whose first draft can be seen in **Figure 1.3**. The device mounts on top of the front suspension fork, occupying the free space near the handlebar, between the instrument panel and the rider. It requires at least two points of attachment: one is fixed to the chassis, the other must be the mechanical link between one end of the piston rod and the relative fork cap.

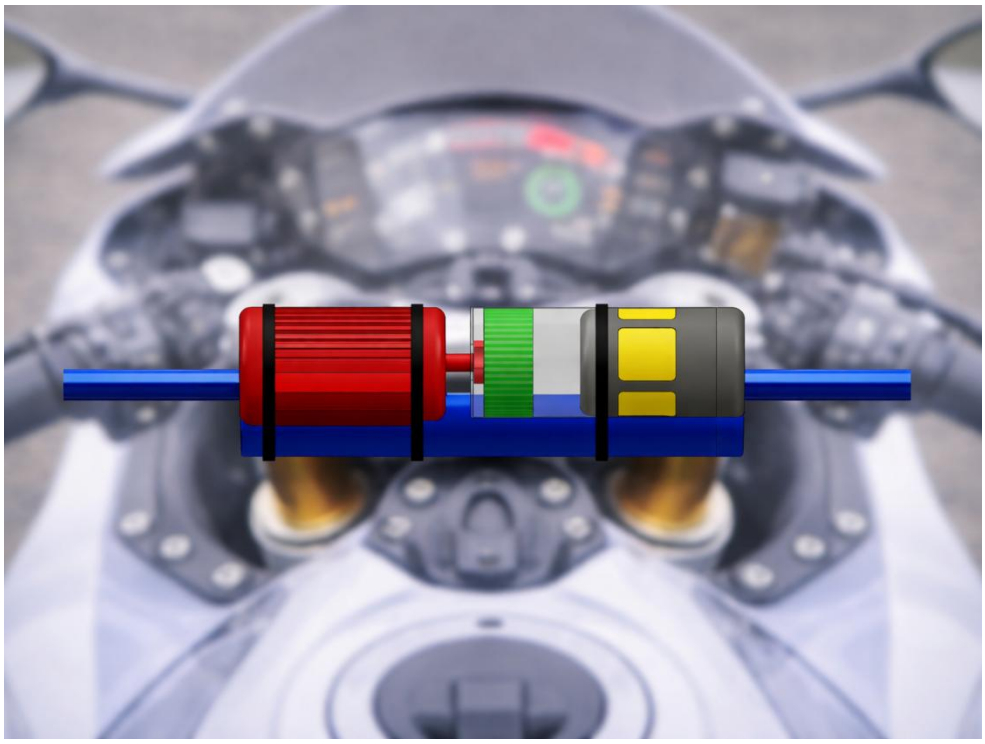

Figure 1.3: *actuator system concept image, possible positioning on generic motorcycle.*

Optionally, a third connection could be made to the other side cap, creating a double-acting piston. Ultimately, the linear motion of the rod pushes (and pulls) against one fork tube, producing the (counter)steering moment necessary to generate the rotation of the front wheel.
A set of stereoscopic cameras should be placed on the front shield of the motorcycle, or inside the lights compartment, directly pointing onto the road. Images are, then, processed to get the lane boundaries in the interested road portion ahead, and transferred to the control unit, together with the states of the vehicle, estimated by the inertial platform and other sensors.
Finally, when the controller decides to intervene, commands are sent to the hydraulic circuit of the device. An electrical prime mover operates the pump that generates the necessary hydraulic flow rate to move the actuator. Its action on the steering system makes the centre of gravity shifting and the motorcycle leaning toward the inside of the corner, exploiting the centripetal effect of cambering.

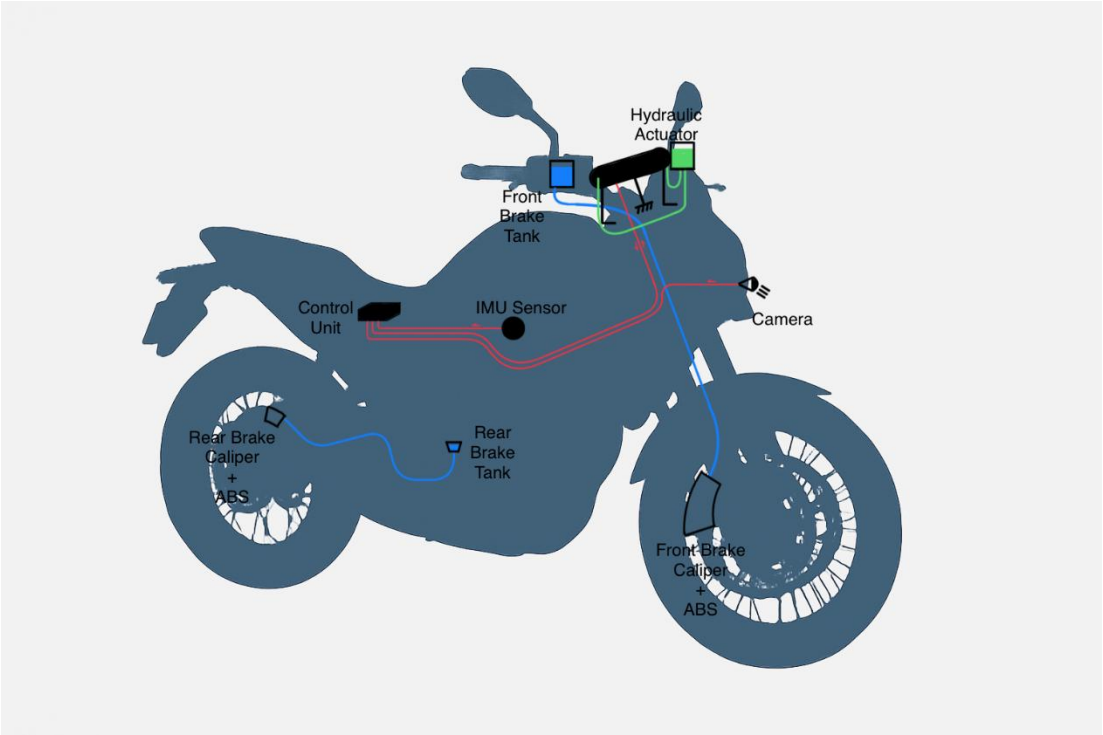

Figure 1.4: *example of system integration: hardware components in black, electrical I/O connections in red, brakes hydraulic circuit in blue, actuator hydraulic circuit in green.*

The controller can be manually activated or deactivated; it should be possible to enable different levels of its decisional power on the steering dynamics. From maximum presence to passive action, this study wants to verify the feasibility of such a device, testing the responsiveness during corners and to find limits of application.

Possible functions that can be exploited with such an active system:

- Always On: based on the data fed by the lane recognition software, the system keeps assisting the rider in leaning the motorcycle. Vehicle speed and maximum camber angle affect the performances.
- Anti-Tucking In (Safety Function): the motorcycle already leaned down when taking a corner, the controller detects the front wheel rapidly self-steering toward the inside (tucking) and maintains the handlebar straight, avoiding the complete loss of adherence for the front tire.
- Obstacle Avoidance (Safety Function): when an obstacle is detected along the path and the rider's actions lead to probable collision, the controller steps in for an emergency steering, if safely possible.
- Off: when deactivated, the device acts as a passive steering damper, to mitigate medium frequency wobbling phenomena of the steering.

CHAPTER II

Methodology

For this study, a generic motorcycle is reproduced for testing kinematics and dynamics. Each feature is taken arbitrarily from various catalogues of past and present vehicles, aiming to have an average composition that represents, as close as possible, reality. The data utilized in the computations are reported in the **Appendix** section.

Once terminated, the vehicle model is able to estimate forces and moments necessary to preliminary size the hydraulic circuit. Testing different scenarios permits the understanding of the worst conditions the device could undergo.

Finally, the data acquisition process and the control logic must be explained, in order to give continuity between sensors and actuation.

1. Vehicle modelling

1.1. Tires

The motorcycle is a road vehicle capable to move on its two wheels; thanks to them, it exchanges moments and forces with the ground. For this reason, the wheel-ground system is given great consideration, by studying some of its non-linear properties and avoid approximations to an ideal case.

Firstly, it is important to define the points of contact with the ground, sited in the front and rear tires. The contact patches show the actual footprint that the tires leave on the terrain; they are variable in size, due to the amount of vertical weight loading the relative tire and its characteristics: geometry and inflating pressure. Usually of elliptical form, they become crooked to follow the vehicle when attending a turn, see right **Figure 2.1**.

A wheel is said to be in pure rolling, when any force nor moment is applied, this condition defines the free rolling radius, which is smaller than the free radius (R_0). When put under this kind of motion, it is subject to a certain rolling resistance: intrinsic characteristic of every tire, it can be parametrised with a linear dependency to load and quadratic to speed, as suggested in equation (1.1.1): the physical result could be imagined as an elongation, or a reduction, of the contact patch, when the tire is under longitudinal effort.

$$F_{rol} = mg\left(f_0 + KV^2\right)\cos(\alpha_{\text{road}}) \qquad (1.1.1)$$

External moments coming from the brakes are always negatively defined, producing a negative longitudinal force; external torques coming from the transmission are generally positive, due to the tractive effort of the engine, but also negative during engine braking; the direction of the force implemented on the contact area varies accordingly. The contact radius (R_c) depends on the vertical load pressing onto the wheel, its length is calculated proportionally to the vertical stiffness of the tire (k_t), see equation (1.1.2), with minimum value limited to 90% of the free radius.

$$R_c = R_0 - \frac{F_z}{k_t} \qquad (1.1.2)$$

The actual rolling radius (R_e) measures the wheel rotation centre relative to the ground, it describes the tire conditions for the longitudinal dynamics: if braking, R_e is higher than the free radius, at the contact point is present a relative longitudinal speed that defines a blocking incipit, this is the case shown in the left **Figure 2.1**; vice versa, during traction R_e decreases, a relative longitudinal speed forms in the opposite direction to define slipping.

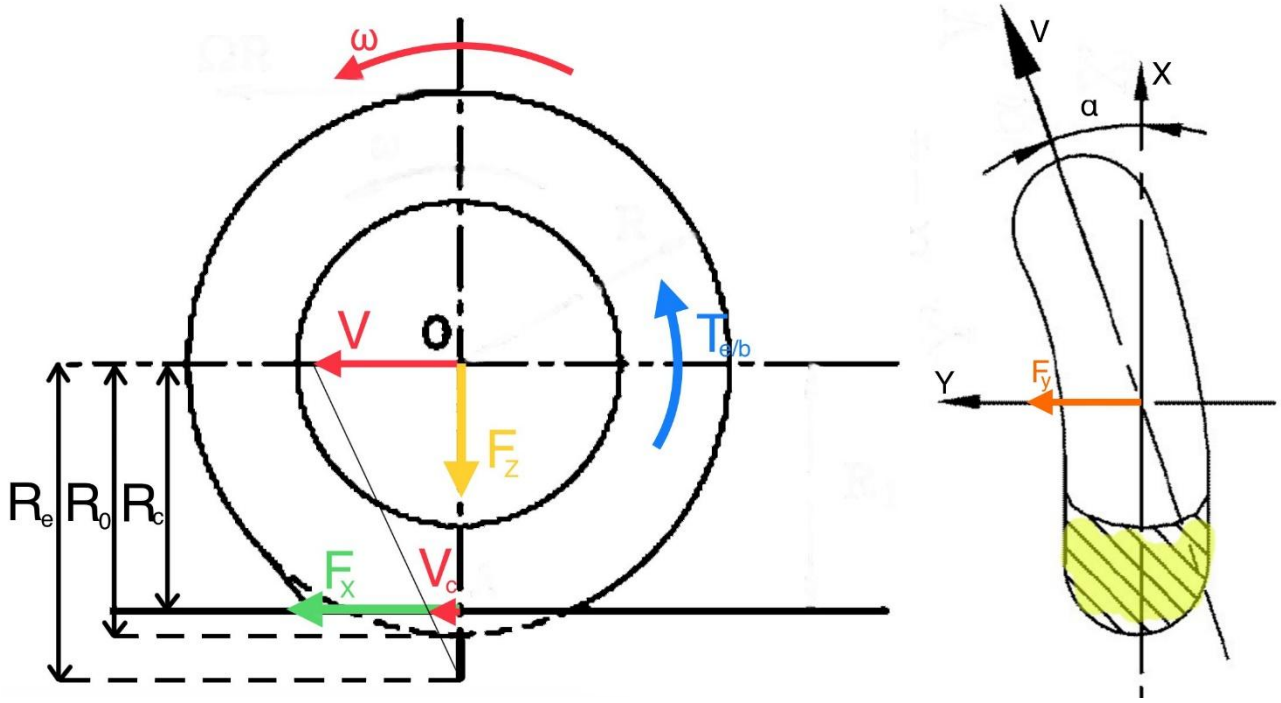

Figure 2.1: *on the left, scheme of forces and moments acting on a rolling wheel; on the right, scheme of a tire contact patch subjected to sideslip angle.*

For motorcycles the front wheel is only subjected to a front braking command (T_{bf}), while the rear wheel receives the contribution from both the transmission (T_w) and the rear braking torques (T_{br}). It is possible to recover the rotational acceleration of the wheel dividing for its inertia the resultant of the equilibrium of those moments around the centre, as described in equation (1.1.3) in a demonstrative example for the rear wheel. It is necessary a successive integration to retrieve the rotational speed (ω).

$$\dot{\omega}_r = \frac{T_w - T_{br} - F_{xr} R_{er}}{J_{wr}} \qquad (1.1.3)$$

It is now possible to define the longitudinal slip as an adimensional value ranging from 0 to 1 in traction, and 0 to -1 in braking. Slip occurs whenever a force is applied to the tire: during a braking action, the force slows down the wheel more rapidly than the vehicle, vice versa, when accelerating, the velocity of the edge of the wheel tends to be faster than the vehicle speed. Extreme cases, respectively, when the wheel blocks (slip equal to -1), or when the wheel spins around itself (slip equal to 1). Due to the mathematical arrangements in the equations (1.1.4a) for traction and (1.1.4b) for braking, it is possible to approximate the rolling radius with the contact radius, so that the longitudinal slip becomes function of the vertical load pressing onto the tire.

$$\sigma = 1 - \frac{V}{\omega_i R_{ci}} \quad (1.1.4a)$$

$$\sigma = \frac{\omega_i R_{ci}}{V} - 1 \quad (1.1.4b)$$

1.2. Longitudinal dynamics

Before computing the longitudinal force, it is better off specify that a Pacejka's tire model [2] have been used, allowing to sum up all the characteristics of the tire in one curve. Suitable for computing steady-state tire forces, the equation (1.1.5) receives the longitudinal slip as input and draws the curve depending on the value of a series of parameters B, C, D, E, shown in **Figure 2.2**.

$$F_x(\sigma) = D\sin\left(C\tan^{-1}\left(B\sigma - E(B\sigma - \tan^{-1}(B\sigma))\right)\right) \quad (1.2.1)$$

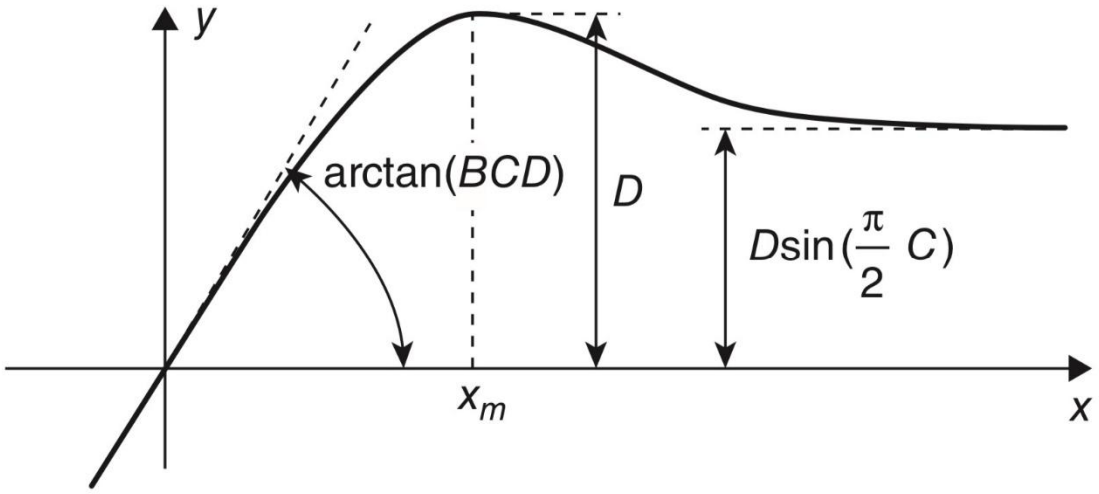

Figure 2.2: *meaning of the main parameters used in the Pacejka's tire magic formula. Redrawn from [1].*

For sake of simplicity, the values of the longitudinal force are normalized for the vertical load, obtaining what is also known as longitudinal coefficient (μ_x), these have been uploaded on a look-up table, function of the longitudinal slip, here reported in **Figure 2.3**. In this way, it is utilized a unique shape of the curve, which is independent of the varying normal load.

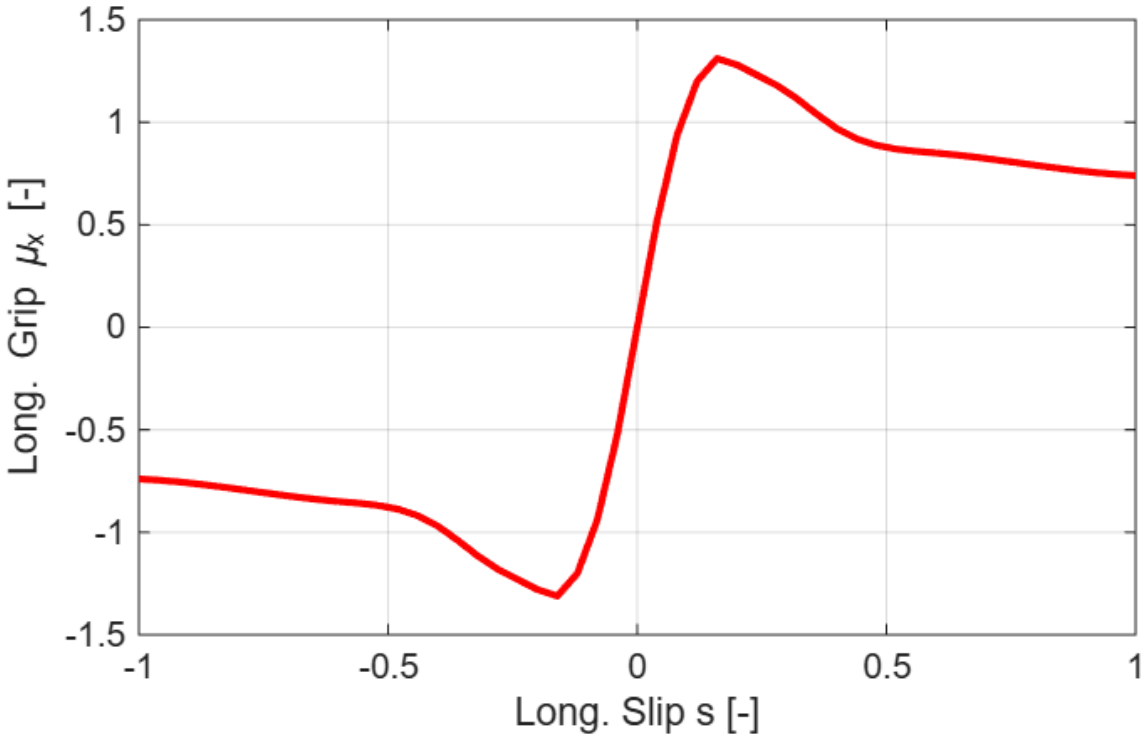

Figure 2.3: *longitudinal friction coefficient function of longitudinal slip, the data are uploaded on a Simulink model look-up table for the computation of longitudinal force of both front and rear tires.*

As it is possible to see, the high peak reached underlines the performative quality of motorcycle tires; though a decreasing trend, the force value remains high for the rest of the curve. The function is valid both for traction and braking, it shows an anti-symmetric shape with respect to the origin. Finally, the product between the coefficient and the vertical load on the given tire generates the longitudinal force.

$$F_{xi} = \mu_x(\sigma)F_{zi} \qquad (1.2.2)$$

The whole process described so far is shown with a Simulink scheme in **Figure 2.4**: the block of rotational dynamics of the wheel, marked in light blue on the left, computes the instantaneous angular velocity of the wheel, necessary to find the slip condition of the tire and to decide if it is accelerating or braking. The slip becomes the variable input for the computation of the longitudinal coefficient, inside the look-up table.

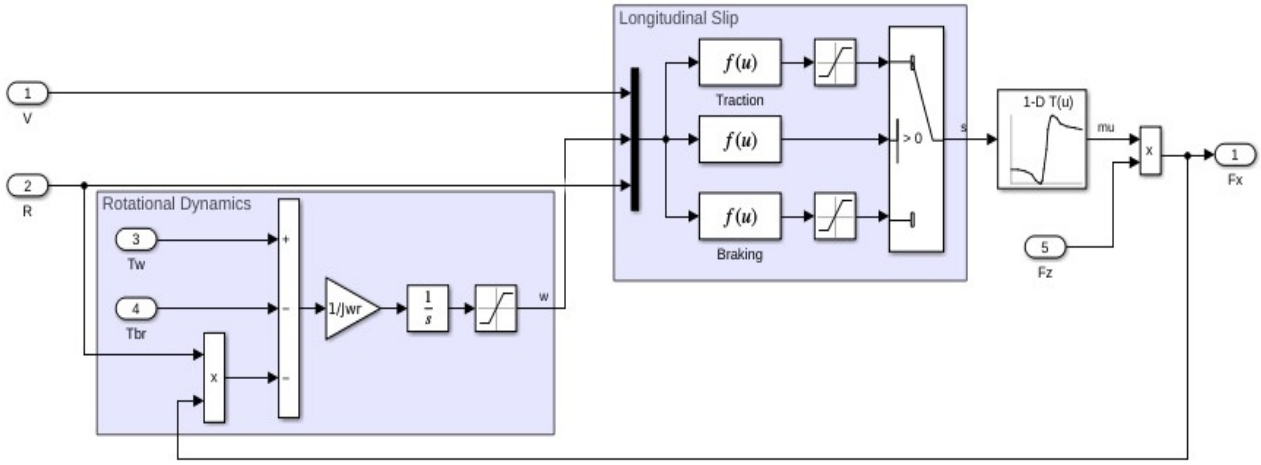

Figure 2.4: *Simulink block diagram for the computation of the rear tire longitudinal force F_x.*

In a real-world case, the estimation of the longitudinal acceleration and the vehicle speed can be done, respectively, via the IMU platform and via sensors at the wheels. The first by linear accelerometers on the longitudinal axis of the motorcycle, the second is usually done with phonic wheels. For this model, the longitudinal acceleration is real time computed in a dedicated non-linear differential system proposed by equations (1.2.3a) and (1.2.3b), then, the speed is gained by integration. The inputs account for the torque at the driving shaft, which is manually modulated accordingly to the simulation requirements, and the longitudinal forces of the front and rear wheels. The states are the position and the speed, only the latter is fed back to system.

$$\dot{X} = V \tag{1.2.3a}$$

$$\dot{V} = \frac{1}{m_e}\left(F_{xf} + F_{xr} - (A + BV^2 + CV^4)\right) \tag{1.2.3b}$$

$$A = mgf_0\cos(\alpha_{\text{road}})\,;\; B = mgK\cos(\alpha_{\text{road}}) + {}^1\!/_2\,\rho S(C_x - C_z f_0);\; C = -{}^1\!/_2\,\rho S C_z K;$$

The apparent mass m_e is chosen to be larger or equal to the vehicle mass, of a proportional factor, for sake of simplicity a more accurate evaluation has no relevance for this study. The components of the resistance to motion account for the linear term A for the rolling resistance, a quadratic term B, with reference to the velocity, mainly due to aerodynamic drag, and the term C, due to the aerodynamic downforce.

Everything necessary to compute the vertical forces on the tires is now available; the load is not constant but varies depending on the dynamics of the motorcycle. It is important to imagine a certain amount of load that transfers, longitudinally, from front to rear, or vice versa, hence adding or subtracting from the static share of the weight. The equation to find the instantaneous value of the forces comprises of the pitching motion and the aerodynamic transfer. The first one is related to the vehicle acceleration or deceleration, it assumes high importance because it can originate

capsizing phenomena, also known as “wheelie”, if at the rear, or “stoppie”, if at the front. The second one depends on the motorcycle velocity; therefore, it becomes relevant at high speed. As already said, this study excludes any suspension effect that can lead to the kinematics mentioned above; nonetheless, the load transfer gets analysed as a dynamic interaction with the ground, reported below in equations (1.2.4a) and (1.2.4b) for both wheels.

$$F_{zf} = mg\frac{b}{l} - m\dot{V}\frac{h}{l} - {}^{1}/_{2}\,\rho S C_x V^2 \frac{h}{l} \quad (1.2.4a)$$

$$F_{zr} = mg\frac{a}{l} + m\dot{V}\frac{h}{l} - {}^{1}/_{2}\,\rho S C_x V^2 \frac{h}{l} \quad (1.2.4b)$$

1.3. Lateral dynamics

For what concerns lateral dynamics, the rider implements two inputs on the motorcycle: steering and leaning. The first one is directly reproduced on the handlebar, and it can be measured as an angle (δ) at the front wheel; the steering system is assumed rigidly connected to the wheel and any geometry variation due to the suspension would not be considered, therefore the rate of change from the input angle to the actual one, acting on the wheel, is considered constant, meaning simultaneous response of the wheel when steering the handlebar.

Though, many riding techniques suggest using the body for laterally shifting some weight and leaning the motorcycle, in this study, the rider seats rigidly and cannot move, therefore the leaning input coincides with the roll angle (φ) at the chassis.

The leaning action can be measured with an angular inclination too. More precisely, the inertial platform IMU estimates the angular acceleration of the centre of gravity along the rolling axis, which lies on the ground, passing through the contact points of the wheels; consequently, the roll angle is easily retrieved.

The rigid linkage between the motorcycle chassis and the rear wheel allows to exactly match the roll angle to the camber angle of the rear tire (γ_r). The front camber angle (γ_f) is subjected to the geometry of the front mass assembly, in particular motorcycle front forks have an inclination along the vertical axis, known as caster angle (ε). Therefore, the leaning input of the driver is influenced by caster geometry and, in case, by the steering angle, amplifying or reducing the front camber angle [3], as reported by equation (1.3.1a).

$$\gamma_f = \sin^{-1}(\cos\delta \sin\varphi + \cos\varphi \sin\delta \sin\varepsilon) \quad (1.3.1a)$$

$$\gamma_r = \varphi \quad (1.3.1b)$$

The generation of lateral force through the tires makes possible to change the direction of the motorcycle. When doing so, the tire undergoes an amount of stress, that, if over its limit, would eventually lead to complete loss of adherence with the ground. This stress can be identified as an angle, sideslip angle (α_i), that derails the tire contact patch from the actual vehicle speed direction. Ideally speaking, cambering is the safest way to produce lateral force, so, it would be the preferred method used during the simulations in the following chapters. This is because, taken as a sole input, it is independent of the sideslip angle formation and its limitations comes with the shape of the tire: in real motorcycle applications, it is usual seeing a rounded tire profile, that allows to safely maintain the contact patch for high lean angles, exploiting the cambering effect.

Returning to the preceding assumption, it can be stated that the sideslip angle values would remain moderate to low and, therefore, the relative model for the computation of the force can be linearized. As already seen for the longitudinal dynamics, the Pacejka's non-linear model can build a function also for the lateral force, with dependency on the sideslip angle; also in this case, the shape of the curve is anti-symmetrical, and the analytical computation depends on fixed parameters. In addition, the lateral force generated by slip is parametrized by the normal load on the tire.
The non-linear outcomes of the Pacejka's magic formula are all replaced with the linearized solution: a product between the sideslip angle and the tire cornering stiffness (C_α), which is, in turn, function of the vertical load pressing onto the relative wheel, its monotonic behaviour can be seen in **Figure 2.5**. The stiffness represents the slope for the initial trait of the Pacejka's function, as already said, if assuming low sideslip angles, the computation of the lateral force is linearized around the sideslip angle.

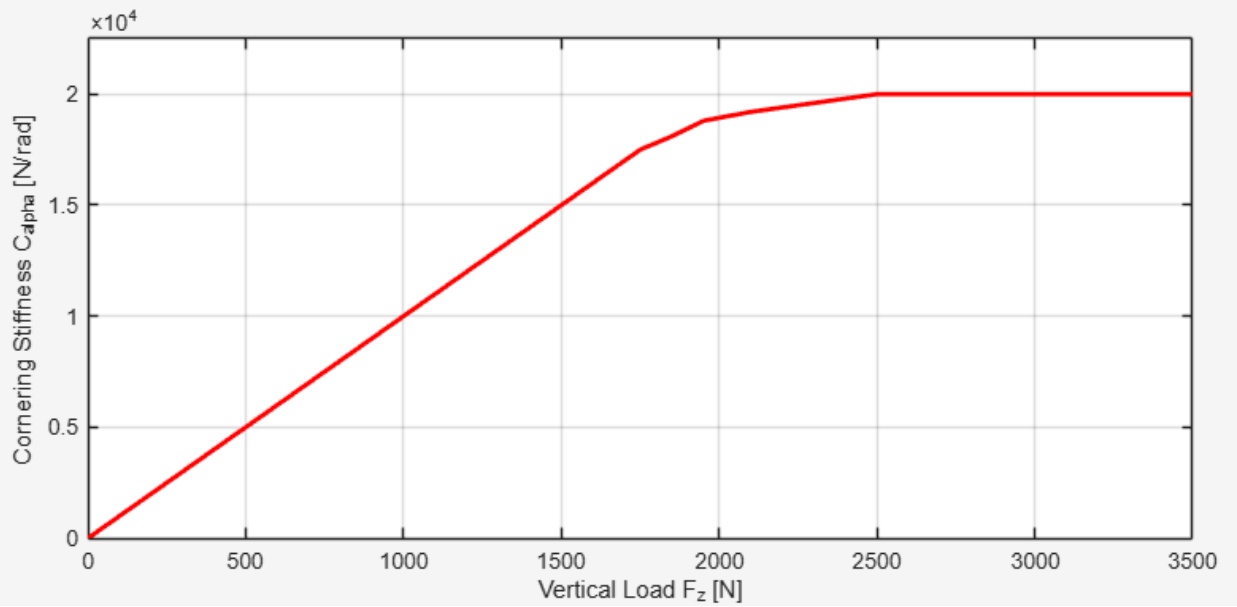

Figure 2.5: *tire cornering stiffness function of the vertical load.*

Now, about the camber angle, in **Figure 2.6**, it is possible to inspect different levels of lateral force generated by the camber angle, each one is linked to a different vertical load, showing an increasing trend that improves the lateral force production, in the case any sideslip angle is not present. Every level grows monotonically for increasing camber, slowly reaching saturation at higher angles. The curves present an anti-symmetry around the origin due to the sign convention; this means that the cambering properties produce the same outcomes for both leaning sides.

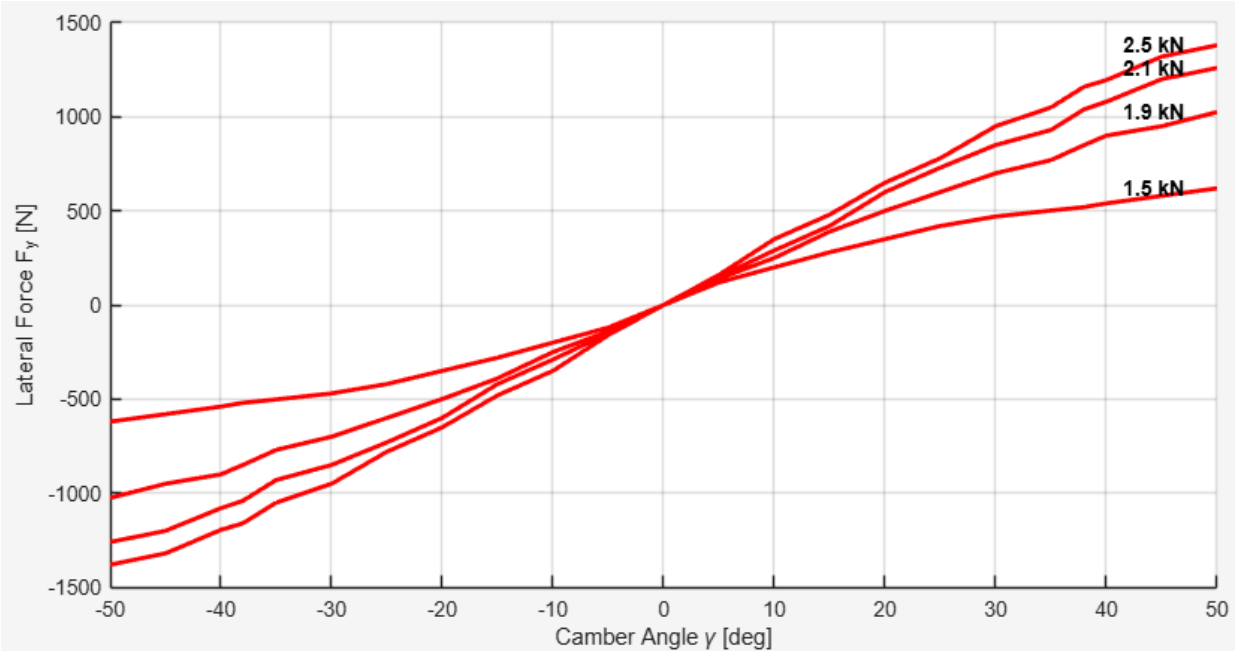

Figure 2.6: *tire generated lateral force, function of the camber angle; multiple curves defined by vertical load, ranging from 1.5 to 2.5 kN [11].*

The lateral force values, generated by camber, are stored inside a lookup table, they can be retrieved with a double interpolation: as first stage, presenting the vertical load computed before; in the second stage, directly inputting the camber angle value.
Both contributions of the lateral force get summed up, even though they come from two different dynamic inputs, they show a common dependency in the vertical force, resumed in the following equation (1.3.2).

$$F_{yitot} = F_{yislip} + F_{yicamb} = -C_{alpha}(F_{zi})\alpha_i + F_{yicamb}(\gamma_i; F_{zi}) \qquad (1.3.2)$$

In **Figure 2.8** are resumed all the passages made so far for the analysis of the forces generated by the tires. It is presented a Simulink scheme accounting for the two look-up tables, one for the cornering stiffness, the other for the camber force; before being summed, as suggested in equation (1.3.2), the stiffness is multiplied to the sideslip angle, obtained with the kinematic bicycle model shown in **Figure 2.7** and explained with the equations (1.3.3a) and (1.3.3b) for both tires.

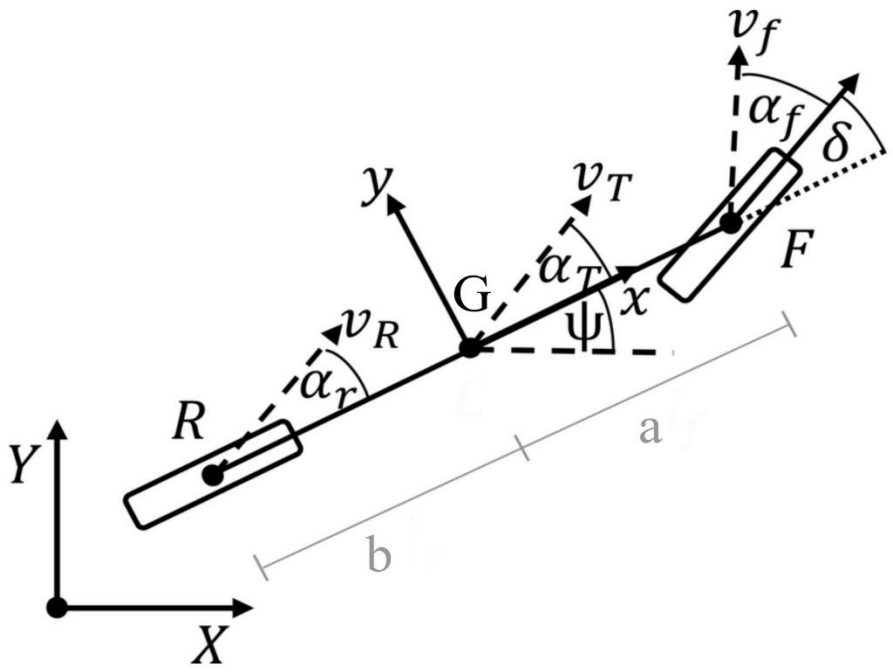

Figure 2.7: *kinematic bicycle model.*

$$\alpha_f = \tan^{-1}\left(\frac{V_y + a\omega_\psi}{V_x}\right) - \delta \qquad (1.3.3a)$$

$$\alpha_r = \tan^{-1}\left(\frac{V_y - b\omega_\psi}{V_x}\right) \qquad (1.3.3b)$$

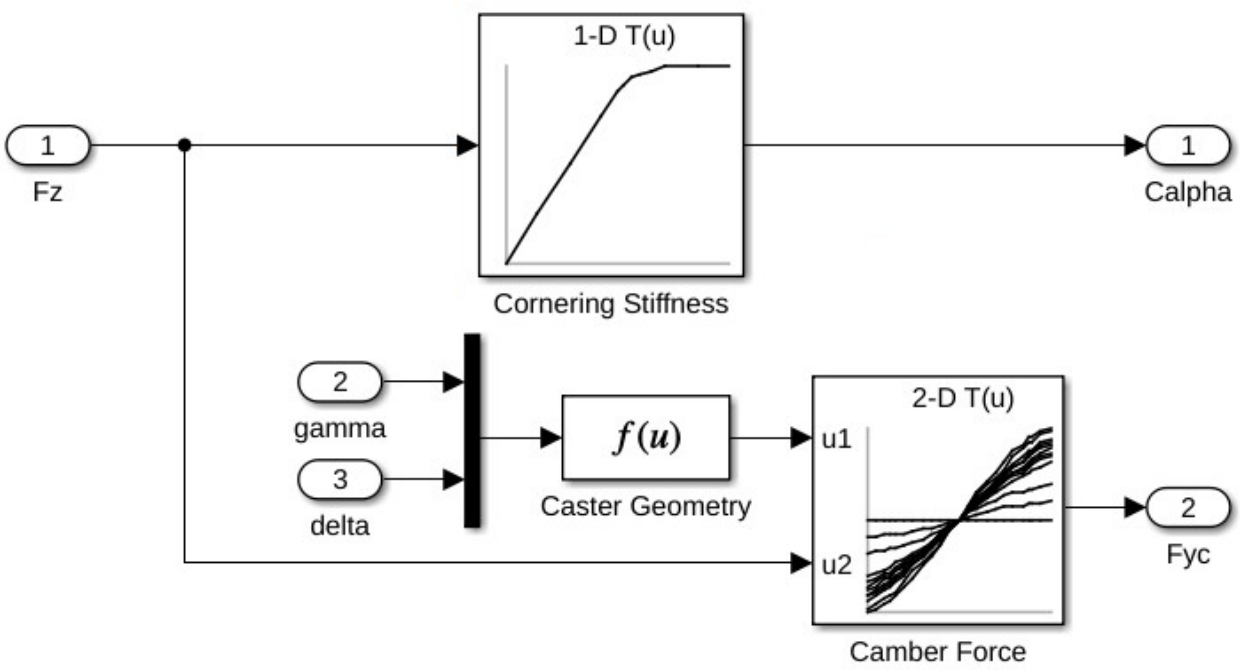

Figure 2.8: *Simulink diagram for the computation of the tire lateral force.*

The actual trajectory of the motorcycle is calculated with the use of a non-linear system, called Dynamic Single-Track model. It receives the steering angle and the longitudinal acceleration as external inputs. The lateral forces from both tires are fed instant by instant, they can be considered as internal states, but actually determined externally, as explained before. The states of the system equations (1.3.4a-f) recount the vehicle position in absolute coordinates (X; Y), the yaw angle (ψ), longitudinal and lateral speed (V_x;V_y)and the yaw rate (ω_ψ).

$$\dot{X} = V_x \cos(\psi) - V_y \sin(\psi) \quad (1.3.4a)$$

$$\dot{Y} = V_x \sin(\psi) + V_y \cos(\psi) \quad (1.3.4b)$$

$$\dot{\psi} = \omega_\psi \quad (1.3.4c)$$

$$\dot{V_x} = V_y \omega_\psi + a_x \quad (1.3.4d)$$

$$\dot{V_y} = -V_x \omega_\psi + \left(F_{yf} \cos(\delta) + F_{yr}\right)/m \quad (1.3.4e)$$

$$\dot{\omega}_\psi = \left(F_{yf} \cos(\delta)\, a - F_{yr} b\right)/J_z \quad (1.3.4f)$$

1.4. Steering torque

From the rider perspective, it is possible to change the motorcycle trajectory by applying a torque on the handlebar. In this way, the rotation of the steering system, i.e. the front suspension fork and the wheel, allows to generate a steering angle. The axis of rotation is not normal to the ground, but it shows an inclination equal to the caster angle. This implicates that the ground intersection, of said axis, does not coincide with the tire contact point, but it leaves a distance ahead, in the longitudinal direction, which is named trail length (a_n) and, for sake of simplicity, it can be considered always constant.

As suggested by Bartolozzi [4], the estimation of the required torque includes a steady-state and a transient contribution. For the former, the vehicle path dictates the necessary conditions to move the steer, these are the velocity and the lateral acceleration; for this case study, it should be considered as if the motorcycle is attending a turn of constant curvature, maintaining constant speed.

Different contributions compose the steady-state moment, each related to different components of the system. Weight and centrifugal forces share the point of application in the centre of gravity of the front assembly, which is often close to the steering rotational axis, thus their moment can be neglected.

The front wheel produces a gyroscopic torque induced by the yaw rate and its angular speed: considering steady-state conditions: $\omega_\psi = a_y/V$ and $\omega = V/R_c$, the vectorial representation of the resulting angular momentum points in the longitudinal direction, with the component on the steering axis subject to caster.

About the contribution of the front tire, it is better off decoupling vertical and lateral from longitudinal dynamics; neglecting the latter, the model lacks in accuracy to estimate cornering

manoeuvres combined with traction efforts, nor braking techniques that prolong the braking phase deep inside the curve trajectory, namely “trail-braking”.
A couple of assumptions are required to link the motorcycle dynamics with the tire forces: equation (1.4.1) remembers the dependency of the lateral on the vertical force, when no steering angle is applied.

$$F_{yc} = F_z \tan(\varphi) \quad (1.4.1)$$

The sum between the two force vectors lies in the YZ plane of the wheel, applied at the ground contact, inclined of an angle equal to the front wheel camber angle; to simplify the computations, it is possible to assume it equal to the roll angle, so that it is possible to obtain the acceleration ratio of equation (1.4.2).

$$tan(\varphi) = \frac{F_{yc}}{F_z} = \frac{a_y}{g} \quad (1.4.2)$$

When the wheel is steered the direction of the force must be described more accurately, distinguishing the kinematic steering angle with the relationship of equation (1.4.3). This curvature gain simplifies the description of the steering behaviour for high roll and high lateral acceleration (fast corners, with small slip angle) from low speed and increased use of steering angle, which will not be considered in this study.

$$\Delta = \frac{l}{R_{curve}} = \frac{la_y}{V^2} = \frac{\delta \cos(\varepsilon)}{\cos(\varphi)} \quad (1.4.3)$$

Now that the resultant force is defined, it must be rearranged to obtain a vector that starts from the ground contact point, parallel to the steering axis. The produced moment is related to the distance of the point of application from the steering axis, which corresponds to the vertical projection of the trail length ($a_n cos(\varepsilon)$); finally, it is possible to say that it is dependent on geometry: sport motorcycles feature a smaller trail to improve steering response, while tourers usually have increased caster angle to improve riding comfort. As shown in **Figure 2.9**, the moment generated by the lateral force, in red, tends to align the wheel with the motorcycle midplane, upward direction, while the contribution of the vertical force, in pink, is non-aligning and tends to follow the steered wheel, downward direction.
Lastly, a cambered tire produces a twisting moment due to its deformation, it tends to self-align the wheel, so opposing a resistance against the steering direction, and it can be linearized using a normalised twisting stiffness (k_{tf}).

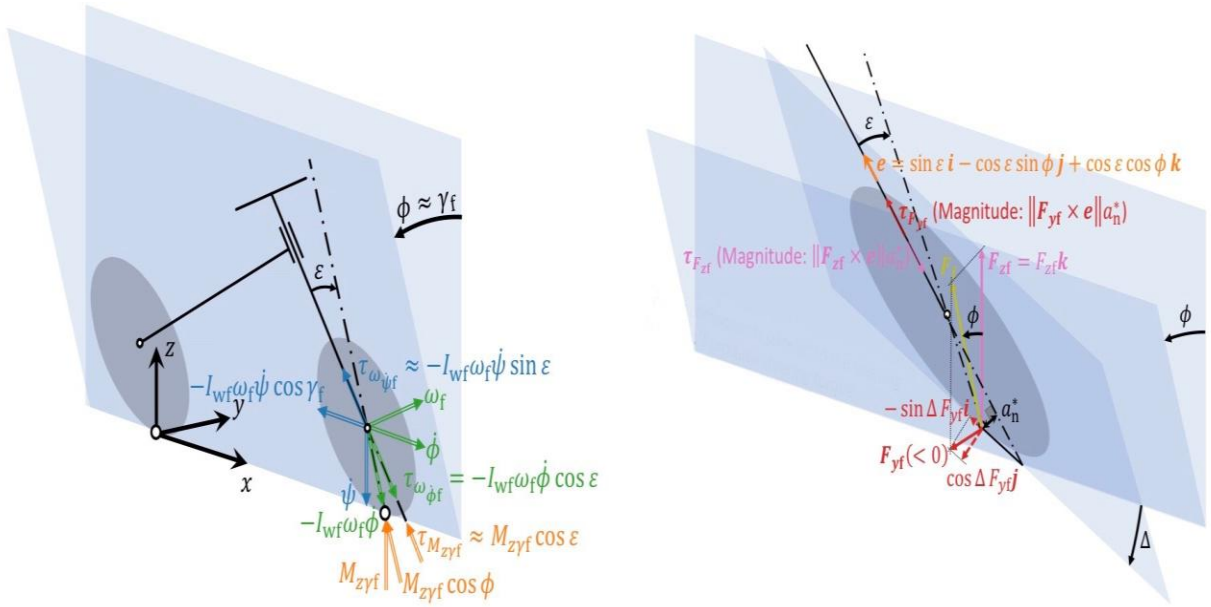

Figure 2.9: *steady-state steering torque contributions, steering, rolling and cambering effects on the left, tire forces effects on the right. Editing from Ref. [4].*

During transient manoeuvres, the torque is mainly affected by the gyroscopic contribution of the rotating wheel, induced by the motorcycle roll rate, the resultant moment tends to increase the steering angle toward the inside of the corner.
Equation (1.4.4) resumes all the contribution to obtain the resultant steering moment; the focus is applied on the value of lateral acceleration, to define the dominant component and, thus, the sign for each different condition.

$$T_{stot} = T_{ss} + T_{tr} = \left(-T_{Mz\gamma} - T_{\omega\dot{\psi}} - T_{Fz} - T_{Fy}\right) + \left(-T_{\omega\dot{\phi}}\right) = \left(-k_{tf}F_{zf}\cos(\varepsilon)\frac{a_y}{g}\right) + \\ + \left(\frac{J_{wf}\sin(\varepsilon)}{R_{wf}}a_y\right) + \left(F_{zf}a_n\sin(\varepsilon)\cos(\varepsilon)\frac{a_y|a_y|}{g^2} - F_{zf}la_n\sin(\varepsilon)\frac{a_y}{V^2} + \right. \\ \left. + F_{zf}la_n\sin(\varepsilon)^2\frac{a_y|a_y|}{gV^2}\right) + \left(\frac{J_{wf}\cos(\varepsilon)}{R_{wf}}V\dot{\varphi}\right) \qquad (1.4.4)$$

1.5. Rolling dynamics

Before explaining the model for rolling dynamics, it must be specified that, from now on, the wheels are assumed to be thin-disk like. This simplification makes the wheel width collapse on its middle plane, the contact patch reduced to a line or, ideally, to a single point. Moreover, when a real motorcycle is leaning, the tire contact points shift from the midplane towards the internal side of the tire itself, and this is also aided by the rounded profile; conversely, in this ideal case, while leaning the contact points remain still, always in the same position, which means that the tires reference frame still coincide with the motorcycle ones. For instance, the vertical midplanes

of both the full body and the wheels share the same rolling inclination and the same roll axis at the intersection with the ground.
The main cause for a motorcycle to lean is the centrifugal torque, dependent on the lateral acceleration applied in the centre of gravity. A secondary effect is played by the gyroscopic precession of the spinning wheels: when a force is applied to a rotating mass, its reaction can be seen in a perpendicular direction to the original force. What should be imagined is that steering the handlebar would apply a moment in the centre of the wheel, depending on the direction that the wheel is being pointed at, it leans in the opposite way. If the rider steers to the left, the right side of the wheel faces forward and starts leaning to the right. The key to read gyroscopic precession in **Figure 2.10** lies in the right-hand rule: a vector defining an angular momentum points out of the plane of rotation so, with reference to the figure, the thumb takes the wheel angular speed, red arrow directed left of the wheel, the index finger points upward, in yellow, for having the wheel steered to the left, and, finally, the resultant direction of the middle finger points straight ahead, in blue, describing a rolling rotation to the right of the wheel.
With increasing rotational speed, thanks to the gyroscopic effect, the wheel obtains a tendency to resist to external disturbances, maintaining its momentum; in other words, it keeps spinning around the same axis of rotation and it is less subject to aligning or misaligning action, like gravity or externa forces.

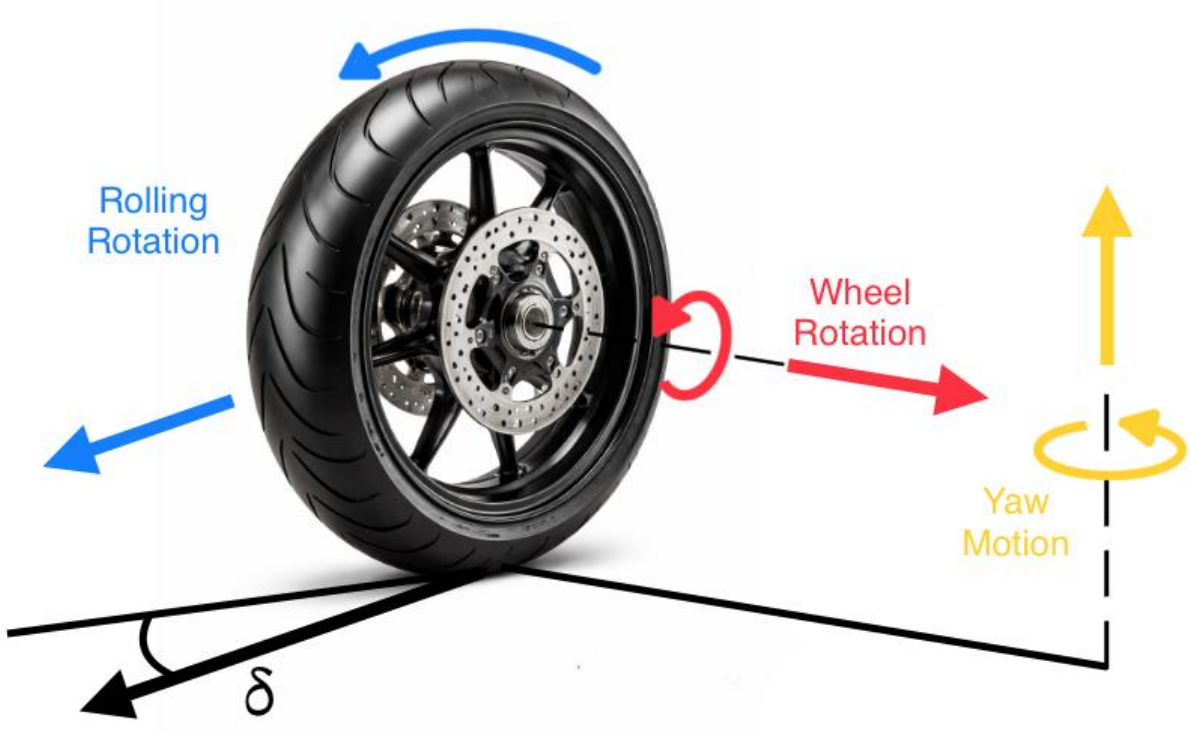

Figure 2.10: *gyroscopic precession applied to a motorcycle wheel steering to its left to lean right.*

The mathematical model suggested by Fajans [5] accounts for a set of three differential equations, linking the change in angular momentum of the front masses (wheel, fork, handlebars,...) to the forces acting in the centre of gravity, defining the rolling motion.

The first equation sets the time derivative of the front assembly angular momentum, pointing in the steering axis direction due to a wheel spinning and leaning. It is caused by the applied moments at the handlebar and the effect of gravitational and centrifugal forces, which self-steer the front wheel, depending on the trail length and caster geometry.
The second equation computes the torque required for leaning, exerted on the front wheel, as the sum of the changes in angular momentum for steering the front wheel, for the gyroscopic effect on the wheel, due to the curvature gain of the motorcycle, and for the rolling behaviour of the front masses.
In the third equation the change in angular momentum around the rolling axis, which lies on the ground in longitudinal direction, is caused by the sum of moments like the torque transmitted to front wheel, computed in the previous equation, the centrifugal and gravitational effects on the motorcycle body, the gyroscopic contribution of the rear wheel and a corrective term due to the change of reference frame between centre of mass and the front tire contact point, as the motorcycle is steering.
The following equations (1.5.1a-e) report the terms explained above, in the respective order, arranged to fit a differential equations system of four state variables: roll and steering angles, roll and steering rates; the steering torque and the velocities as inputs, dependent on time.

$$\dot{\varphi} = \frac{d\varphi}{dt} \tag{1.5.1a}$$

$$\dot{\delta} = \frac{d\delta}{dt} \tag{1.5.1b}$$

$$J_{wf}\omega\dot{\varphi} + J_{f\delta}\ddot{\delta} = T_{stot} - mg\frac{b}{l}a_n\varphi - m\frac{V^2}{l}\frac{b}{l}a_n\delta \tag{1.5.1c}$$

$$T_{\varphi wf} = -J_{wf}\omega\dot{\delta} - J_{wf}\omega\frac{V}{l} + J_{xf}\ddot{\varphi} \tag{1.5.1d}$$

$$J_x\ddot{\varphi} = -T_{\varphi wf} + m\frac{V^2}{l}h\delta + mghh\varphi + J_{wr}\omega\frac{V}{l}\delta + mV\frac{b}{l}h\dot{\delta} \tag{1.5.1e}$$

Finally, it is possible to analyse a countersteering action explaining the physics behind it. The process of making a countersteered right turn, hence having as final objective to lean the motorcycle to the right, begins when the rider applies a torque to the handlebars that steers the front wheel to the left. The rate of increase of the steering angle is determined mainly by the moment of inertia of the wheel, fork, and handlebars about the steering axis, and by the trail, with an aligning torque if the length develops ahead of the tire contact point.
As the motorcycle turns left, centrifugal effects lean both the rider and motorcycle body to the right, while gyroscopic effects also contribute a small right-leaning torque. After receiving the leaning torque, the front wheel responds gyroscopically by tending to steer to the right, i.e. realigning the wheel, counteracting the applied steering torque and halting the increase of the steering angle.
The lean continues to increase as the motorcycle is still turning left. Due to the acquired lean angular velocity, the lean does not stop immediately, causing the steering angle to pass through zero and become positive to the right. As the steering reverses, centrifugal torques change direction, eventually balancing gravitational torques and stopping the lean increase; with no further leaning torque applied to the wheel, the steering angle stabilizes and the motorcycle executes a steady right turn. These five passages are graphically represented in **Figure 2.11**.

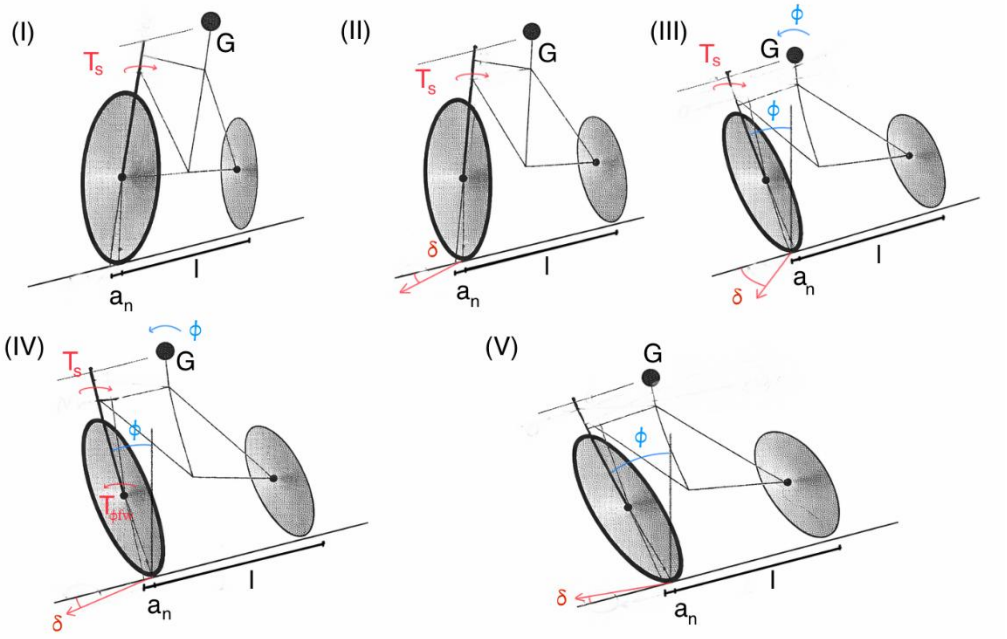

Figure 2.11: *breakdown of countersteering manoeuvre to turn right in stages, in red the moments applied around the steering axis, in blue the rolling dynamics.*

2. Hydraulic Circuit Design

First step for the design involves the study of different scenarios, trying to recreate real world conditions to apply the formulas seen before. Case one and two wants to reproduce two different corners of constant curvature, travelled at constant speed. The aim is to simulate, respectively, highway and rural road conditions, taking the harshest features from the Italian state regulation document [6], differences of speed and trajectory are reported in **Table 2.1**. In both cases, the computed steering moment represents the maximum value needed to move the handlebar against the loads generated by weight, speed and lateral acceleration, that is constant as it is a matter of steady-state manoeuvres.

For the third case, the speed is lowered to a value suitable for an urban scenario and it is staged the detection of an obstacle at a distance of 50 m. The manoeuvre is thought to resemble a single lane change, to evade of 4 m laterally the static object.

If in the previous cases simply steady-state conditions were attained, this one tests the fastest transient dynamics that the system can reach. Once again, it is assumed null steering angle, therefore the objective is to fulfil an acceptable roll rate that makes the motorcycle change its trajectory within the available distance.

Table 2.1: recap of each case scenario results.

Case Scenario	Curvature Radius [m]	Velocity [km/h]	Estimated Roll Angle [deg]	Estimated Roll Rate [deg/s]	Maximum Torque [Nm]
1	250	140	32	-	7.6
2	118	90	29	-	7.1
3	-	60	-	26.4	15

The third scenario is pinned on as the ultimate choice: the computed torque almost doubles the other cases; therefore, it should be taken as starting point for the design. Even though the other scenarios differ in the approach made for calculations, this computation represents an instantaneous value too and it can be suitable for steady-state corners of worse conditions. It is possible to say that, in theory, the system can attend corners similar to the first and second case at a higher speed or with a lower radius, further raising the limits of the first two cases.
The hydraulic circuit is based on an Electro-Hydraulic Actuator (EHA) unit, in closed circuit configuration. An example is given in **Figure 2.12**, showing a real unit, already on the market, for maritime, agricultural machinery or ground static applications.

Figure 2.12: compact Electro-Hydraulic Actuator developed by Parker.

The actuator is simply fed by a pump, originally moved by an electric motor, this clearly defines a high pressure and a low-pressure side and, consequently, the direction of motion of the actuator rod. Hydraulic closed circuits struggle in maintaining sufficient pressure on the low-pressure side. If the pressure level is inadequate, the pump may not receive enough fluid, increasing the risk of cavitation. The flow rate in the low-pressure side can be compensated, if necessary, by the accumulator, which is filled, in turn, by the drainage flow from the pump, recovered into a separate channel. The hydraulic circuit scheme is presented in **Figure 2.13**.

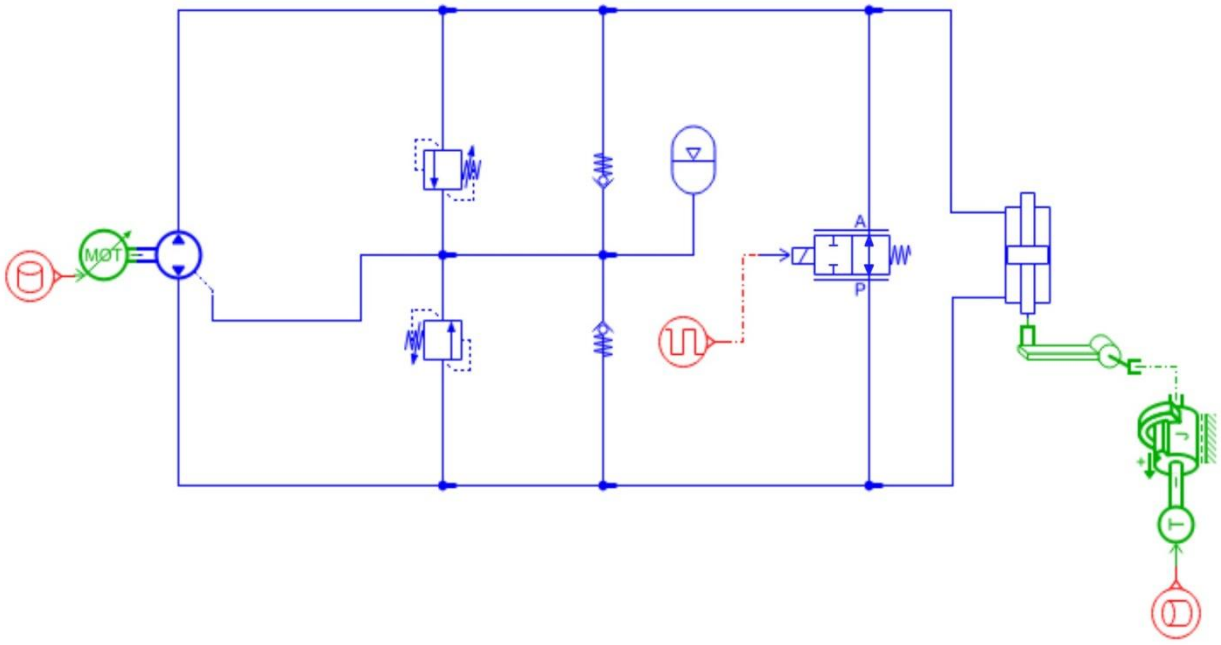

Figure 2.13: *hydraulic circuit overview, sketched on Simcenter Amesim software.*

In the figure it is possible to distinguish the hydraulic components in blue, from the mechanical elements in green. Normal operations start with the electric motor, on the far left, transmitting the shaft rotation to the pump rotors; it is generated an oil flow that moves from left to right, finally reaching one chamber of the cylinder actuator and pushing the piston along its linear travel. It has been already described the high-pressure line, conversely, the reverse flow rate, exiting the other chamber and returning to the pump, defines the low-pressure line.
The actuator linear displacement is transformed in the rotation of the front mass assembly, here schematically represented by a rotating arm of half the distance between the fork stems, and an inertia around the steering axis, accounting for the suspension fork and the wheel. This last element, as the interface with the ground, exchanges the torque computed in the previous paragraphs, represented, in red, as a generic input.
The other inputs correspond to the variable speed command for the electric motor, regulated by the control unit, and the electro-valve activation signal, represented with a squared waveform that defines the On/Off condition related to the motor activating or idling.

2.1. Actuator

First element of design is the actuator, which is the mechanical link to the motorcycle, accounting for a fixed attachment to the frame and a point where to transfer the linear motion to the front suspension fork. It is reasonable to assume the distance between the fork stems (l_f) to be only 200 mm: this gap checks out when considering the 120/70 R17 tire model, which is one of the most common front tire sizes with 120 mm of width, then, adding a gap of 20 mm each side, plus fork tubes of 40 mm in diameter.

Retrieved the maximum handlebar moment from the third case scenario (T^{III}_{stot}) from the previous paragraph, it is necessary to apply a safety coefficient (SC_T) of at least 2. Moreover, the actuator cannot be placed horizontal, parallel to l_f, but tilted of a minimum angle (θ) of 22° on the horizontal plane. In this way the maximum linear force operated by the device would be 400 N, retrieved by equation (2.1.1).

$$F_{lin} = \frac{SC_T T^{III}_{stot}}{l_f \sin(\theta)} \quad (2.1.1)$$

The actuator body is cylindrical, with a double-acting double-ended piston rod inside, so that the fluid pushes against an equal surface for both directions of motion. Next step is to decide its geometrical features: providing two similar solutions of external diameter (D_a) 50 mm and 30 mm, maintaining the same internal-external diameter ratio at 0.5. Among the maximum operating pressures, computed for each case in equation (2.1.2), the choice falls on the smaller solution: though almost doubling the resulting value (7.54 bar against 3.66 bar), compactness is preferred to limit weight and cut operating times. Being the piston symmetric, the two active surfaces (S_a) are equal, meaning that identical operating pressure conditions are repeated for both direction of motion; furthermore, it is assumed that any differential pressure does not form between inlet and outlet ports, and that, ideally, there are no other pressure drops nor disturbances along the low-pressure side, thus the term p_{out} for the cylinder outlet pressure value is null.

$$p_{max} = \frac{F_{lin}}{S_a} + p_{out} = \frac{F_{lin}}{1/4 \pi (D_a^2 - d_a^2)} + p_{out} \quad (2.1.2)$$

The cylinder length (l_a) is arbitrarily chosen at 200 mm; ideally, it avoids the device to exceed the distance between the fork stems, and, for a real application, the reduced size allows to better position and install the mechanical linkages between the fork and the piston rod. This also means that the maximum piston displacement would be 100 mm for each side, considering the component ideal for this preliminary design. For sake of completeness, equation (2.1.3) computes the useful volume to be filled of oil inside the cylinder, while **Figure 2.14** shows an overview of the component and its main characteristics.

$$V_a = S_a l_a = 1/4 \, \pi (D_a^2 - d_a^2) l_a \quad (2.1.3)$$

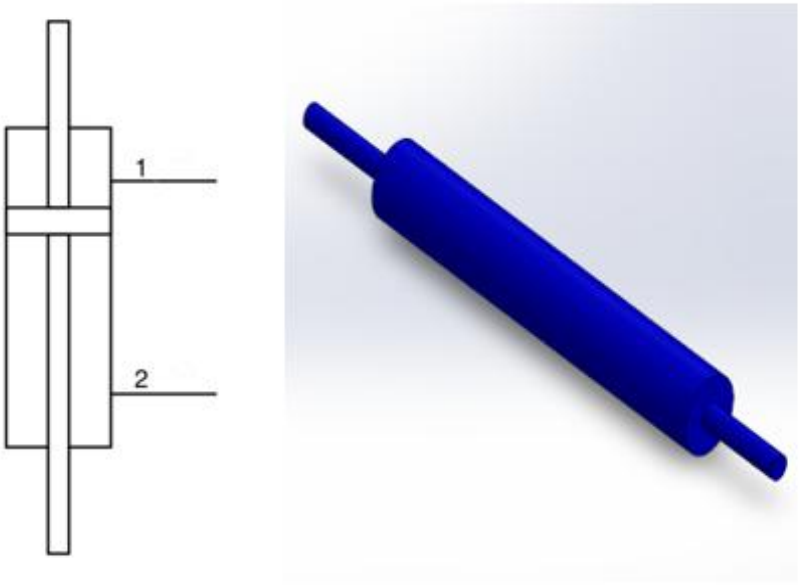

Ext. Diameter (D_a)	30 mm
Diameter Ratio (d_a/D_a)	0.5
Piston Surface (S_a)	530.1 mm^2
Cylinder Length (l_a)	200 mm
Useful Volume (V_a)	106 cm^3

Figure 2.14: *left, double-acting double-piston rod linear actuator standardized ISO 1219 symbol; centre, simplified 3D CAD drawing; right, actuator dimensions and useful data.*

Once known the total volume to be filled, now it is possible to find the last requirement for this component, which is the maximum operating flow rate. A couple of hypotheses must be formulated: firstly, when the device is active, to a linear motion of whichever amplitude it corresponds an instantaneous rotation of the handlebar and the front wheel. Remembering that the steering axis is not perpendicular to the ground, but it presents an inclination from the vertical direction that forms the so-called caster angle; the length (e), found by equation (2.1.4), is equal to the projection on the ground, along said axis, of the distance measured from the top of the steering head, where to locate the hinge centre of rotation at certain height (h_{hinge}), down to the centre of the wheel, at a height corresponding to the contact radius (R_{wf}).

$$e = \left(h_{hinge} - R_{wf}\right) \tan(\varepsilon) \qquad (2.1.4)$$

During a countersteering action, the wheel is turned towards the outside of the curve, while the rest of the motorcycle body pivots around the same hinge point of the handlebar, the so-called steering column, causing the centre of gravity to move towards the inside, leaning with a certain angular rate. In **Figure 2.15**, it is shown the correlation between the two pivoting bodies, front and rear masses, at the initial instant of a countersteering manoeuvre; it is worth noticing that they both share a common point in the hinge of the handlebar, red point.

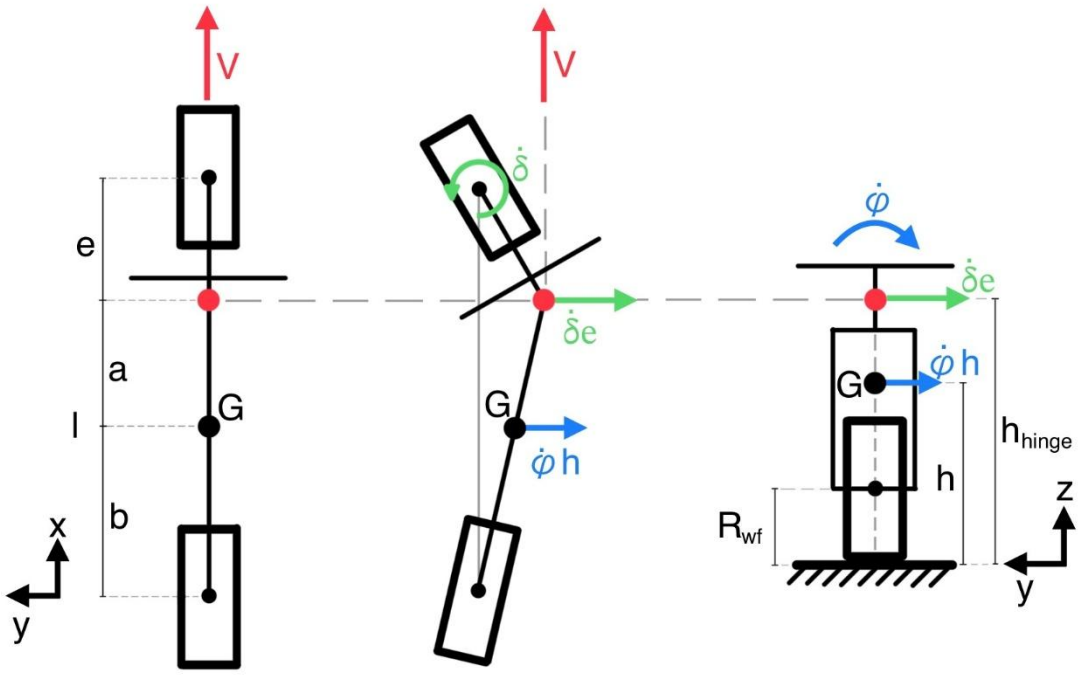

Figure 2.15: *representation of countersteering action initial instant: left, motorcycle top view; centre, top view with exaggerated focus on steered front wheel; right, rear view.*

The second hypothesis assumes that the roll rate, i.e. the leaning action angular velocity ($\dot{\varphi}$), is proportional to the steering rotation angular velocity ($\dot{\delta}$); this means that the response to whichever handlebar motion is immediate. Though the rolling dynamics are governed mainly by the centrifugal forces that rise when steering, this assumption serves as limit case to find the maximum operating speed for the device. Nonetheless, when simulating high speed scenarios, the generation of strong centrifugal forces validate the hypothesis for this rolling behaviour.
The contact point of the front tire needs to be taken as fixed reference, so that, when the wheel is steered and the motorcycle starts leaning, the hinge point of the handlebar moves of a relative tangential speed equal to steering angular velocity multiplied for the distance e. The same point is shared with to the rear body, so it is possible to say that it is also rotating with the same angular velocity of the centre of mass (G), which corresponds to the roll rate. Knowing the respective heights from the ground, it is easy to calculate the proportional relationship between leaning and steering rotation, reported in equation (2.1.5).

$$\dot{\delta}e : (l-e) = \dot{\varphi}h : b;\ \dot{\delta}_{max} = \dot{\varphi}_{max} h \frac{l-e}{be} \qquad (2.1.5)$$

Getting back to the initial purpose, the maximum flow rate entering the cylinder considers a device intervention where the piston displaces half the stroke. A full lock-to-lock displacement is not taken under consideration, because the operation starts from the middle point of the actuator, having the front wheel straightly aligned. Crossing it would change the direction of steering, drifting away from the purpose of the manoeuvre in the case studied.

Therefore, the linear speed is related to the maximum roll rate, which is retrieved from the computations made in the third scenario, and computed in equation (2.1.6).

$$\dot{X}_{dmax} = \dot{\delta}_{max} \, {}^{1}/_{2} \, l_d \tag{2.1.6}$$

Finally, the maximum flow rate is computed in equation (2.1.7) as the product of the maximum linear speed with the useful surface, which is the annular area of the piston.

$$Q_{amax} = {}^{1}/_{4} \, \pi (D_a^2 - d_a^2) \dot{X}_{dmax} \tag{2.1.7}$$

2.2. Pump

During operation, the flow rate entering the cylinder determines the high-pressure side of the circuit. In this way the actuator is directly connected to the pump delivery port, receiving the totality of the flow. For this purpose, the pump ratings must satisfy the previously computed value for the actuator, augmented of a safety factor (SC_p) equal to 1.5, to cover possible external leakages and the drainage flow.

The pumping element and its casing are meant to be placed coaxially with the electric motor and the accumulator; therefore, a cylindrical shape better suits the premises. Compactness is a much-preferred characteristic to look for, along with the costs minimization, these are key factors contributing to the choice of a gear pump type, more precisely a gerotor. This positive displacement rotary pump is composed of an inner gear rotor with N teeth and an outer gear rotor with N + 1 teeth, driven by the internal one. During rotation, sealed chambers form between the rotors; these chambers volume expands at the inlet to draw in fluid and contracts at the outlet to deliver it. With respect to the central illustration of **Figure 2.16**, the sense of rotation of the pump is defined by the input rotary speed of the electric motor shaft; intake and delivery ports switch accordingly.

The gear profiles are conjugates cycloidal, presenting an eccentricity between the centres of rotation: for one revolution completed by the outer gear, the inner one has rotated of (N+1)/N revolutions.

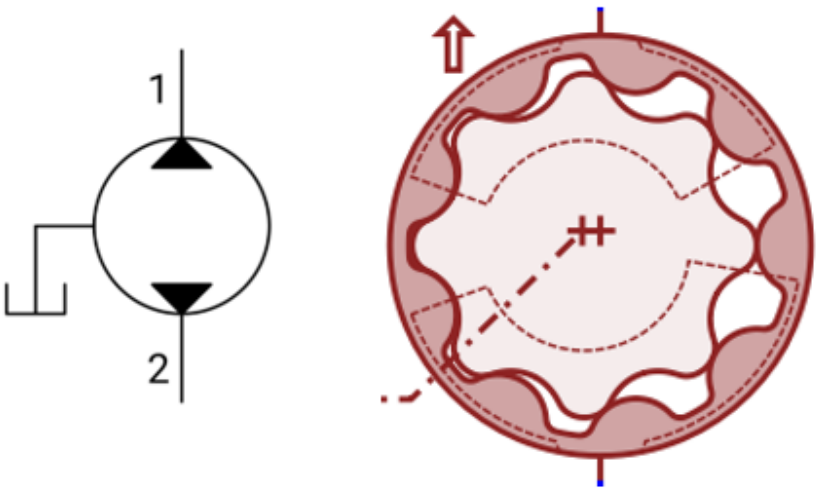

Ext. Diameter (D_p)	50 mm
Displacement (V_p)	18.9 cm^3/r
Max. Casing Thickness (l_{pc})	50 mm
Gear Thickness (l_p)	20 mm

Figure 2.16: : *left, fixed displacement pump, bidirectional flow with external drain standardized ISO 1219 symbol; centre, section view of gerotor pump from Amesim; right, pump dimensions and useful data.*

The pump instantaneous flow rate is not constant, since fluid is delivered in discrete number of volumes. This causes flow ripple, which depends strongly on the number of chambers, affecting the generation of noise and vibrations. A higher number of chambers (corresponding to higher teeth count N) increases the frequency of flow fluctuations while reducing their amplitude, resulting in a smoother overall delivery. Conversely, fewer chambers lead to larger volume variations per cycle and higher flow ripple. Furthermore, an odd number of chambers disrupts more easily the symmetry that is created between intake and delivery volumes every cycle: the flow pulses are out of phase, attenuating the fluctuations.

The gear elements are required to work as a pump for both direction of motion of the prime mover, also to revert into motoring mode when the controls are inactive and the steering handlebar manned by the rider.

The maximum operating speed (n_{max})of the inner rotor is arbitrarily set at 400 rpm; in this way, the required pump displacement (V_p) remains slightly below 20 cm^3/rev, avoiding oversizing problems when selecting a standardized component off a catalogue. Equation (2.2.1) reports the calculation for the pump displacement: the safety coefficient is a way to mitigate the negative effect of the possible actual volumetric efficiency of this pump, in a real case. As it is possible to see in the graph of **Figure 2.18**, the volumetry is strongly limited at lower rotating speed, loosing most, if not all, the generated flow rate in leakages.

$$V_p = \frac{SC_p Q_{amax}}{n_{max}} \qquad (2.2.1)$$

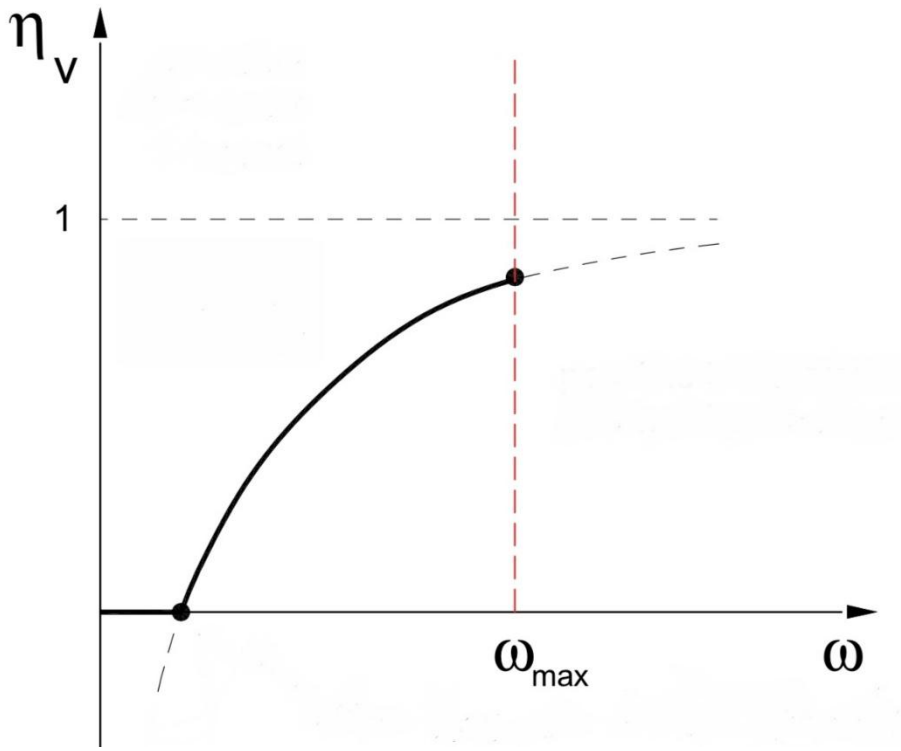

Figure 2.17: *volumetric efficiency function of the speed of a generic pump. Editing from Politecnico di Torino – DENERG FPRL.*

The external diameter (D_p) is limited at 50 mm, while the gear thickness (l_p) does not have any constraints, so a suitable value can be of 20 mm. These measures set the maximum dimensions of the pump, enclosed inside a casing element that must take into account to leave enough volume for oil suction, even though the maximum operative speed is low as the risk of cavitation. Therefore, the maximum available case length (l_{pc}) is set at 50 mm.

2.3. Accumulator

The undetermined pressure level in the low-pressure side is one peculiarity of hydraulic closed circuits, mounting a second charging pump with a dedicated relief valve, always ensures continuity of flow rate at a certain pressure level, but this solution is suitable for larger systems, such as hydrostatic transmissions.

For the kind of circuit considered in this work, the low-pressure side is determined by letting the high-pressure side close the relative check valve and isolate itself; because of symmetry between the two annular surfaces, the actuator motion pushes out the exact quantity of oil that enters the cylinder, so the only source of flow losses comes from the pump leakages. For this purpose, an accumulator must be placed to guarantee correct recirculation and establish a minimum pressure level at pump suction. When needed and available, the charge stored inside flows through the open check valve of the low-pressure side, reaching the pump suction port.

Either a compressed gas accumulator, as seen in the scheme of **Figure 13**, or a spring kind can be suitable, differences rise in the pressure trends function of displaced volume.

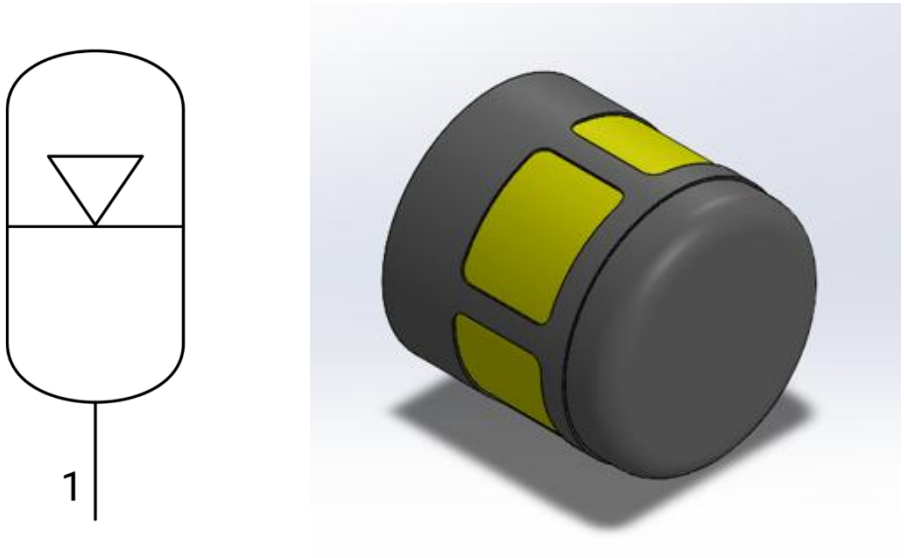

Figure 2.18: *left, gas charged accumulator standardized ISO 1219; right, simplified 3D CAD drawing.*

In the first typology, the gas, in a separated chamber, gets compressed when the oil flows inside, then release it, in the discharge phase, decreasing its pressure. Considering polytropic processes, with ideal gas exponent equal to 1.4, the pressure-volume characteristic follows the related non-linear law, which matches an adiabatic. In the spring type accumulator, the oil pushes against a piston, displacing the spring. Neglecting the non-linearities and hysteresis issues, the volume variation depends on the constant stiffness of the spring, generating a linearly increasing or decreasing force counterposing the oil pressure. The qualitative trends of both accumulator typologies are reported in **Figure 2.19**, the gas pre-charged one, on the left, distinguishes from the other for being non-linear, so that it can actually represent multiple cases, depending on the gas exponent, from adiabatic to isotherm.

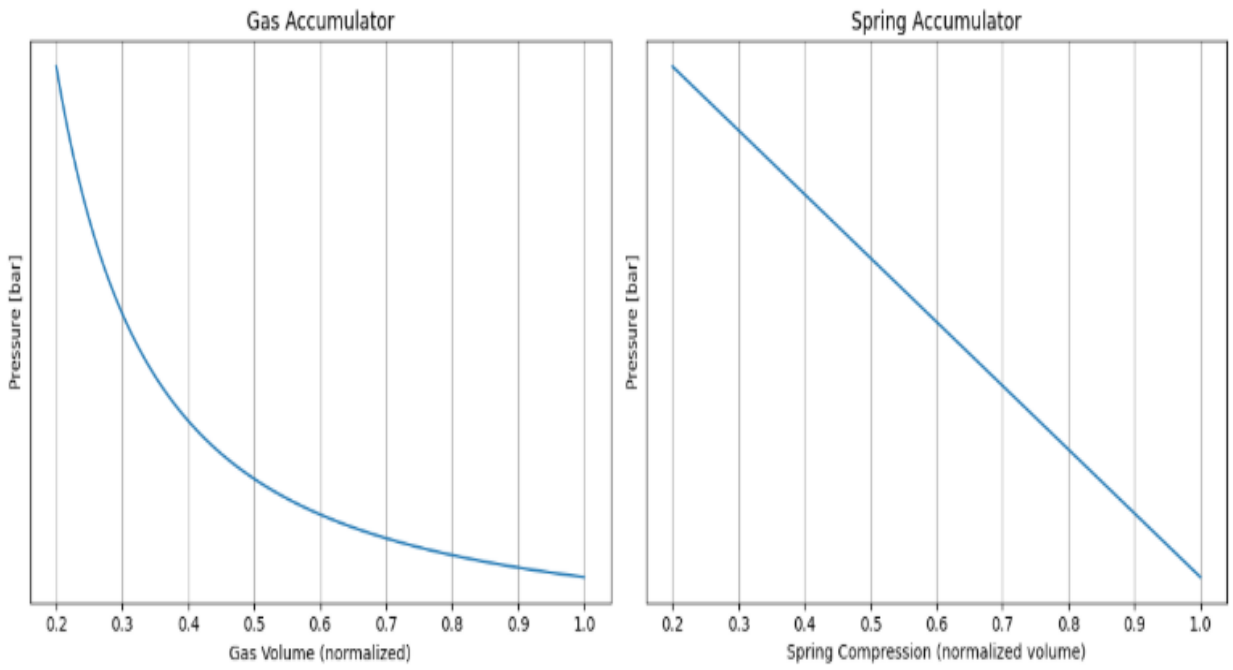

Figure 2.19: *different pressure dependency against volume variation (oil filling) of a gas charged accumulator (left) and a spring accumulator (right).*

When comparing the two types, compressed gas accumulators show a smoother pressure trend when the useful volume of oil is low, this reflects in a higher filling and faster initial charging phase, keeping constant the inflowing oil pressure. Ambient temperature influences, usually negatively, the adiabatic dependency of the gas; considering that the accumulator location highly exposes it to the environment, temperature can condition operations, only for this reason, a spring accumulator might be preferred.

The accumulator is then sized according to the volume displaced by the actuator. In particular, the extreme case when the actuator displaces the full stroke, the missing oil quantity corresponds to the piston volume, also increased of a 20% factor.

The component would be placed in series with the pump, coaxially, with a maximum external diameter of 50 mm. This position allows to link the accumulator duct to the pump drainage collector, which is the direct way to recharge the lost volume.

The pump drain flow rate is modelled as function of the delivery pressure, it shows an increasing trend for increasing the pressure at delivery; for similar displacements and operating pressures the estimated drain flow rate ranges between 20-40% at an average value of the operating speed, and about 10-20% at maximum operating speed [7], these values follows the trend of the volumetric efficiency function shown in **Figure 2.17**. Therefore, the accumulator functioning depends on its pressure level: when sufficiently high, meaning sufficiently charged to overcome the pressure of the pump drain, it permits discharging into the low-pressure side of the system. When the accumulator has emptied enough, it receives part of the flow rate coming from the drainage, recharging its chamber; the rest of the drain flow rate directly recirculates in the low-pressure side, passing through the relative check valve.

2.4. Generation unit

The pressure relief valves, placed downstream the pump, control the high-pressure side and protect the actuator from overpressure. This configuration is called “Continuously Variable Flow Generation Unit for Closed Circuits”, for this case the continuous modulation is obtained with a fixed displacement pump, free to operate at any velocity imposed by the electric prime mover. The variable speed command is sent by the controller, based on a closed-loop regulation of the actuator control: the electric motor increases or decreases its velocity, depending on the actuator position feedback. The relief valve is put downstream of delivery, in series, acting as a safety valve for the high-pressure line, seen in **Figure 2.20**.

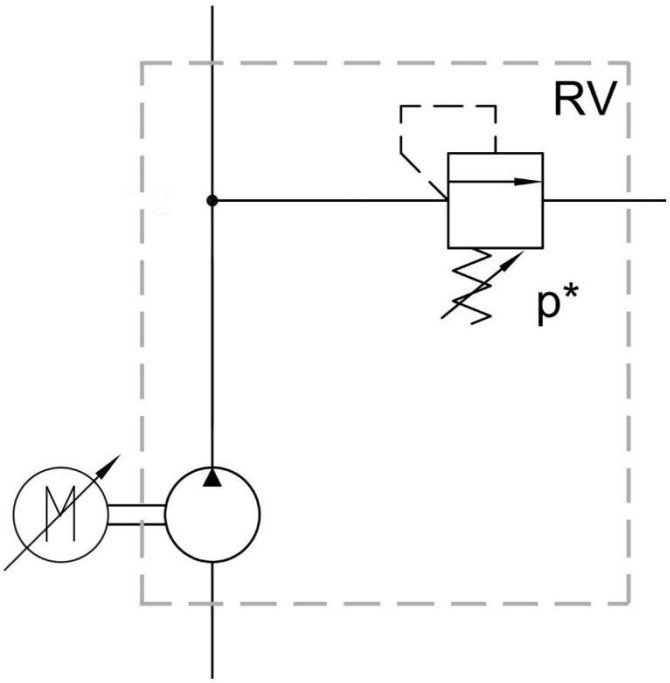

Figure 2.20: *Continuously Variable Flow Generation Unit.*

For an ideal component, once the pump delivery pressure overcomes the set “cracking” value, the valve opens up, diverting the flow rate from the user and keeping a constant pressure level.
For an actual component, the valve progressively enters in regulation stage: further pressure increments, above the cracking level, increase the valve opening and, consequently, the amount of diverted flow rate. This is due to the spring element inside the valve, which counteracts the pressure action with a force, that can be considered linearly dependent on the spring travel. Therefore, when the valve is fully open no flow rate reaches the actuator, the pressure remains at a stable level but higher than the cracking pressure. For the design of this component, it is applied a 20% margin to the highest operating pressure, setting the cracking value (p^*) at 8 bar.

2.5. Dynamic restrictor

When the whole system is inoperative, either if it is shut down or the electric motor stands still, the rider must be able to steer the handlebar at his own will. The necessity of making the actuator floating freely arises; the piston must be decoupled from the rest of the hydraulic circuit, by creating a recirculation of oil back into the cylinder. In this way, when manually rotating the handlebar, the oil pushed outside the cylinder, by the linear motion of the piston, is redirected straightly to the other port of the actuator.
This is made possible by installing a directional control valve, connecting inlet and outlet of the cylinder. More precisely, it is required a two states, two gates, normally open (NO), electrically actuated valve, represented by the scheme of **Figure 2.21**.

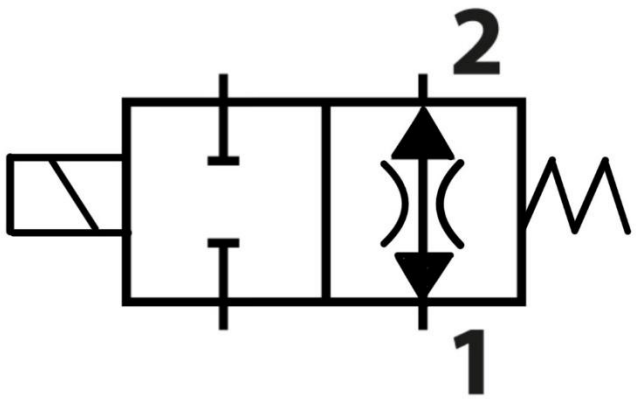

Figure 2.21: *2/2 NO Electro-Valve symbol following ISO 1219 standard.*

The spool of the valve can switch between only two possible stages: open and closed; for this reason, fast dynamics are preferred, especially for close-to-open transitions, to avoid that the pump starts generating flow with the valve still partially open. For the open stage, it must be ensured bidirectionality and symmetric characteristics at both ports. The normally open condition meets safety requirements, in case of fault of any upstream components, the rider can always operate the handlebar without resisting against the inertias of the motor and the pump. Therefore, the spring element pushes back the spool in the open configuration, while a solenoid coil, when electrically powered, produces a larger opposite force that lets the valve close the passage.
The disadvantage brought by the presence of the whole actuator system is felt with an effort increment: when the rider decides to apply a moment to rotate the steering system, it is faced additional resistance, due to the viscous friction for the fluid circulation. Nevertheless, the actuator enhances safety also when inactive, producing passive influence on the vehicle, while riding.
During a straight motion, the motorcycle is still subject to out-of-plane dynamics; generally speaking, these account for yaw, roll and steering, affecting lateral stability and safety. The involved degrees of freedom permit the decoupling of every other behaviour that belongs to the

in-plane dynamics, lying on the body symmetry and affecting riding comfort, such as pitching and the vertical motion of both suspensions.

In particular, the rotation of the front steering assembly, around its axis, may give rise to a vibrational mode, named wobbling. The causes to attribute to this phenomenon are multiple and often a combination of disturbances coming from road irregularities, loading or unloading tire transients, hitting the wobble resonance frequency. The oscillations of the handlebar become perceivable to the rider in the range 6-10 Hz and the motorcycle velocity plays an important role in the stability of the model, when studying the frequency response: the eigenmode is unstable for lower speed, while the wobbling amplitude stabilizes for higher values [8].

The model to consider represents a simplified version of the front assembly, with a single degree of freedom, that is the rotation around the steering axis. The front wheel, the fork and the handlebar are assumed as a rigid body, decoupled from the rest of the motorcycle and independent on the rolling motion. These are all resumed in a single inertia ($J_{f\delta}$) around the steering axis, characterised by an equivalent stiffness, taken at the ground and projected to the vertical axis, therefore influenced by geometry, as the caster angle and the trail length. In addition, the rider handling of the steering system contributes to said stiffness, meaning that a relaxed grip would decrease it, causing less resistance against the oscillating torque.

Equation (2.5.1) shows the homogeneous solution in the frequency domain of the undamped model:

$$J_{f\delta}\omega^2 + k_{f\delta}a_n \cos(\varepsilon) = 0 \tag{2.5.1}$$

To a single degree of freedom corresponds a single vibrational mode, whose natural frequency of resonation is computed in equation (2.5.2).

$$\omega_n = \sqrt{-\frac{k_{f\delta}a_n \cos(\varepsilon)}{J_{f\delta}}} \tag{2.5.2}$$

Ideally, at this frequency the amplitude of the oscillation can diverge to infinite, thus, it is necessary to introduce the damping effect. Each element of the model presents an intrinsic damping characteristic that contributes to attenuate the magnitude of the oscillations. Wheel, suspension, handlebar and rider produce an effect inversely proportional to the motorcycle velocity, therefore, at high speed the attenuation is limited.

The need for a sufficient damping in all conditions is filled with the passive work of the actuator system. It brings up a constant damping (c_a) that sums to other components. The effect is due to the passage opened by the electro-valve, working as a dynamic restrictor. For this reason, the allowed flow rate is regulated sizing the opening, assumed circular, thus only dependent by its constant duct diameter (D_r). The resultant simplified equivalent circuit is shown in **Figure 2.22**, with the valve open the oil can recirculates into the cylinder.

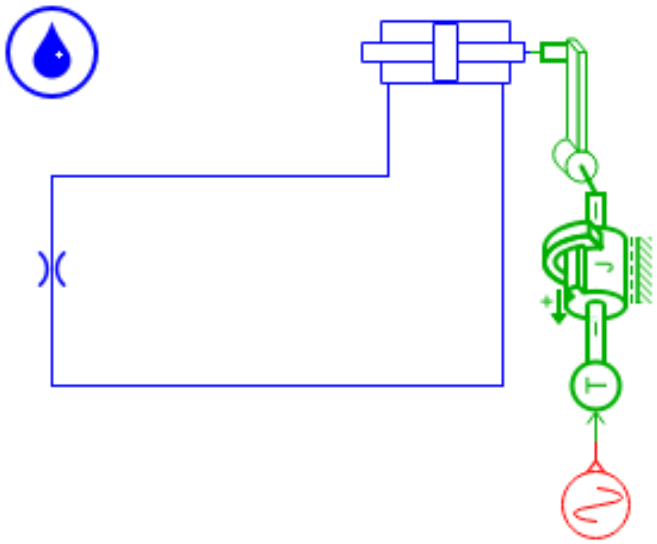

Figure 2.22: *equivalent circuit when the electro-valve is open: in blue hydraulic components, in green the simplified mechanical rotating elements for the front assembly, in red a sinusoidal torque input representing the vibrational mode.*

The restrictor works as an obstacle for the flow, increasing the pressure and propagating upstream, back to the cylinder chamber related to the outlet port. The piston, moving toward this port, is slowed down by the braking action of the oil at higher pressure, ultimately decreasing the amplitude of the oscillation, here retransmitted from the linear motion of the actuator to the steering rotation.

The relationship between the pressure drop and the flow rate is described by the Hagen-Poiseuille law for laminar regime, equation (2.5.3); with μ the viscosity of the fluid, l_r the length of the restrictor duct. Higher damping effects are, therefore, related to a higher pressure difference, which, in turn, is inversely proportional to the opening dimensions and the fluid properties, resumed in G.

$$\Delta p = \frac{Q}{G} = \frac{8\mu l_r Q}{\pi {r_r}^4} \tag{2.5.3}$$

From the complete damped model [9] can be computed, as seen in equations (2.5.4) and (2.5.5), the new resonance frequency, different due to the damping effect, and the damping ratio (ζ): ranging from 0, undamped case, to 1, corresponding to the critical damping, observed in the term under squared root at the denominator of equation (2.5.5).

$$\omega_d = \sqrt{\left(\left(c_a + \frac{k_{f\delta} {a_n}^2}{V}\right)\frac{1}{2J_{f\delta}}\right)^2 - \frac{k_{f\delta} a_n \cos(\varepsilon)}{J_{f\delta}}} \tag{2.5.4}$$

$$\zeta = \frac{{}^1\!/_2\left(c_a + \frac{k_{f\delta} {a_n}^2}{V}\right)}{\sqrt{J_{f\delta} k_{f\delta} a_n \cos(\varepsilon)}} \tag{2.5.5}$$

3. Control Logic

The automation of the whole system must ensure efficiency and safety, during operations. The controller logic expands to two different and semi-independent layers. Each one has its own control variables, and when the respective targets are met, one logic can exclude the other for the computation of the actuator command. There is not a predefined master or slave layer, they can alternate the roles depending on different conditions; furthermore, this design ensures stronger safety in case of a generic failure.

3.1. Upper layer controller

The first level checks if it is necessary to lean the motorcycle, so it enables the actuator to operate. It requires the absolute error of the leaning angle, difference between a target and an actual value. To obtain the former, it is necessary to compute the value for the roll angle required to attend a corner of a certain curvature radius R_c.

As it is possible to see from the following formula of equation (3.1.1), the value is purely theoretical and valid when no steering angle is applied, so that all the work to turn the motorcycle should be completed by the device, leaving no space to human interventions.

$$\varphi_{ref} = \tan^{-1}\left(\frac{a_y}{g}\right) = \tan^{-1}\left(\frac{V^2}{gR_{curve}}\right) \quad (3.1.1)$$

The radius is estimated by algorithms that analyse the images coming from the camera, the velocity is simply measured with on-board sensors, in the end, the computed value is taken as the reference. Raw image frames are captured from front-facing cameras, usually configured in stereo. Once acquired, they undergo preprocessing to enhance lane visibility and reduce noise. Regions of interest are selected to focus computation on the road surface. A perspective transformation is then applied to map the camera view into a bird's-eye representation of the road, seen perpendicularly from above. Following this, lane feature extraction is performed to isolate visual prompts corresponding to lane markings. Depending on the approach, this may involve classical computer vision techniques such as edge detection, gradient thresholding, and colour filtering, or learning-based methods that produce pixel-level lane probability maps. The goal of this step is to generate a representation of the road where lane markings are clearly separated from the background. The extracted road features are then used in the lane candidate detection stage, where potential lane lines or boundaries are identified, validated and given a confidence estimation, to finally assess them as reliable. The steps of this process are reported in **Figure 2.23**, using Active Contour Model method.

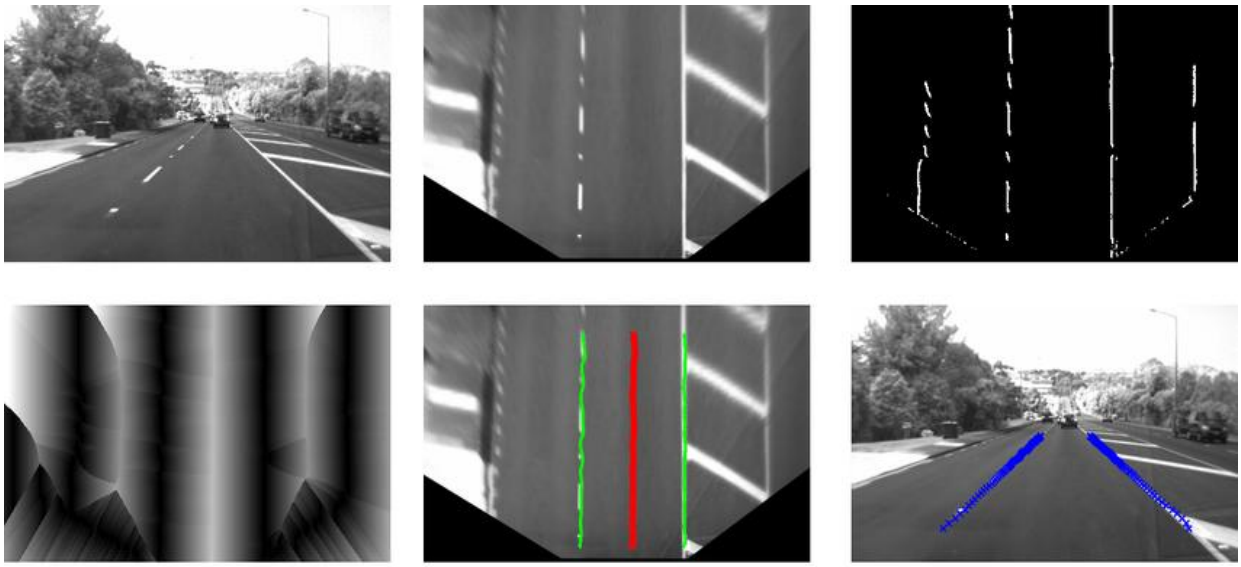

Figure 2.23: *image processing for lane detection with Active Contour Model method.*

The actual roll angle, instead, is estimated by the inertial platform sensor, it reproduces the measurement for the centre of gravity of the motorcycle.
If the difference, taken in absolute value, between these two parameters differs from zero, the second layer of the controller is allowed to provide the command to the actuator, for whichever direction the motorcycle needs to lean. It is ought to remember that for straight roads the curvature radius tends to infinite. Therefore, for a null target roll angle and the vehicle already in equilibrium, i.e. going straight, the device cannot move because this first layer control is preventing any command.
The impediment also occurs when the roll angle difference is equal to zero, this means that the motorcycle lean angle is sufficient to attend the estimated curvature, the device operation has approached the upper layer control target, so it should be stopped.

3.2. Lower layer controller

In a first moment, the second layer controller provides the actual command to the device, which is a position target for the piston linear motion; then, it manages the displacement error in closed loop feedback. The architecture comprises of a Stanley kinematic controller in series with a 1D Body position controller, enforced with a Proportional-Integral controller.
To get aware of the motorcycle orientation and position along the road, a software elaborates the images from the camera to extrapolate the heading (e_h) and the cross-track (e_{ct}) errors. The first one refers to the angle between the vehicle and the reference direction, here taken in the lane centre, the second one regards the distance from the reference trajectory, which lies on the lane centre.
Steering the motorcycle by leaning, and exploiting the cornering effect of the camber angle, would produce an overestimation of the heading error. The front of the leaned vehicle points outwards of the corner, while the actual curvature gain is higher; this understeering behaviour is wrongly picked by the camera and needs to be reduced.

The adjustment is made by subtracting an angular quantity from the heading error. This is done starting from the reverse of the equation (3.1.1), it is possible to obtain the curvature in rad/m, using the actual roll angle estimated by the sensors, as seen in equation (3.1.2). The curvature is transformed into an angular gain if multiplied of a certain distance horizon: this results in a sort of prediction of how much of a corner, of constant radius, the motorcycle would complete in the next meters ahead. Equation (3.2.3) computes the corrected heading error.
Increasing the horizon enlarges the adjustment, possibly further misleading from reality the estimation of the motorcycle heading; thus, keeping it low creates a trade-off between accepting some understeering and improving the responsiveness of the controller.

$$\frac{1}{R_{curve}} = \tan(\varphi)\frac{g}{V^2} \tag{3.2.2}$$

$$e_h^* = e_h - \frac{[hor]}{R_c} \tag{3.2.3}$$

The Stanley lateral controller is a nonlinear function that relies on the kinematics of the vehicle. It receives in feedback the cross-track and the orientation errors from the reference trajectory, and it computes the needed steering angle. The choice falls on this kind of control law instead of others, like optimality concept controllers, because it does not require any specific parameters related to the vehicle on which is implemented, allowing the controller to be used universally on every motorcycle.
Primarily, it is imposed a directional control type, meaning that the controller output matches the heading error, so that to any trajectory variation corresponds a steering response. In addition, when the lateral error increases, the related nonlinear term further raises the output command to reinstate the vehicle onto the trajectory path. The ratio between the cross-track offset and the longitudinal speed is put under arctangent function: resulting in an initial proportional like contribution, as suggested in equation (3.2.4), for low values of this ratio; subsequently, the output behaviour saturates asymptotically for higher values.

$$\delta = e_h^* + \tan^{-1}\left(\frac{k_S e_{ct}}{V}\right) \tag{3.2.4}$$

To sum up, for this case, the controller inputs account for the longitudinal velocity, the cross-tracking error and the modified heading error, while the generated output is the theoretical steering angle, which should be adopted if one wishes to conduct the motorcycle only by steering the front wheel. The longitudinal velocity buffers down the output command; the steering angle of whatever vehicle, especially motorcycles, should be limited at high speed. For this reason, the maximum command is limited to 25° in each direction, in order to avoid potentially dangerous countersteering actions and that the actuator remains stuck at the end of the stroke, causing overpressure.
The cross-track term is multiplied of a proportional gain (k_S) to increase its contribution weight; it also qualifies as the only parameter to be tuned inside this stage of the controller layer.
Few steps are required to transform the Stanley controller output, which is an angular quantity intended for the front wheel, into a linear displacement, to be encoded by the device controller. Starting from the bottom, the front wheel is rigidly connected to the front suspension fork which, in turn, extends to the handlebar; hence, neglecting any vertical motion along the suspension travel, the steering action is rigidly transmitted among the components of the motorcycle front body. The already computed wheel steering angle lies on the ground plane, from a vertical point

of view, the origin is located in the centre of the tire footprint and the arc develops from the longitudinal symmetry axis of the contact patch.
Although, this cannot be said for the steering angle at the handlebar (δ^*), which lies on a plane with an inclination from the vertical that, for sake of simplicity, can be assumed very close to the caster angle: for this premises, the axis is supposed to pass in the wheel centre. This kind of geometry impacts on the steering rotation by dropping a few degrees at the handlebar, meaning that to produce a certain steering angle at the wheel, the required input would be larger for the rider, as seen in equation (3.2.5).

$$\delta^* = \frac{\delta}{\cos(\varepsilon)} \tag{3.2.5}$$

In a second moment, this angular quantity, that lies on the same plane perpendicular to the steering axis, must be transformed into a linear displacement (X_d). The centre of rotation of the fork stems, the same for the handlebar, is located in their middle point. In real application the steering plate accounts for a small offset from the triple clamp, from which departs the actual steering axis; by neglecting it, the steering angle rotates around a smaller circle, with diameter equal to the distance between the fork stems. Therefore, it generates an underestimation of the displacement, which is, actually, more favourable for the design, because it considers worse conditions.
From the rotating motion, it is firstly isolated the tangential displacement of the stems and, secondly, it is extrapolated the device travel, remembering that the actuator is horizontally tilted of the angle θ, the formula is reported in equation (3.2.6).

$$X_d = \frac{X_{ft}}{\sin(\theta)} = \frac{{}^1\!/_2 d_f \sin(\delta^*)}{\sin(\theta)} \tag{3.2.6}$$

Once computed the linear displacement, it is transmitted as target position: it is defined as the distance taken from the central point of the actuator available displacement stroke, therefore, the piston direction of travel is defined accordingly to the sign of command received. The passages to determine the target position can be seen in **Figure 2.24** with a Simulink scheme.

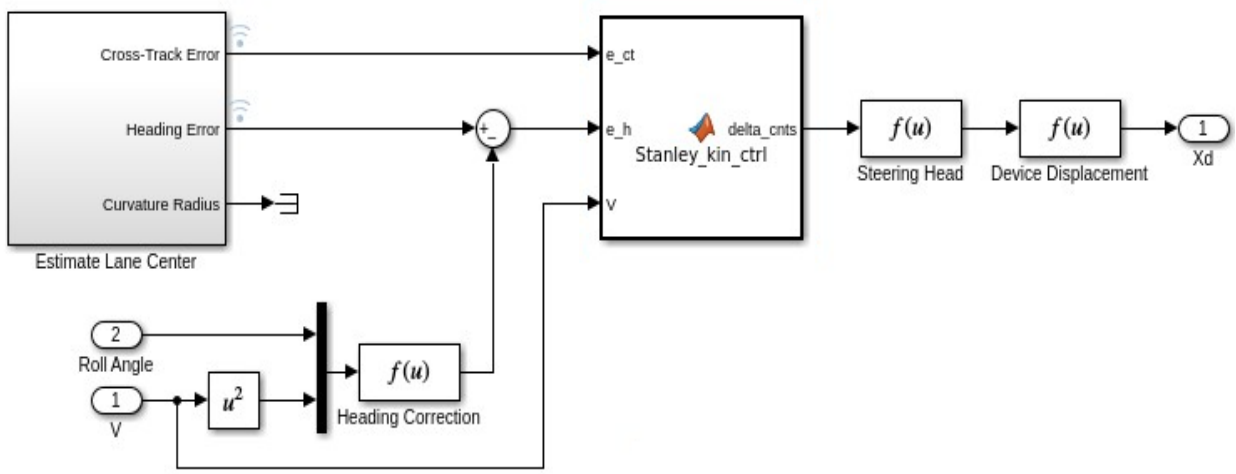

Figure 2.24: *Simulink block diagram of lower layer controller: detail of the Stanley kinematic controller and linear displacement computation.*

The position controller computes the drive command, so that actual position along the actuator stroke reaches the position setpoint. Lower and upper limits for the command signal correspond at the maximum travel in each direction. The first operation of the control logic is the computation of the position error as the difference between the reference command signal and the actual position signal, sensed on the actuator stroke by a potentiometer and received by the control unit in feedback closed loop.
The error is then processed by the controller to obtain the driving command signal, to be sent to the electric motor. Therefore, it is done the transformation from a position error to an angular velocity. Finally, the command signal is enhanced with a PI (Proportional-Integral) controller. The proportional term focus on the control of the error value at each time instant; the tuning of its magnitude k_P regulates the steady state behaviour. If too small, the correction on the position error would not be sufficient to track the reference, resulting in a wrong drive command signal: for instance, too low angular velocity to generate a sufficient flow rate. If too large, also the error correction would be overestimated, this results in an oscillating behaviour around the target, because the controller cannot generate a command of adequate accuracy. The fluctuations cascade from the prime mover angular velocity to the piston displacement, reproducing the same behaviour in the steering system and creating discomfort or potentially dangerous conditions.
The integral term k_I introduces a correction on the position errors of the past instants, performing the integral sum of the previous samples. This leads the controller to perfectly track any steady-state error; nevertheless, if the magnitude of the term is too small, the transient behaviour, before reaching the target, will be too slow. Conversely, if the magnitude is too large, the transient time will be fast but the behaviour too aggressive, resulting, for instance, in an overshoot of the piston displacement. The actuator position, closed-loop feedback can be seen in **Figure 2.25**, of the hydraulic circuit only the actuator is visible, representing the interface with the motorcycle, the rest is shadowed inside the block SC_1. The green mechanical parts show a mass (m_{feq}) only capable of moving in one dimension, equivalent to the motorcycle front assembly; it defines the load at the actuator, receiving as input the force derived by the moment necessary to steer the handlebar. In red it is represented the position feedback loop, serving the position controller; the other parameters regard the stroke limits and the ratio to scale the output, which is unitary. The resulting command (u) is regulated by the PI controller before reaching the electric motor.

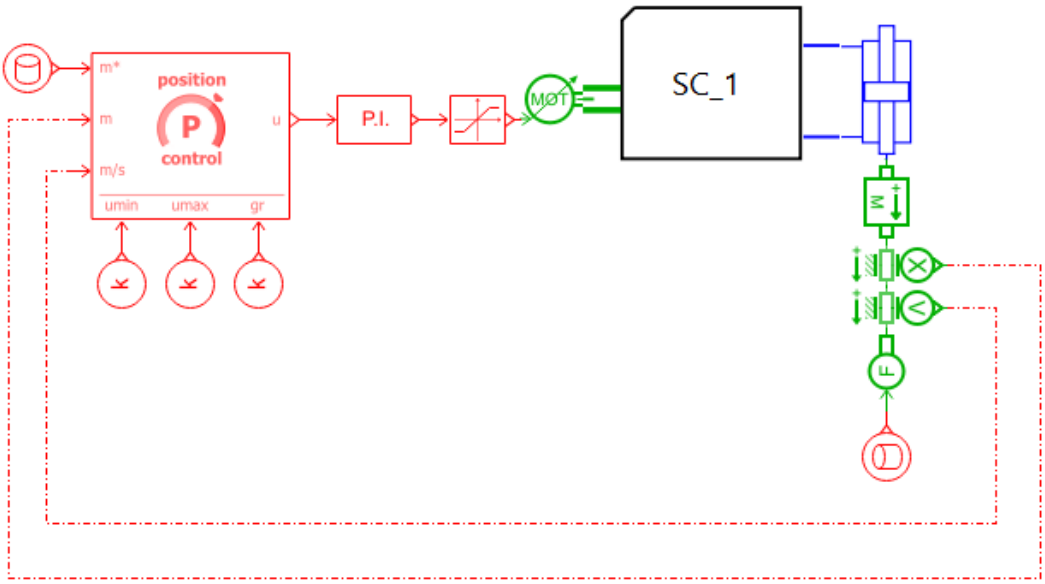

Figure 2.25: *Amesim block diagram of lower layer controller: detail of the position controller and position control closed-loop feedback.*

The tuning of the two parameters must avoid spiking behaviour at all, to improve the accuracy in displacing the actuator piston, but also focus on rapidity of execution.
Before being sent to the electric driver, the command signal gets saturated: a lower and an upper limit are imposed to avoid infinite values. The saturation occurs, for both senses of rotation, at a speed 25 % higher than the maximum operating rating.

CHAPTER III

Simulations and Results Analysis

1. Software Setup

This section describes the main settings adopted on the two software programs, to run the following simulations. It will be explained the process to combine the results, what kind of data is exchanged and the setup of environment.

1.1. Matlab/Simulink

The system modelling, done in the previous chapter, needs to be implemented on software to visualize the results. In general, Matlab/Simulink program formalizes the mathematical problems that regard the physics of the vehicle and the control systems.

In particular for this work, the process starts on a Matlab file, resuming all the needed data of the motorcycle, like geometry features, wheels size and characteristics, useful physical parameters to define the ambient. Moreover, on the same file are recalled the functions to design the road scenarios and the parameters to run the simulations.

The vehicle is properly reported on a Simulink file, following the structure of the described model, therefore split in a section that computes the dynamics (longitudinal, lateral,...) to find the trajectory in the space, and a section dedicated to the controller. Both parts are strictly connected and communicates with a closed-loop feedback input-output relationship. It is also present an interface that reads the road scenario.

The whole process begins with the road profile uploaded, together with the initial conditions, to define the starting position, velocity and orientation of the motorcycle. The other set of inputs, predefined in the Matlab file, accounts for the commands related to the rider, these are the throttle opening, simplified to an amount of traction torque available at the rear wheel, and the braking torque, differentiated between the two systems front and rear. Although not being of particular importance for the following simulations, they can be modelled as time signals, synchronized with the simulating time, as a human rider intervening on the ongoing motorcycle. For instance, it is possible to recreate the braking action before a corner, or an accelerating phase, totally independently on the system actuator dynamics.

For the simulation to run, it means that the road features are extrapolated and processed, then fed to the controller, that computes, instant by instant, the actuator input command: the linear displacement target. This data is packed and sent to the Amesim file, from which returns the actuator actual position. This gets retransformed in a steering angular quantity (countersteering), to have the rolling dynamics ready to be sent to motorcycle block as input signal.

It is necessary to explain that the angle produced for counterteering the front wheel does not induce any disturbing result on the orientation of the motorcycle; as already described, in a real-world manoeuvre the handlebar is countersteered for a small period of time, preceding the corner, so for the rest of the curve it is assumed that the front wheel points straight, perfectly aligned with the rest of the frame, while the vehicle is cornering, leaned down. Furthermore, the rolling model

immediately responds to any input, hence, any heading variation can be neglected also for the initial countersteering part.
It is also possible to reproduce the steering angle and use it solely as input signal, considered as an action of the rider.
The vehicle block closes the Simulink loop, because it updates the state of the motorcycle, i.e. speed and actual trajectory, after receiving the inputs related to the preceding instant. At this point, the simulation steps onto the next time instant, so that a new portion of the road ahead can be scanned.
Finally, the relevant results can be extracted and brought back to a dedicated new Matlab file to be consulted and analysed.
The Simulink blocks call the needed variables from the Matlab file, which are saved as single values, vectors or even in matrix form to manage the bidimensional lookup tables. Part of this data is taken from literature, other is arbitrarily selected from existing models, or produced ad hoc; with the purpose of recreating a motorcycle with generic and average characteristics, respecting the feasibility and the reproducibility of outcomes that can be compared in the real world.
The road scenarios are created with a Matlab function that draws the road segments and put them together. Among the geometrical requirements, there are the length of straight traits, the radius and the arc of every corner; furthermore, it can be decided the width and the number of driving lanes, so that it is possible to imagine several cases that reflect reality. The ultimate result of the function works like a spline, it approximates every curvature with a line interpolated in a series of waypoints, that are placed in the centre of each road. Therefore, for small corners it is best to increase the number of waypoints for obtaining smoother resolution.
The road created is totally compatible with the Simulink reader, which interconnects as a shared world, merging the same system of absolute coordinates, where the motorcycle and other objects can move inside. The graphic result can be appreciated in **Figure 3.1**.

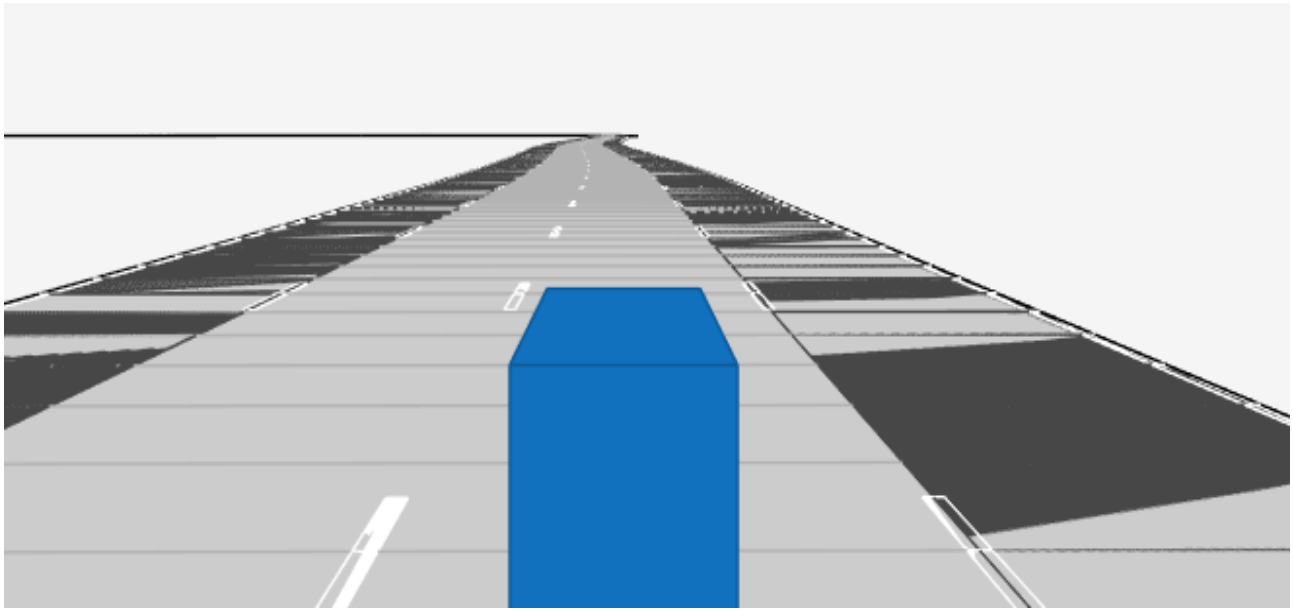

Figure 3.1: *generic road scenario reproducing virtual road perception: drivable lane (light grey), non drivable lane (dark grey), road markings (white) and estimation of motorcycle occupied space (blue).*

Once the road is uploaded on the Simulink scenario reader, it must be configured to output all actors in world coordinates, so that the following vision detection block can output the objects and the lane markings in the vehicle coordinates.

This last block simulates the camera sensor, for this reason it needs to be properly set up as if it is done for a real case. The correct positioning must be done along the longitudinal axis of the motorcycle, at a certain distance ahead of the centre of mass and at a sufficient height: for this reason, it is placed 0.8 m longitudinally and at 1.1 m of height, to replicate the position of the motorcycle lights. The camera is also given 1 degree of pitch inclination, which means it points down to the road.

The estimation of the lane centre is computed in a dedicated subsystem that outputs the data from lane sensors to the controller block as the heading and the deviation errors, or the as the calculation of the curvature radius. The detector in this case is configured to report the left and right lane boundaries of the current lane in the current field-of-view of the camera, that is the image processed at that instant. Each boundary is modelled as a length of a curve whose curvature varies linearly with distance (clothoid curve). Both detected curves are offset toward the centre of the lane by the width of the motorcycle and a small margin, that can be adjusted in a way to increase or decrease the error calculation, triggering faster or slower responses of the controller. Each of the resulting centred curve function is weighted by the strength of detection and the averaged result is passed to the controller.

Last setting that is worth to know regards the sampling time used in the simulations. Elements like the camera, the image processor and the BUS lines used to recreate the network for internal electronics communication among the system different elements work with a sampling rate of 10 Hz, this means that, during a simulation, these actors play a frame every 0.1 seconds; the overall sampling period, used by the Simulink compiler, is equal to 0.001 seconds.

As mentioned before, it can be created a model for the rider, aiming to simulate the execution of actions to be translated as input signals. As for the camera sensor, it starts from the perception of the road markings; in particular, it needs to be written a Matlab function that reads the waypoints on the centre of lane and compares them to the position of the rider, which obviously coincides with the motorcycle. This wants to simulate the human perception of the vehicle heading along the road and its surroundings, it takes as inputs the series of road centre marks, retrieved from the Matlab file for the creation of scenarios, and the current position from the Simulink ongoing simulation. The output is the relative orientation from the current heading to the target waypoint at the end of a road segment. In this way, it is generated a target value, that varies instant by instant depending on the motorcycle trajectory; it also resembles a human behaviour that tries to focus on the portion of road up ahead.
In a second moment the output of the function is multiplied to a proportional factor, that ranges from zero, no human intervention, to a positive value, to increase the amplitude, and so the promptness, of the human action.
The signal generated from the rider block is suitable for a steering input but also for the leaning angle. In the following simulations the first option will never be used, while the second one will be added to the actuator effort to create the wanted roll angle. Therefore, the ultimate input signal for rolling is going to be a combination of the two actors never antagonizing themselves, nor excluding one another.

1.2. Simcenter AMESim

The second software in use to realize the model is Simcenter AMEsim: it enables the modelling of multi-physics systems and components. As a matter of fact, it must operate on components that see hydraulics, mechanics and control electronics. These are taken from different libraries and combined together: the software provides interfacing to integrate the different mathematics behind each one.
The aim is to compute the actuator linear displacement and pass it to the Simulink model; to do such, it is necessary to synchronize the sampling time in order to let Amesim operate on the same Simulink time step transmitted as input. As already explained before, this model receives the target position for the actuator position controller and stop command from the controller upper layer. Therefore, it accounts for the control part, that transmits electrical (logic) signals to the electric motor, which is a simplified component, that, in turns, put in motion the hydraulic circuit; in the end, the actuator piston motion is intended as an unidimensional moving mass, that constitutes the mechanical part of the model.
The whole procedure seems like the testing of the actuator physical object, whose 3D concept can be seen in the previous chapter, as Hardware-in-the-Loop (HIL) simulation based. The physical hardware, under test, is integrated into a real-time simulation environment that emulates the behaviour of the system it is intended to control.
After sketching the hydraulic circuit, every component is assigned a sub model to get into detail about its functioning and its characteristics, in different levels. For example, one can describe accurately the non-linearities of a retaining spring; conversely, one another can totally neglect the internal leakages of a valve.

Last passage, before running the simulation, is the definition of the parameters for every component. To be more precise, these data can represent dimensions, technical characteristics or even functions to describe the behaviour of a variable.
It is important to mention the characteristics for the oil intended to be used inside the hydraulic circuit; these are taken off a sheet of specifics for the Motul FORK OIL EXP M 10W[1]. This is a fluid suitable for motorcycle suspension forks, with density of 0.859 kg/l at 20 °C. It is defined with elementary properties, with calculated kinematic viscosity; meaning that the kinematic viscosity of the liquid is calculated and is dependent on the fluid temperature, provided two points to interpolate the inversely proportional function: 35.9 cstoke at 40 °C and 6.1 cstoke at 100°C.

2. Scenarios and Operations

2.1. Motorway Environment

All set to begin virtual trials, the first scenario intends to test the device in a high-speed environment, like it could be a motorway. Therefore, though the aim is to create difficulties and harsh conditions to discover the limit of the controller, the road follows few regulations for its design.
As a motorway is defined as high traffic capacity, it accounts for three lanes of 3.5 m of width each, that follow the given profile by placing the waypoints of the curve running along the central lane. Three segments are visible: an initial straight of 50 m, pointing along the longitudinal direction, a wide 90° corner towards the left and a final straight segment of 100 m.
The curvature is the maximum possible, findable on the Italian motorways network, depending on the regulation documents. It includes a radius of 250 m for the most internal lane, which is the left one, considering the direction. The resulting road scenario can be seen in **Figure 3.2**.

[1] Hydraulic Fluids for any type of telescopic forks Technosynthese®, Motul, FORK OIL EXPM 10W.

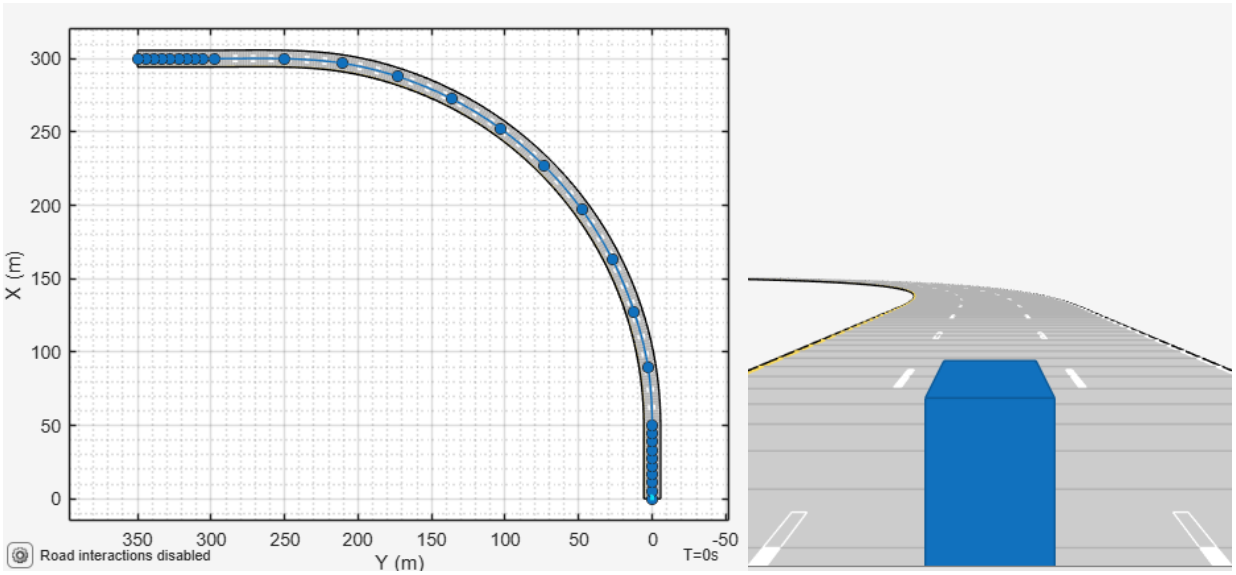

Figure 3.2: *road scenario overview: left, world coordinates with central path waypoints in blue; right, concept view from the ground.*

The initial whereabouts of the motorcycle coincide with the origin of the world coordinates frame, which corresponds to the first segment first waypoint, in the middle of the central lane. It is launched at a speed of 140 km/h, in longitudinal straight direction. It is applied neither a steering angle, nor a rolling angle; in this way, its heading can perfectly match the road, to avoid corrections in the early stages of this simulation.

About the other input parameters, no braking actions are requested during the simulation, while a constant tractive torque is applied at the rear wheel. The vehicle is free to march and take the single corner without any other kind of disturbance, at a speed kept almost constant for the whole time.

Excluding any type of external factor, it is wanted to reproduce a typical behaviour to attend this kind of road scenario, with a speed slightly over the current limits, however, all decisions, about changing the trajectory of the vehicle, are left to the controller to take. This first simulation would like to represent a sort of testbench to refine the tuning parameters for control and identify any sort of criticality from the preliminary sizing of the hydraulic circuit.

The expected outcomes would be qualitatively acceptable, since the radius of curvature is enough high to permit the actuation of small, not too challenging, corrections. In the design phase, previous chapter, the identical conditions have been used to calculate the torque necessary to steer the handlebar, although, that was a simplified case for the steady state contribution. Accounting for transient behaviour and on-time continuous corrections, the total moment required could be slightly higher.

The outcomes of this simulation can be read in two ways: from an imaginary rider perspective or from the response of the actuator system. At the beginning of the curve, in **Figure 3.3**, the controller waits for the errors to rise, before enabling a displacement of the actuator; this leads the trajectory to deviate from the ideal path, in the centre of the lane, and the vehicle to attend the corner somehow delayed from the optimal timing.

Nevertheless, once finished the initial part, the lateral offset is recovered, maintaining the motorcycle acceptably inside the lane.
In a second moment, the same conditions show up as before: the increase of both errors induces the controller to activate. The cause of it must be attributed to the simulated absence of any human control; therefore, the motorcycle path is left to deteriorate any time the actuator completes its intervention and restores the actual trajectory, closer to the optimal one.
This process repeats itself several times in the course of the corner arc, until the motorcycle approaches the final straight segment. In this last part the trajectory oscillates around the straight line, compromising the decent behaviour had so far.
From the point of view of the actuator, the response occurs in the best manner, even though a bit late, as said before. The trajectory correction happens as a last resort to save human negligence, done in the less invasive possible way; on one hand, the more the delay, the higher the risk to compromise safety, on the other hand, it wants to avoid overreaction or superimposition of actuator and rider's actions.
The solution for a faster response could be found with a stronger tuning of the lane departure control, though the Stanley kinematic law reaches saturation, and any further increase of its parameters is vane.

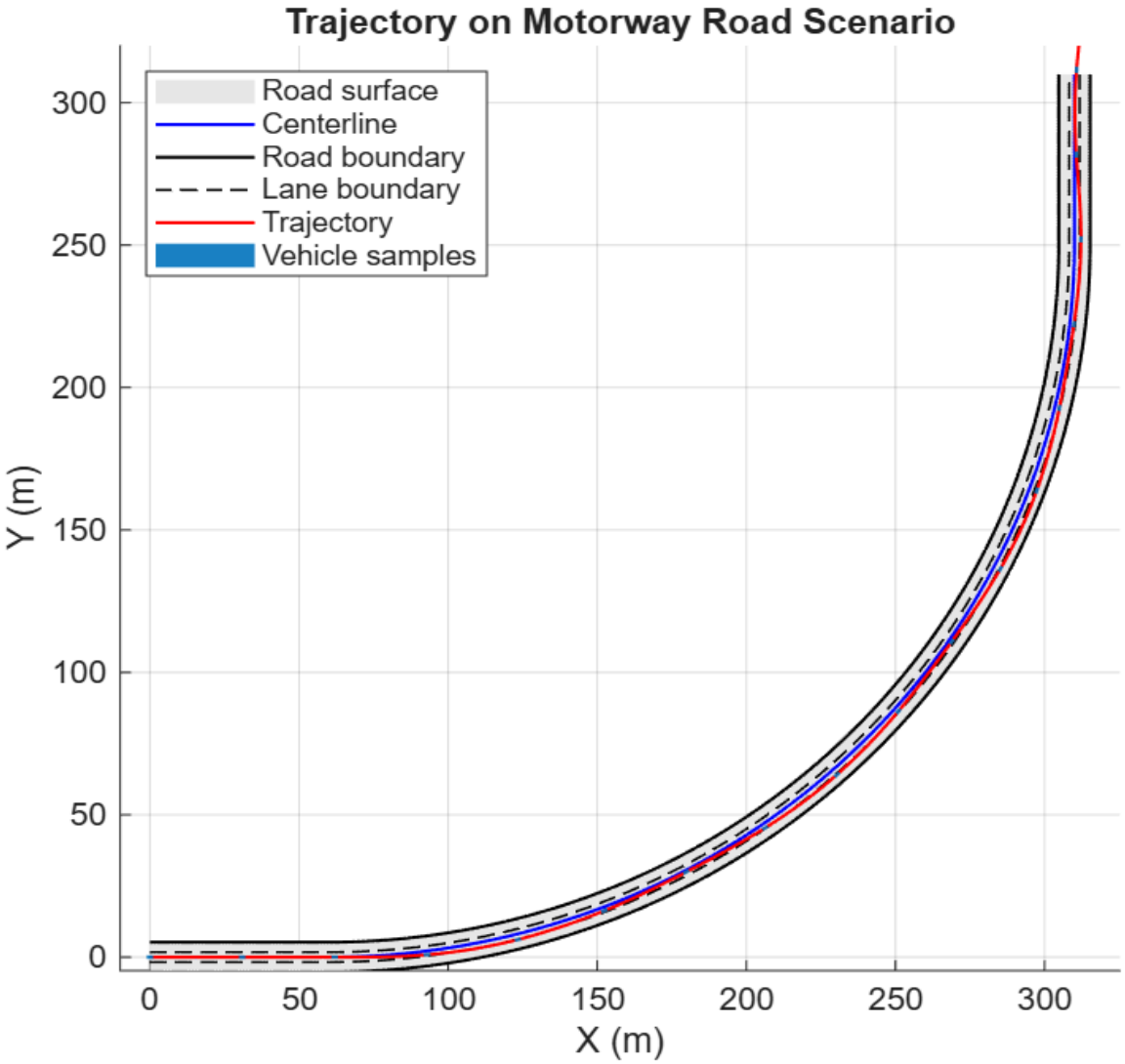

Figure 3.3: *motorcycle trajectory (red line) and centre line path (blue line) for the Motorway Environment road scenario.*

The simulation can be examined under quantitative terms, looking at **Figure 3.4**, the trend of the cross-track error is characterized by fluctuations and several crossings of the lane boundary, represented as a black dashed line. It should be explained that the changes of sign occur when the controller engages the central path line of the adjacent lane, when the motorcycle invades it. In this case a negative error, with respect of the motorcycle reference frame, defines the right side, and so the crossing from the central to the right lane.
The heading error shows a fluctuating trend too: the pattern tells that when the motorcycle orientation is pointing outwards the corner, right side in this simulation, the error turns negative. This is also linked to a faster increase of the lateral offset, leading to overcome the lane boundary. It is also possible to see the amplitude of the heading error unstably increasing in the final moments; this confirms the mentioned behaviour of the vehicle along the last straight segment.

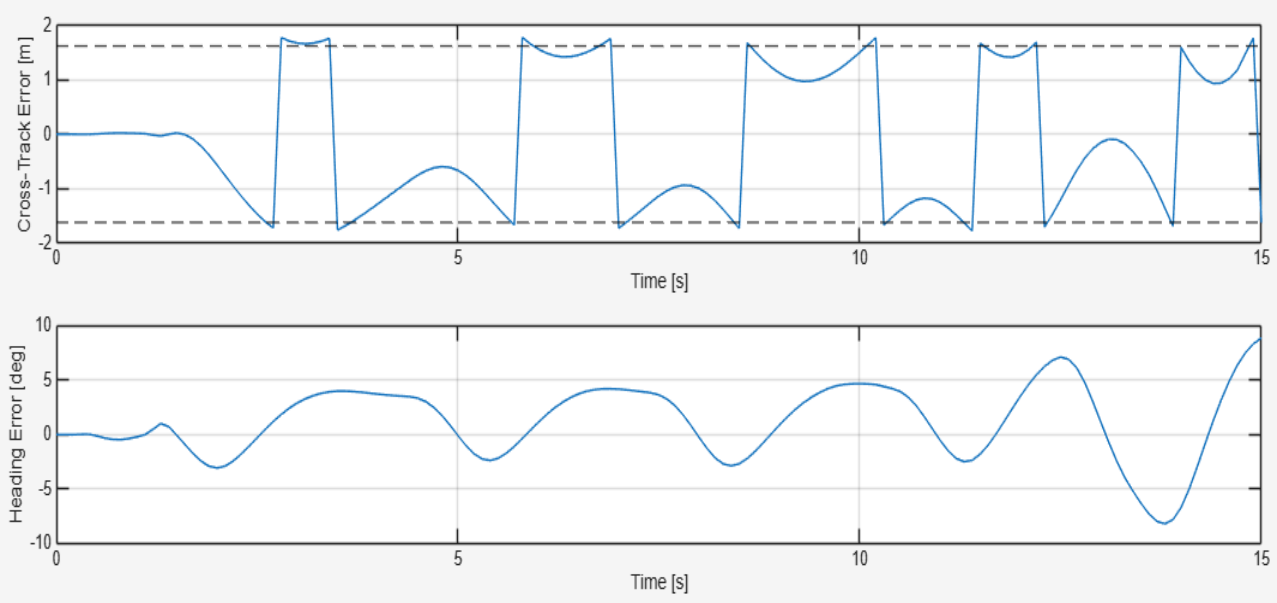

Figure 3.4: *cross track (up) and heading errors (down) of the Motorway Environment scenario.*

To better understand when the actuator is activated, it could be useful to look at other parameters that define the motorcycle behaviour. With the constant input torque, the longitudinal speed drops only few points for attending the corner; as it is possible to see in **Figure 3.5**, also the speed function shows an alternation of decelerations to few seconds of increment. The small accelerations fall exactly when the motorcycle trajectory has got closer to the central path of the lane, meaning smaller lateral error; in these moments the actuator is not intervening, straightening the vehicle path. On the contrary, when the velocity decreases the motorcycle trajectory is following the curvature, meaning that the actuator system is actually correcting the heading.
Longitudinal velocity is connected to the lateral acceleration, especially for steady-state behaviour, the latter is involved in the calculation of the moment needed to steer the handlebar with a given steering rate, which in turns, is related to the development of the roll angle.
Recalling that a positive roll angle defines the motorcycle leaning to the left side, the trend shown in the right figure is consistent with the pattern demonstrated by the actuator system, which is a sequence of trajectory corrections, resulting in the wanted lean toward the inside of the curve. The maximum value reached is slightly lower than the one it is possible to calculate as target to attend a steady-state similar curve, and which is, therefore, considered by the upper layer controller as the threshold to stop the actuator.

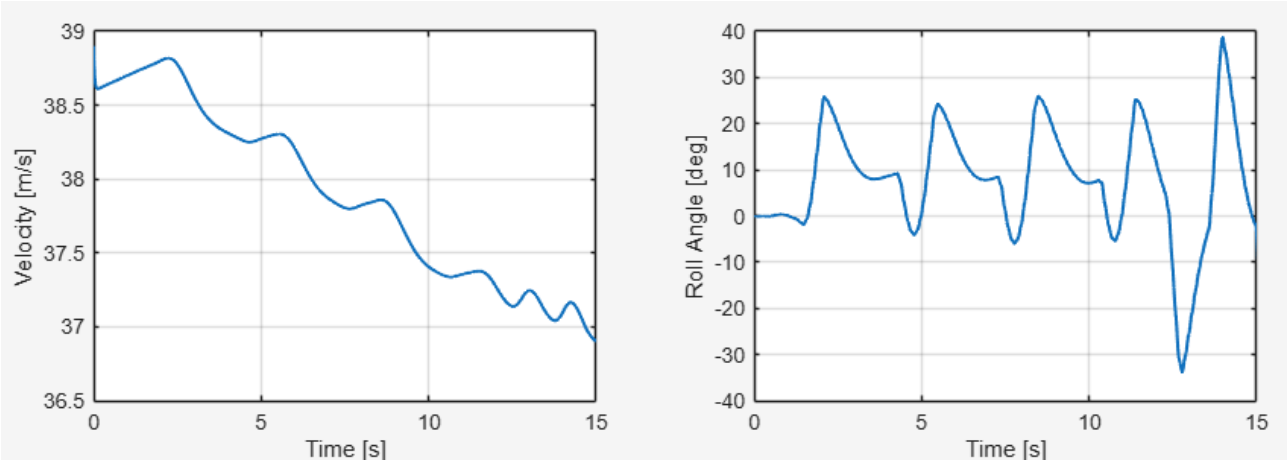

Figure 3.5: *motorcycle longitudinal velocity (right) and roll angle (left) trends over simulation time.*

The oscillating behaviour is repeated in the torque transmitted from the handlebar through the steering axis, as it is possible to see in **Figure 3.6**. From this trend is computed the linear force that applies either a resistant or a dragging load at the piston ends. To lean the motorcycle to the left, the handlebar steers to the right, needing to overcome a positive moment; intuitively, when the actuator changes direction of motion, it faces a negative torque. Though the high speed conducted by the vehicle, the large curvature radius keeps low the lateral acceleration; this characteristic influences the moment at the handlebar, it defines its behaviour as resistant, tending to realign the front wheel with the longitudinal direction. For this purpose, during the inverting motion, the torque amplitude is lower, because aided by the spoken aligning effect.
The peak value revealed to be lower than the one studied for the design, this could be explained by the trajectory kept by the controller, which resulted to be slightly wider than the desired path.

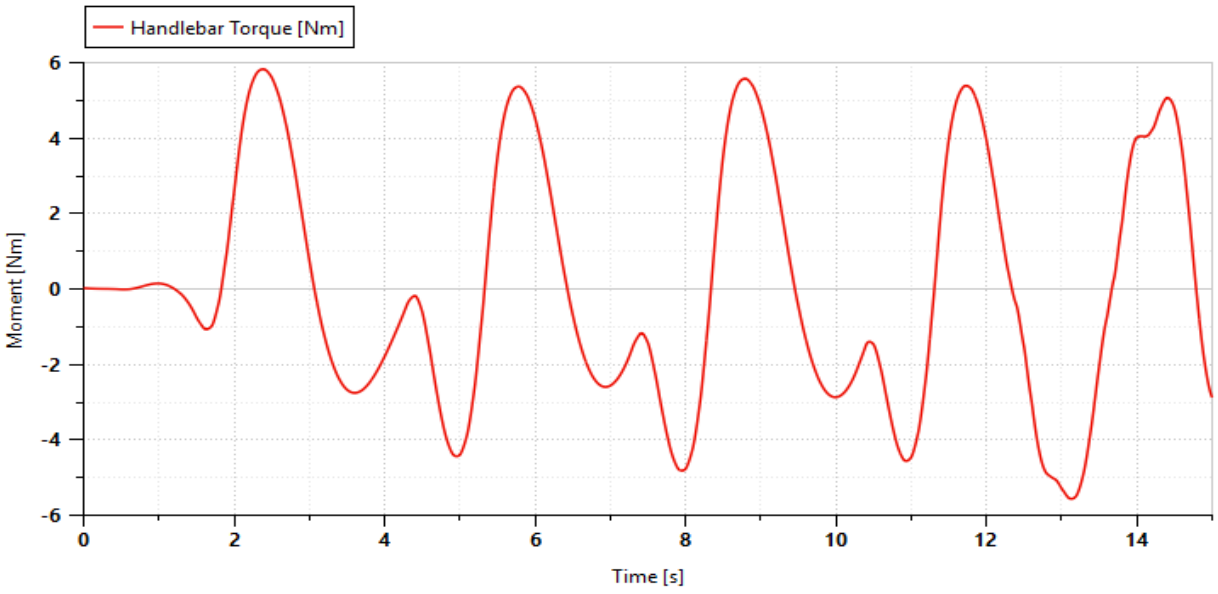

Figure 3.6: *evolution over time of the torque applied at the handlebar.*

The **Figure 3.7** describes the flow rate entering the cylinder actuator, at the corresponding left port. It should be recalled that to rotate the handlebar to the right, it is necessary to push on the left side, in this case the piston pushes onto the left fork stem. From the perspective of the actuator, the piston must slide to the left, therefore, the cylinder receives an ingoing flow rate at the right port, and an outgoing flow rate at the left port, here represented by the negative peaks.
It is worth noting that the flow rate peaks occur slightly delayed from the torque peaks, some tenths of second; nonetheless, the trend respects the recurring fluctuations, here generating the sliding, linear, motion of the actuator.

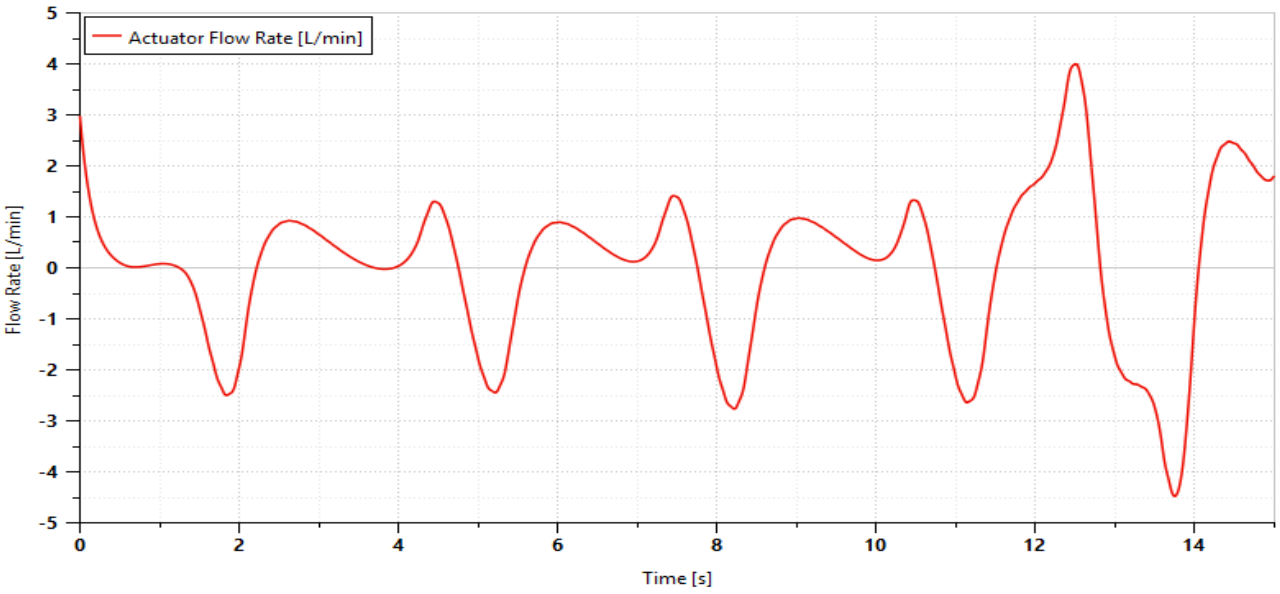

Figure 3.7: *evolution over time of the actuator flow rate at left port.*

It is useful to describe the functioning of the Electro-Hydraulic Actuator; in particular, the behaviour of the pump, depending on the level of charge stored in the accumulator. Being able to operate bidirectionally, inlet and outlet ports of the pump switch accordingly to the requested flow rate direction. Therefore, when delivering, a pressure difference rises, while the accumulator must ensure continuity of flow at suction and constant level in the low-pressure side.
In **Figure 3.8** is reported the pump delivery pressure trend, shown for three cases, each one related to a different filling level of the accumulator. The red line corresponds to empty volume and the accumulator gas pre-charge pressure at 1 bar: the pump works around 0 bar, so to an increase of pressure at the delivery side corresponds an equal decrease at suction, the compensation for the drainage oil flow cannot happen and this condition will not last for a real component.
In the other cases, green and yellow lines, the accumulator volume is filled at, respectively, 47% and 66%, initial level of pressure of 4 and 8 bar; in both cases, it is established a constant head level. This permits to maintain the low-pressure side as it is, when a positive pressure difference is generated at the pump delivery.

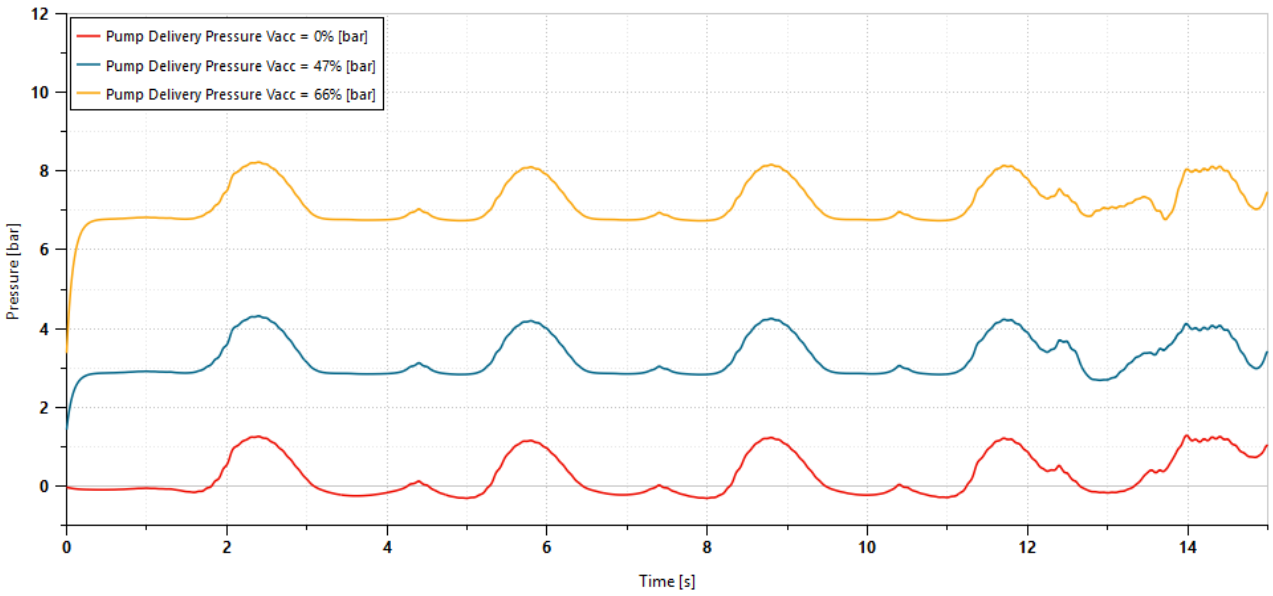

Figure 3.8: *batch run simulation of the accumulator volume level to study the pump delivery pressure over time.*

The observed pressure peaks occur coincidently with the maximum values reported for the torque at the handlebar and so for the load acting on the piston.

Now referring to **Figure 3.9** and recalling the dependency of the drain leakages of the pump on the pressure drop of the component, said peaks of pressure generate a leakage flow with the same trend. More precisely, the flow rate pulses in figure, which are due to the increment of pump pressure, correspond to the initial rotation of the handlebar to the right, facing a resistant load. The drainage flow rate never drops to zero, even when the rotation is inverted, counterclockwisely to realign the wheel; the load at the piston generates a minor pressure increase at the new delivery port, which has swapped after the rotor changed sense of rotation, this causes the minimum leaks between two pulses, observed in the figure.

For the whole simulation, the majority of the drainage flow rate is immediately redirected to the low-pressure side, at pump suction, passing through the relative check valve, that opens because of a higher pressure level imposed by the accumulator line. To actually fill the accumulator volume, having ingoing flow rate from the drainage, the delivery pressure must be higher than the accumulator-imposed level. This condition occurs either if the volume discharges enough oil to lower the pressure level, or if the actuator load induces a sufficient increase at the pump delivery. In this case study, it is the second option that generates the small flow rate fluctuations for the accumulator, green line visible in **Figure 3.9**.

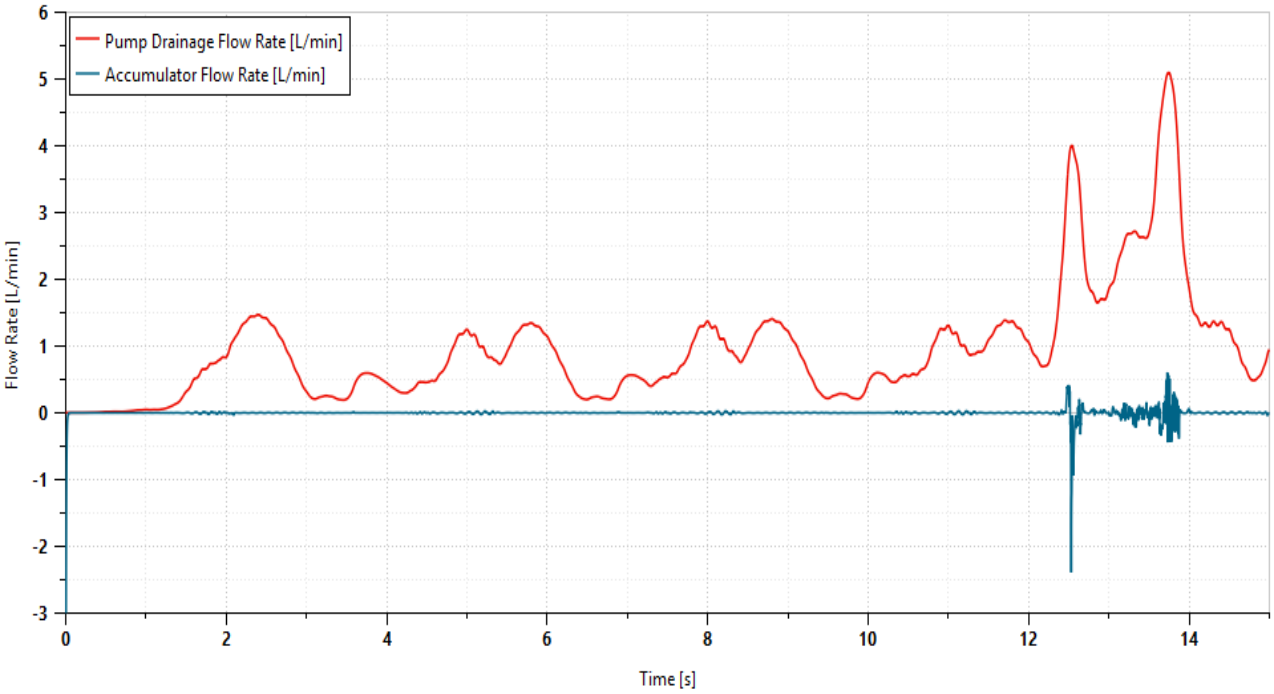

Figure 3.9: *flow rates over time in the drainage line, from pump to accumulator.*

2.2. Rural Environment

The second scenario wants to reproduce the kind of conditions that can be found in a rural environment, outside of living areas. For this reason, the road must show several changes of direction, i.e. multiple corners, mixed with straight segments, creating a dynamic and variable environment.

The characteristics of the road are the simplest: a single drivable lane, only 3.5 m wide, on the right side of a second non-drivable identical lane, reserved for vehicles coming in the opposite direction. Though, the only actor present will be the motorcycle. Therefore, the waypoints for the creation of the ideal path are placed in the middle of the drivable lane.

The first road segment is a straight of 50 m in the longitudinal direction, it follows a double curve of different characteristics: first turn of 45° to the left has a curvature radius of 120 m; the second turn begins right away, it accounts for an arc of 90° to the right and a smaller radius of 80 m. Before the last corner, the road features another straight segment of 50 m, after that, a turn of 45° to the left with curvature radius of 100 m. A final straight segment of 50 m concludes the track of the scenario, pointing again in the longitudinal direction. All the road features can be seen in **Figure 3.10**.

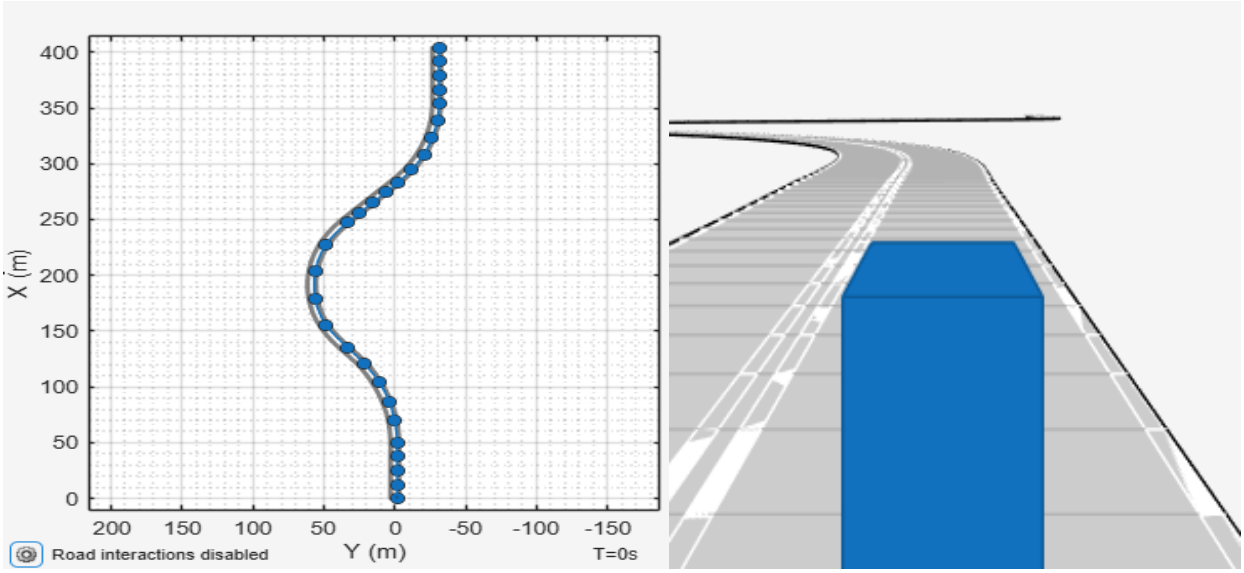

***Figure 3.10**: road scenario overview: left, world coordinates with central path waypoints; right, concept view from the ground.*

The initial conditions of the motorcycle coincide with the origin of the world coordinates frame, it is travelling at a speed of 100 km/h, perfectly aligned with road direction, in the middle of the lane. After one second from the start, it is commanded a braking action lasting one second, where both wheels receive some braking torque; after this period, the brakes are released and the motorcycle attends the double curve free of any other input. In the second straight segment it is simulated a moderate acceleration, inputting a positive tractive torque at the rear wheel, this also lasts one second. The aim is to restore a longitudinal velocity about 90 km/h, before the last corner. The vehicle keeps travelling until the end of the road scenario.

With the description provided above, given the track characteristics, together with the series of commands, it is clear that this scenario wants to test conditions closer to reality. In particular, the system actuator is called to operate simultaneously with the rider, or even respond to a rider action with a trajectory correction: for instance, an acceleration risks making the motorcycle take a corner too wide. The challenge arises, given the fact that the actuator works alone in correcting the trajectory.

The harsher conditions, with respect to the previous scenario, lead the system to fail in two different moments, during the course of the simulation. The first time occurs at the beginning of the second curve, here controller and actuator are too late to follow the inversion of curvature, from left to right, as it is possible to see in **Figure 3.11**, and the motorcycle invades the non drivable lane. During the acceleration phase along the straight segment, the motorcycle is still trying to return in the right lane, this means that it is produced a leaning action, whose effects sum to the acceleration and result in the failure to begin the last corner in time.

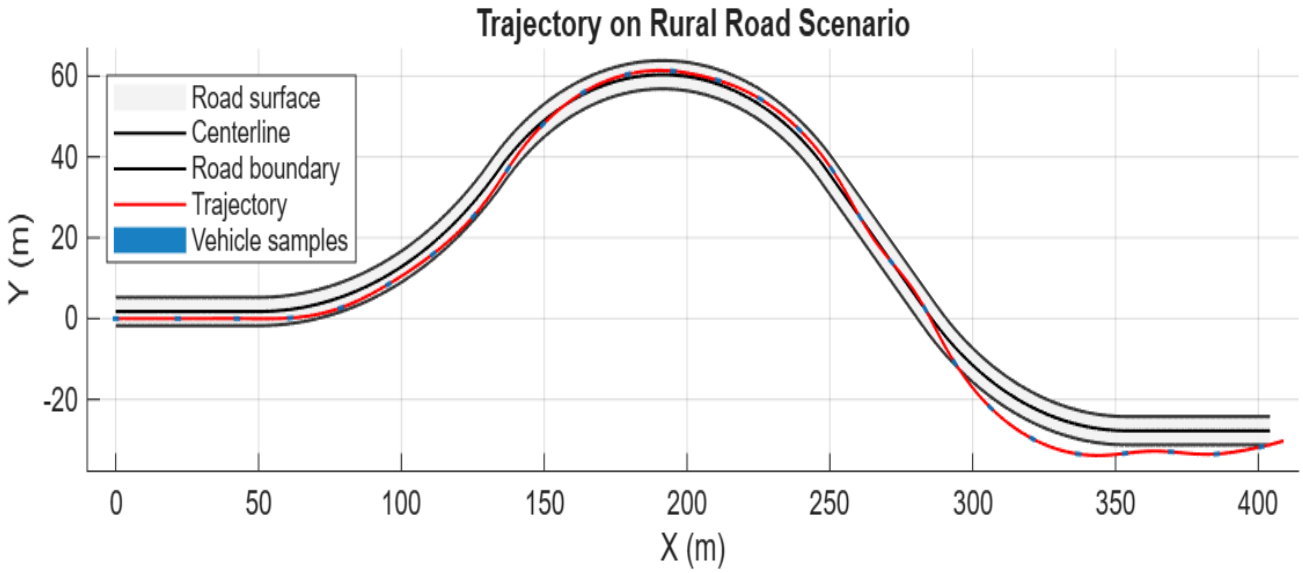

Figure 3.11: *motorcycle trajectory (red line) and centre line path (blue line) for the Rural Environment road scenario.*

This road scenario proves the limits of the controller and states that the system cannot be used as much as a lane keeper, as done so far in these two simulations. Nonetheless, the positive aspect can be appreciated in succeeding the first corner, as single correction delivered by the actuator.

2.3. Rider Leaning Assist

The third simulation pairs the system operation with the action of the rider. More precisely, the motorcycle can still take a corner only by leaning its body, hence without steering the handlebar, but counting on the contribution of the actuator, by countersteering, summed with a generic leaning input from the rider. The model representing the human intervention is purposedly tuned to act poorly, like delivering an input too small or performing with delay. The aim is to recreate a situation similar to a loss of focus or a misjudging of the curvature.

The road scenario, visible in **Figure 3.12**, is composed of an initial a final straight segment of 50 m, in between is present a double curve. Both turns feature the same radius of 100 m, first one is directed to the left with an arc of 45°, the other continues to the right, symmetrically in their central point.

The run starts in the origin of the world coordinates, launched at 70 km/h longitudinally heading along the initial straight segment. No other input adds to vary the motorcycle speed during the simulation time; while the rolling contribution coming from the rider model depends on the orientation error, which is calculated inside the rider function block.

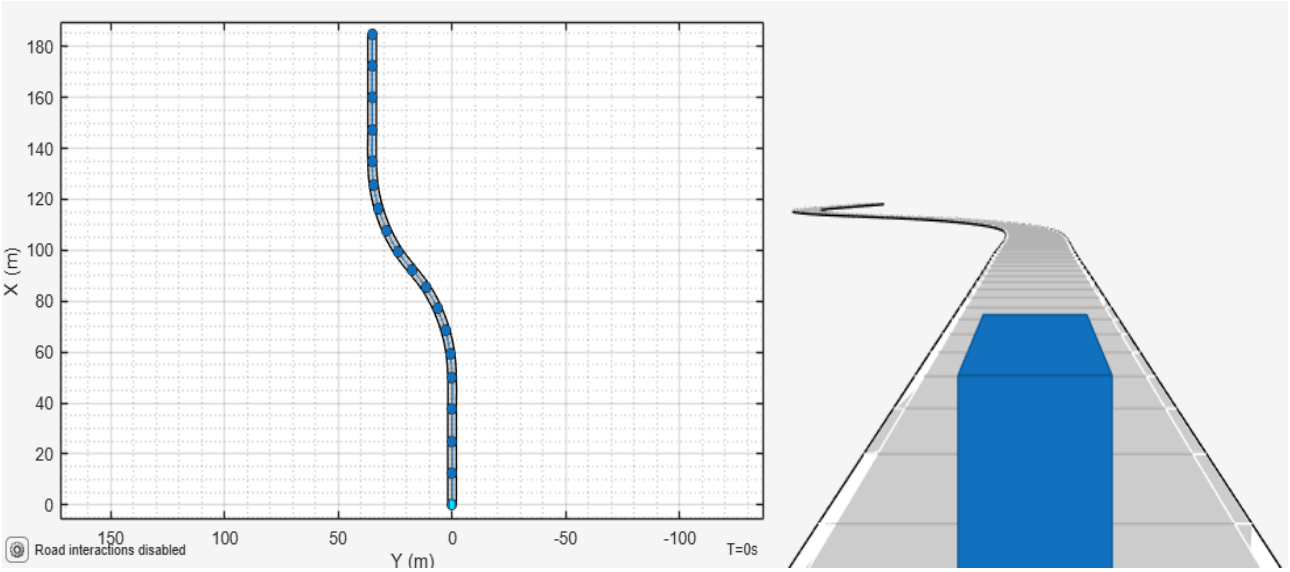

Figure 3.12: *road scenario overview: left, world coordinates with central path waypoints; right, concept view from the ground.*

The two trajectories, visible in **Figure 3.13**, belong to two separate simulations on the same road scenario. This aims to compare the possible path of a misconducted motorcycle, yellow line, to the result of combining the rider with the intervention of the controller, red line.
The first run ends prematurely out of the lane, when approaching the first corner to the left. The leaning input is clearly underestimated and insufficient to keep the motorcycle within the road boundary.
Conversely, in the second run the motorcycle completes both curves and succeed in maintaining itself inside the lane. It is worth noting that, also for this case, the rider model is tuned to underperform, just like for the previous one; this means that the actuator fulfils to provide assistance instead of only substituting the rider, as seen so far in the previous tests.

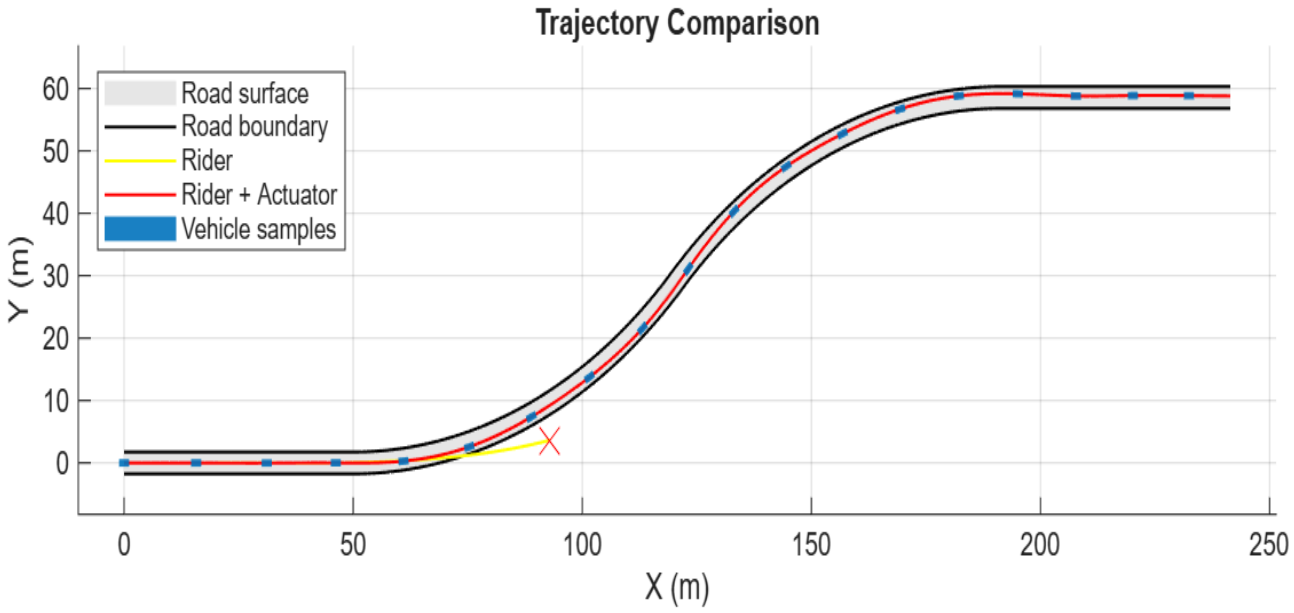

Figure 3.13: *motorcycle trajectories describing the "only rider" simulation (yellow line) and the assisted simulation (red line).*

About the way of intervention, there are differences with the first road scenario to point out: here, the actuator does not correct the trajectory with a series of actions that lasts small periods. The motorcycle attends the curve with a single, long lasting, leaning action for both the corners. This is confirmed by the trend of the cross-track error, in **Figure 3.14**, the fluctuations are reduced to a minimum, while the error almost stabilizes to a constant value for most part of the turn. It must be said that the speed is halved, with respect to the first case scenario, so the controller can respond with greater time to less stringent dynamics.
This behaviour can theoretically describe how to approach the ride of this kind of road scenario, in real situations. Though, this test reports simplified conditions, the result is not only acceptable for the limited deviation from following the ideal path, but also for the manner the system can integrate and support on the motorcycle, during the riding.

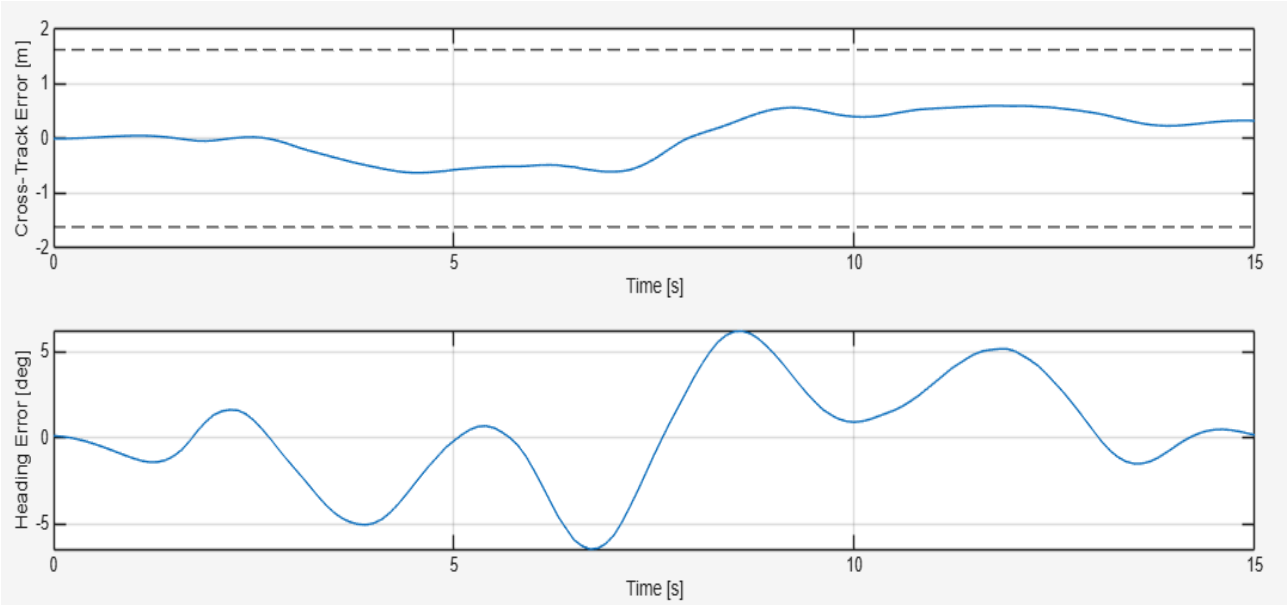

Figure 3.14: *cross track (up) and heading errors (down) of the Leaning Assist scenario.*

In the following **Figure 3.15** is possible to look at the instant when the actuator starts the operation for the curve: exactly at 2.5 s it imposes a steep roll rate to recover the lateral error, which has been rising for two reasons. Firstly, the vehicle has been subject to a disturbing slalom around the straight path for the preceding second, caused by the controller to command an unnecessary rolling oscillation. Secondly, the rider input for the roll angle is too small to satisfy the corner trajectory line, which has already begun to curve at that instant.
In the figure it is also possible to compare the motorcycle trajectory, done with the actuator assistance in red, with the one failed by the rider alone, yellow function. As demonstrated in the figure, in both runs the human preparation to attend the curve is the same, meaning that in both cases the vehicle would have finished off the road. The red dashed line, initially superimposing on the yellow one, stops increasing and remains almost stable for the rest of the curve, while the actuator contribution guarantees the application of the roll angle.

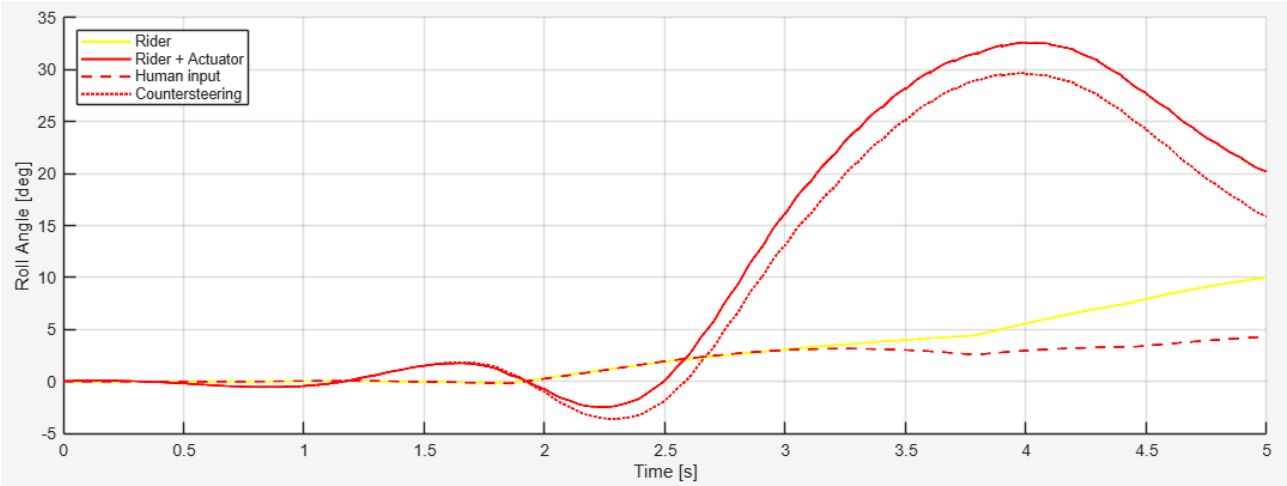

Figure 3.15: *time evolution of the roll angle, detail of the first corner.*

The trend of the linear displacement reflects the roll angle generation; this means that for the piston moving in one direction, the motorcycle responds by leaning toward the same side. This statement is valid both for theoretical and real-world application.

For the simulation of this case scenario, the trend, reported in the upper graph of **Figure 3.16**, highlights the double curve road profile, showing the piston passing from negative to positive, hence from left to right.

In the lower part of the figure, it is possible to see the trend of the flow rate, at the left port of the cylinder. It is defined as the time derivative of the piston displacement, independent of its surface, being constant. This demonstrates the fact that an increase of ingoing flow rate (positive) accelerates the motion from left to right, producing a steeper slope. As seen in the figure, at the time coinciding with the highest peak of flow rate.

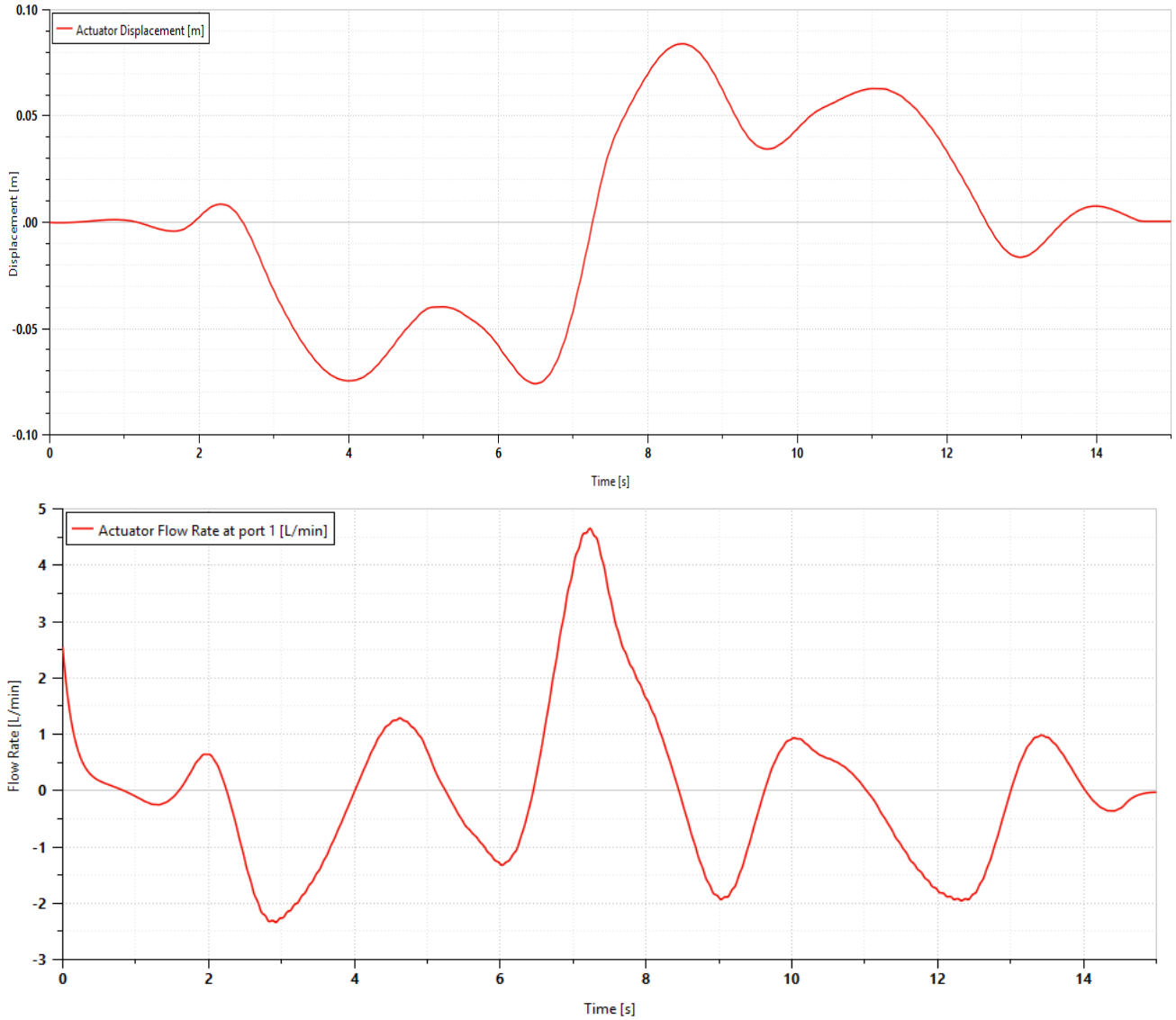

Figure 3.16: *piston displacement (up) and actuator flow rate at left port (up).*

2.4. Actuator Size

The aim of this simulation is to study the influence on operations, after varying one design parameter. The dimension under test is the external diameter of the actuator cylinder, keeping the size of the piston rod unchanged. Starting from the original design, one of the try-outs compares an increase of the size, while the other one a decrease. The variation of the diameter makes other parameters dependent on it, **Table 3.1** resumes the new data for the diameter ratios, the piston surfaces and the volumes.

Table 3.1: *set of actuator external diameters for batch simulation and variation of dependent dimensions.*

External Diameter [mm]	Diameters Ratio [-]	Piston Surface [mm^2]	Useful Volume [cm^3]
20	0.75	137.4	27.5
30	0.5	530.1	106
45	0.33	1413.7	282.7

Firstly, the system will be given a slow sinusoidal input of frequency 0.1 Hz, both for electric motor speed, and torque, with maximum +/-10 Nm, always resistant to the piston motion and synchronized with the angular speed of the motor. The test wants to analyse the different behaviours of the hydraulic system, with focus on the linear actuator.
The flow rate, entering the cylinder, is independent of the size of the cylinder diameter; **Figure 3.17** demonstrates that each case follows the sinusoidal wave and shows the same values for the peak. For the smallest cylinder, red line, the flow rate interrupts from the sinusoidal function and drops to zero almost instantaneously: because of the piston arriving at the end of the stroke, the pressure rises in the duct until the pressure relief valve opens and divert all the flow rate from the cylinder.

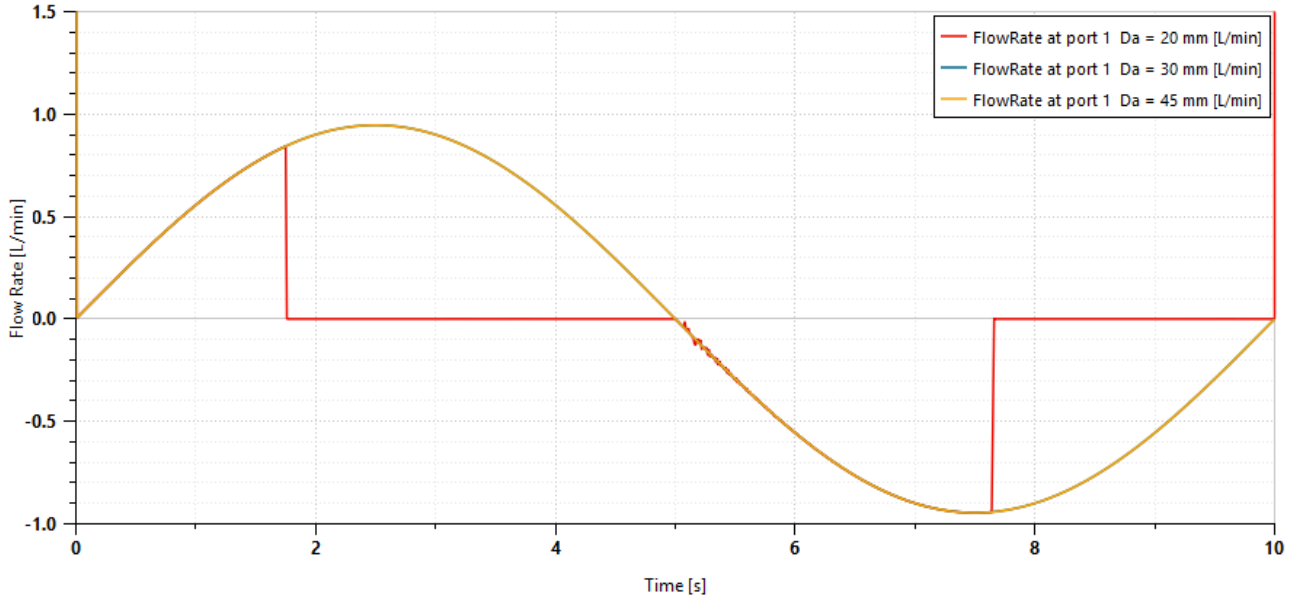

Figure 3.17: *flow rate at the left port of the actuator cylinder.*

Having an actuator with a smaller external diameter, hence a smaller useful volume, could become an advantage when targeting rapidity. As observed in **Figure 3.18**, for the same duty cycle, the smaller the cylinder size, the sooner the piston is displaced. While for the other two cases the end stroke has never been reached, for the 20 mm diameter, the piston finishes its run twice: first against the left side, then the right side after the electric motor inverts the speed.

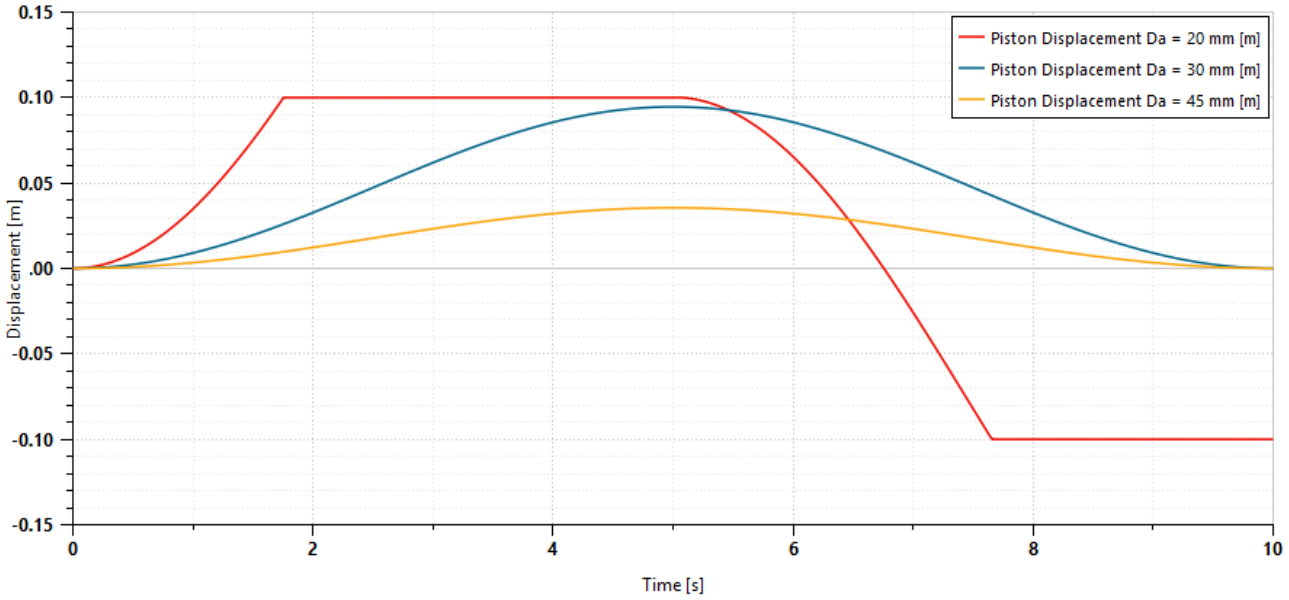

Figure 3.18: *piston displacement.*

With a reduced external diameter, the pressure reaches a higher level in the line upstream the actuator. At the pump delivery port, the pressure difference from suction port becomes more than four times between the 20 mm and the 30 mm cylinder; the smallest test case hits the piston end-stop and, as already said, the level rises almost vertically.

When increasing the useful volume of the actuator, the pressure characteristic at the pump decreases, as seen in **Figure 3.19**. If the objective is to avoid overpressure issues and potential damages, it is preferable to increase the size of the cylinder

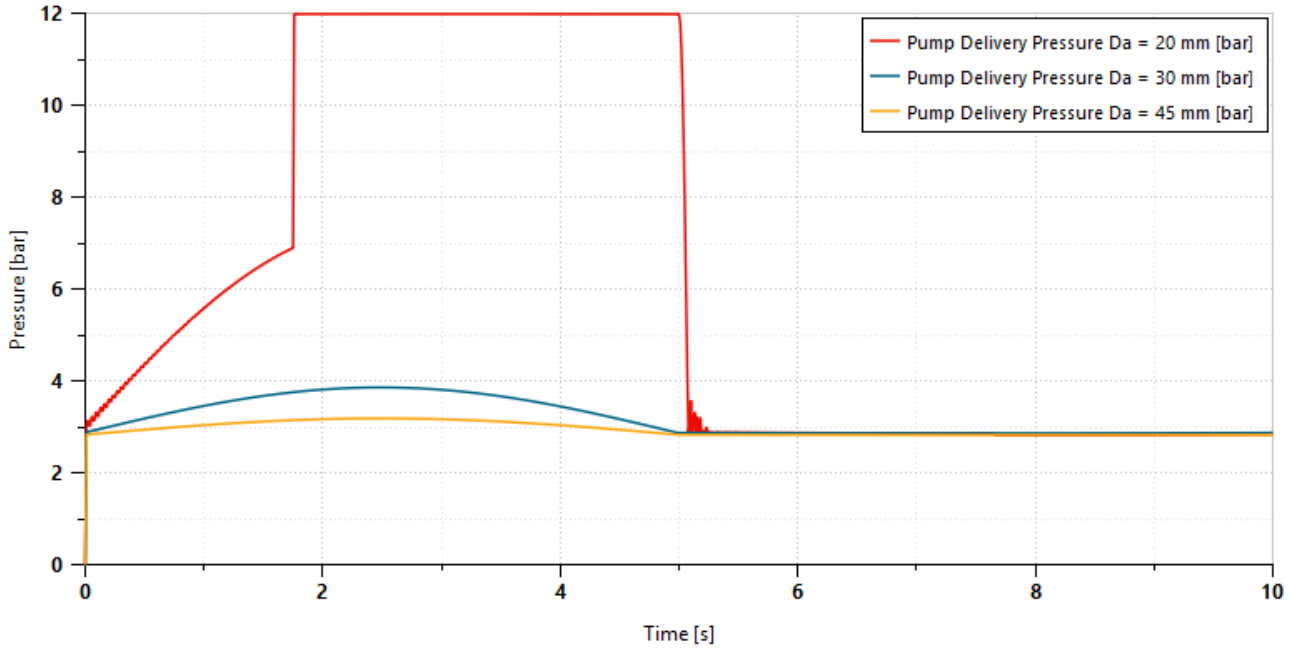

Figure 3.19: *absolute pressure level at pump delivery port (left side actuator).*

2.5. Pump Size

The aim of this simulation copies the previous one, this time, the dimension under test is the pump displacement, keeping all the other components unchanged. Also for these tests, the size used for the original design is compared to an increased and to a decreased dimension. The size variations are reported in **Table 3.2** as positive displaced volume per revolution.

__Table 3.2:__ set of pump displacements for batch simulation.

Pump Displacement [cm³/rev]
15
18.9
25

For this simulation the angular speed input is a ramp signal with slope of 20 rpm/s, while the load applied at the piston is constant, due to a moment of 20 Nm. For the same applied conditions, the pump displacement size influences the production of flow rate. As it is possible to see in **Figure 3.20** and **Figure 3.21**, the 15 cc/rev pump penalizes the piston run, as the slowest among the tested measures, the smallest generated flow rate delays the actuator from reaching the end stop.

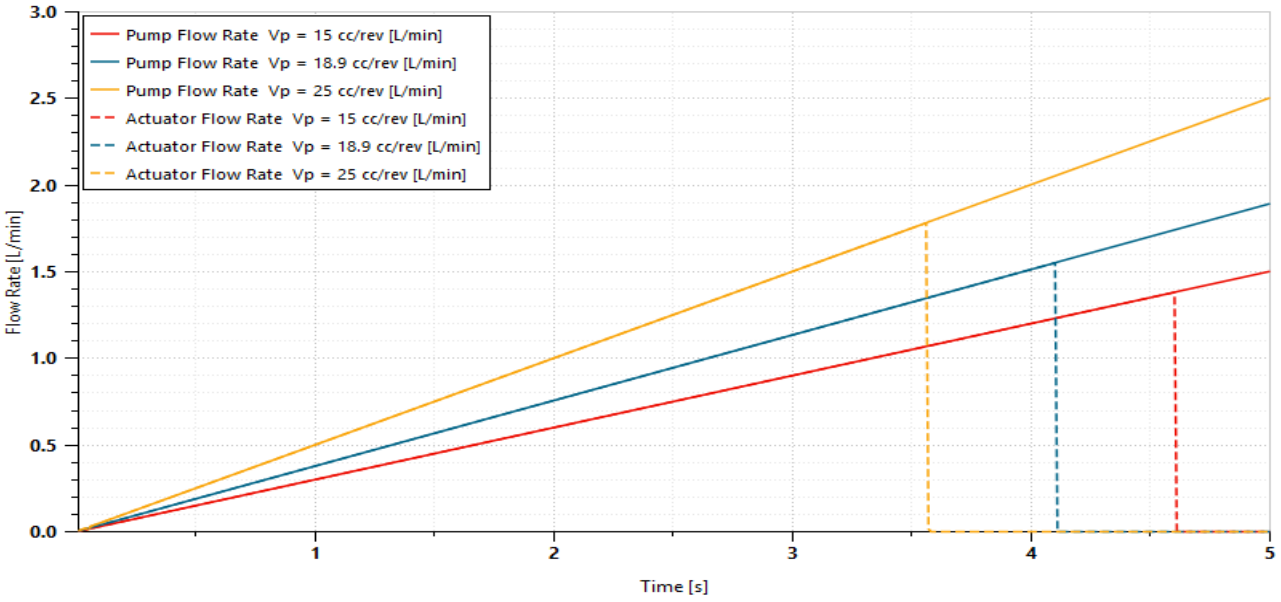

__Figure 3.20:__ pump delivered flow rate (solid lines) and actuator flow rate at left port (dashed lines).

Conversely, the increase of the pump dimension leads to a higher flow rate, delivered for the same angular speed of the prime mover. Consequently, the piston arrives sooner at the end of the stroke and the pressure rise lets the relief valve open up.

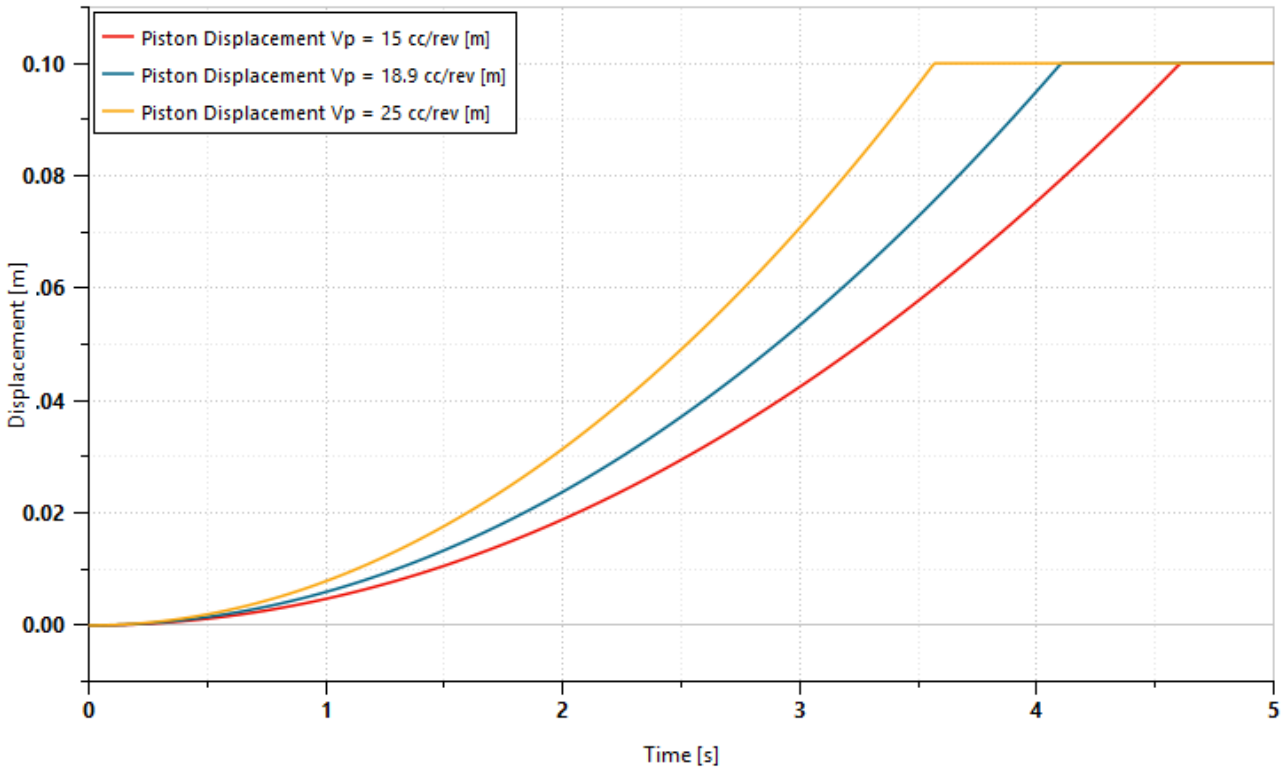

Figure 3.21: *piston displacement.*

3. Passive Operations

In this paragraph will be shown the functioning of the system when turned off. The aim is to allow the rider to easily rotate the handlebar manually, feeling the lowest resistance. Remembering that the system control unit deenergizes the electro-valve to short the oil flow around the actuator, and this occurs whenever the electric motor stops. It is possible to simulate the rider steering the handlebar and the response of the hydraulic circuit.

The manoeuvre does not start before the valve receives the step command, in this case an ideal electrical low signal, precisely at instant 1 s; from then, the rider rotates the front wheel and the mass assembly of a semi-sinusoidal wave function, slowly varying at 0.33 Hz frequency. It is implemented a low load on the handlebar of just 3 Nm of maximum amplitude, yet it is enough to angularly displace the wheel of 50 degrees, as visible in **Figure 3.22**. The operation is completed after three seconds, when everything returns to the initial conditions.

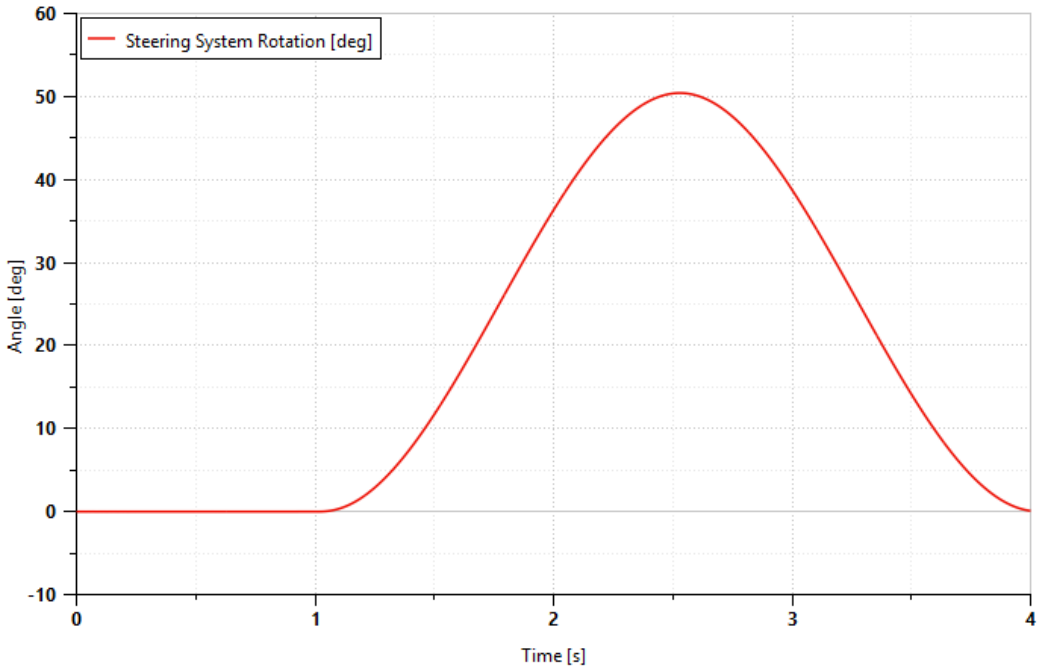

Figure 3.22: *rotation of the front assembly for a manual steering manoeuvre.*

From the actuator point of view, the piston is dragged along its stroke by the external load. In this way, inside the hydraulic circuit form high and low-pressure sides, but switched, with respect to the normal functioning of the system. Due to the symmetry of the piston surfaces, the same quantity of oil, displaced outside the outlet port, flows inside the inlet one; this is confirmed by **Figure 3.23**, imagining a second flow rate curve for the other port, exactly mirroring the shown function. During normal operations, an outgoing flow rate, negative for sign convention, defined the low-pressure side, with the oil sent to the pump suction; now it characterizes a pressure rise in the line starting from the actuator exit port to the restrictor. This is also explained in terms of work done by the piston onto the oil initially at rest.
In the second half of the simulation, the wheel changes the sense of rotation, as well as the actuator inverting the direction of motion and, consequently, the oil recirculation inside the restrictor, producing an ingoing flow rate through the port observed by the figure.

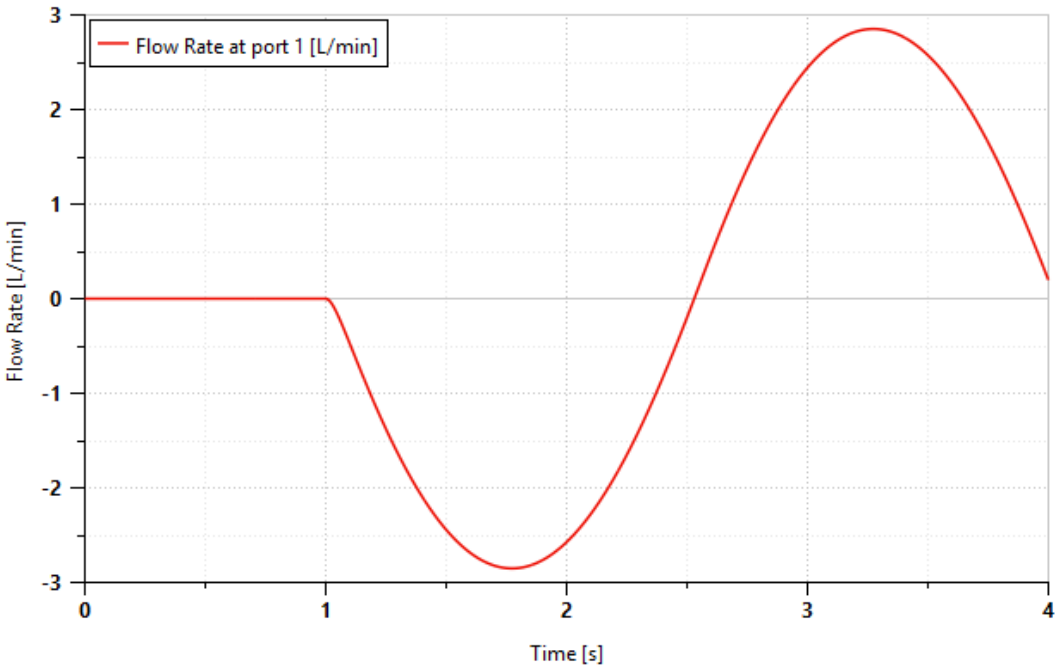

Figure 3.23: *flow rate trend at actuator left port.*

The situation is a bit different for the pressure trends, seen in **Figure 3.24**, the alternating behaviour is proposed only in the first half of the actuator stroke, showing the rising high-pressure side, of the red curve, matching the same port observed in **Figure 3.23**, while the other side presents a slight decrease from the initial pressure level.
In the second half of the actuator stroke, the level in the low-pressure side starts increasing above the initial value. The increment ends when the pressure level is the same for both sides, occurring when the piston returns in the initial position.

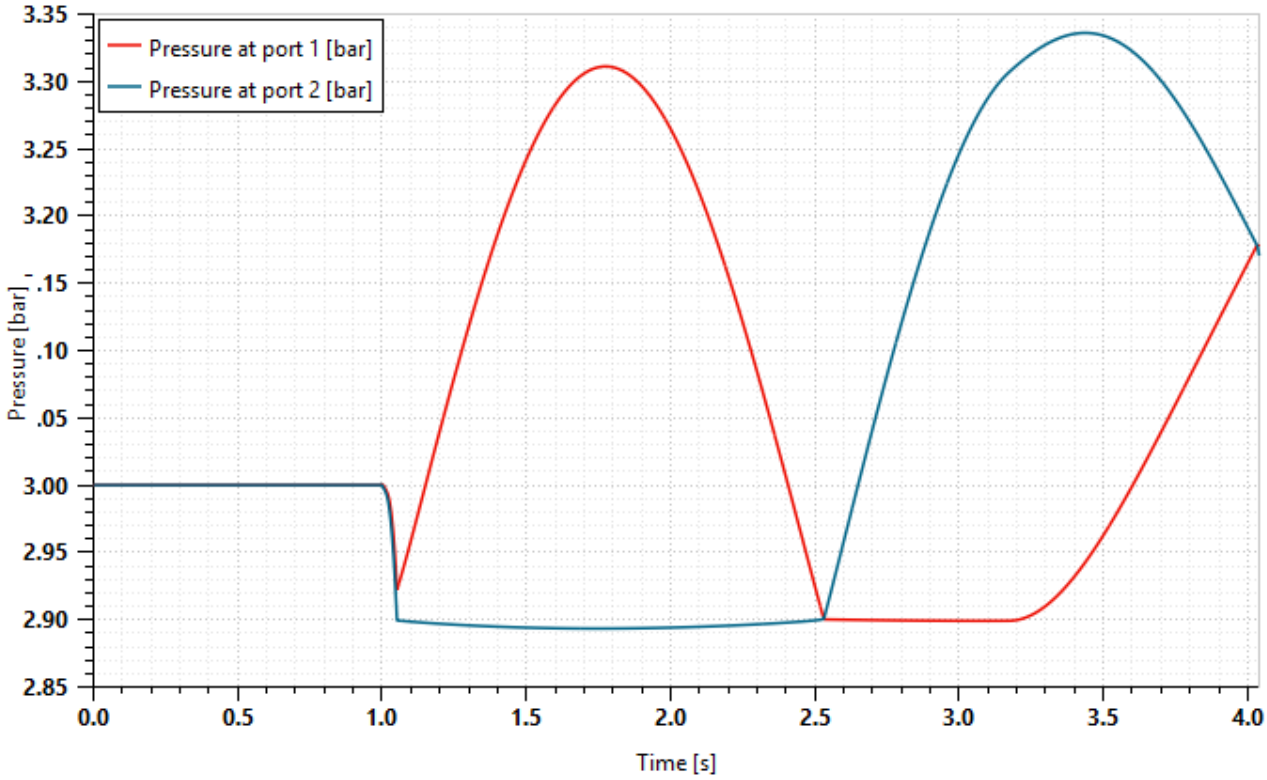

Figure 3.24: *pressure trends at the actuator ports.*

In the second simulation of this paragraph are tested the effects of damping against the wobble phenomena. Recalling the equation (2.5.2), with the parameters in use, the natural frequency at which the undamped system resonates is 9.83 Hz, compliant about the frequency range where wobble appears. Therefore, it is created a torque input from a sinusoidal wave at that frequency, with time dependent amplitude, increasing at a rate power of five. The input function is suggested in the following equation and visible in **Figure 3.25**, as the resulting rotation of the steering system with very low damping.

$y(t) = t^5 \sin(2\pi f_n t)$

Again, the electro-valve connects the actuator ports after one second from the start, but the oscillations become perceivable (visible) only in the last two seconds.

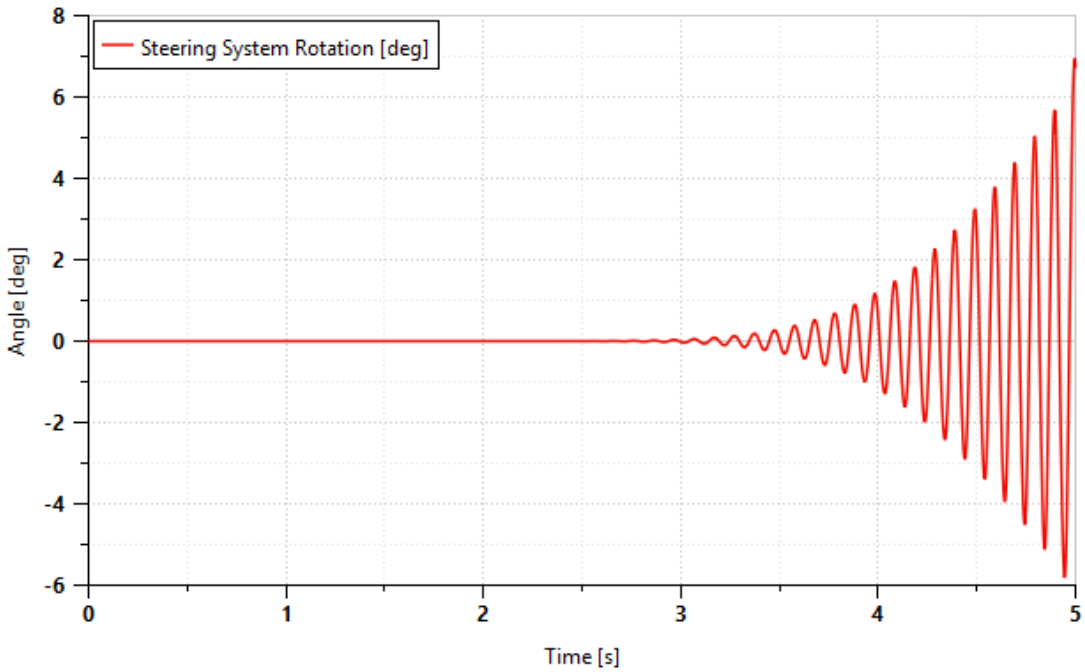

Figure 3.25: *wobbling oscillations of the undamped steering assembly.*

The solution against this vibrational mode is to reduce the amplitude of the oscillations, acting on the damping effect of the restrictor. As it is possible to see in **Figure 3.26**, reducing the oil passage through the valve, which is reducing the diameter and, so, the surface of the orifice, decreases the amplitude of the oscillation. As seen in the figure, at varying the diameter, the resulting displacement of the actuator lowers down with an inverse quadratic proportionality. In addition, it can be observed that, for a smaller restrictor, the peak of every oscillation is anticipated, slightly increasing the frequency of the output sine wave, with respect to the input torque. For the restrictor diameter of 2 mm, the system vibrates at 9.91 Hz.

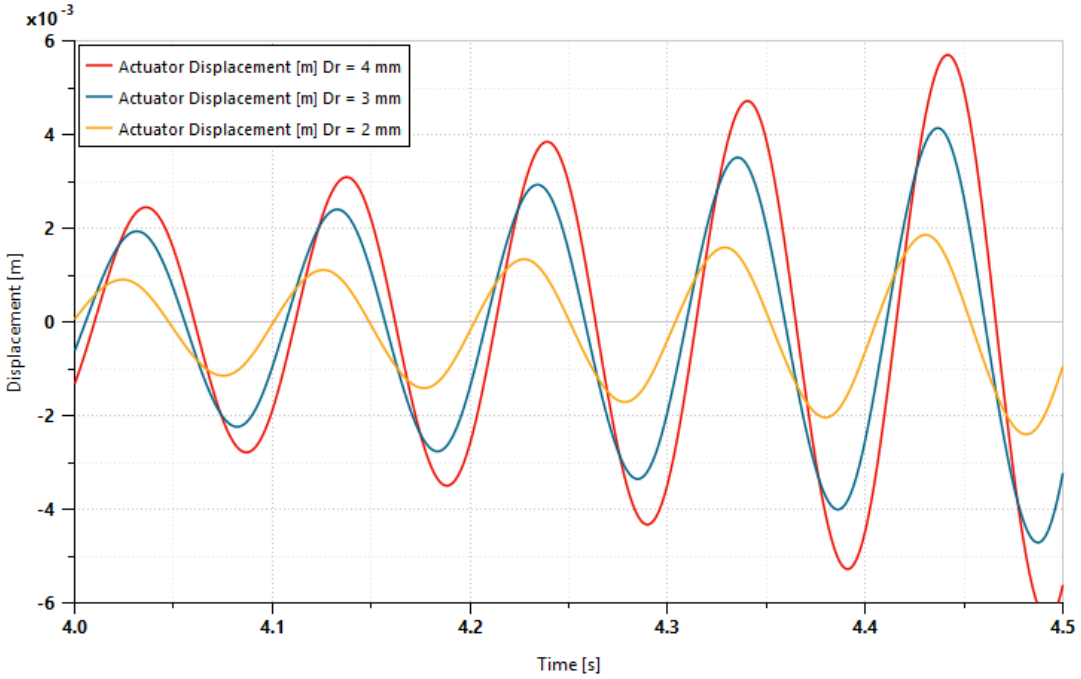

Figure 3.26: *detail of the damped oscillations for different restrictor diameters.*

Among the effects brought by the dynamic restrictor, a negative outcome is the pressure increment in the hydraulic circuit, risking the damaging of the components. As it is possible to see in **Figure 3.27**, a larger orifice generates a smaller pressure drop that can propagate to the actuator. Therefore, the increase of damping, and pressure so on, would give to the rider the perception of increasing effort when steering the handlebar, the actuator travel would result braked, being detrimental for safety.

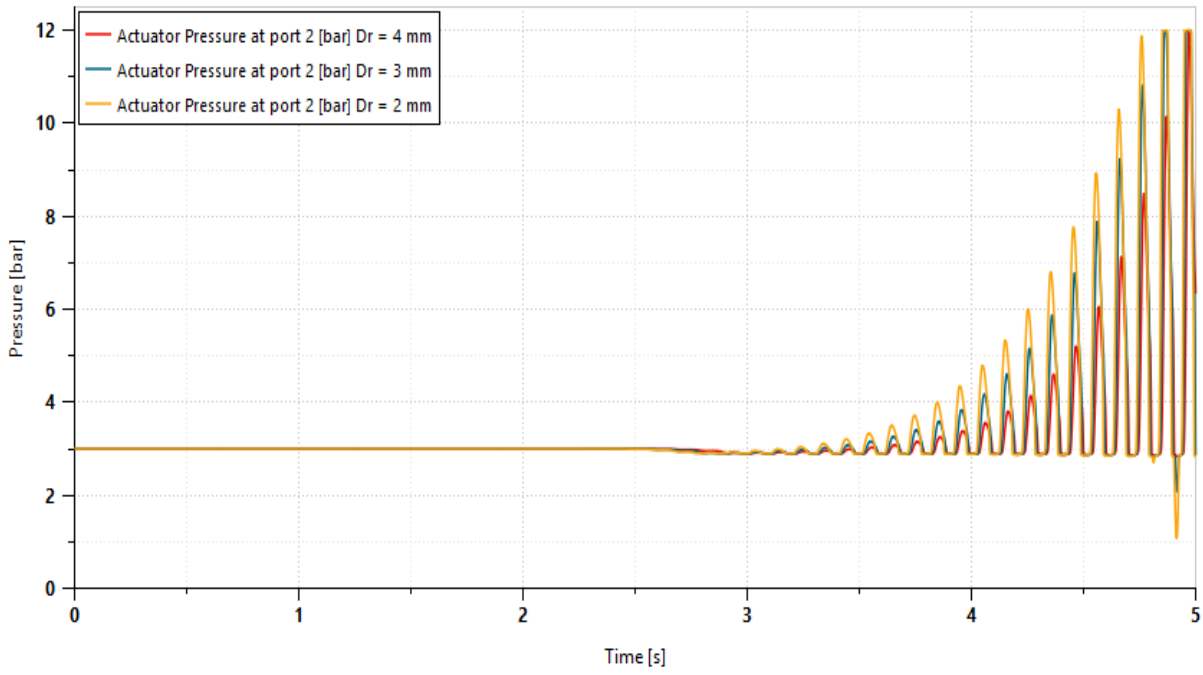

Figure 3.27: *actuator pressure trends for different restrictor diameters.*

CHAPTER IV

Conclusions

The results brought by the simulations cannot fully express if the designed system is feasible for a real-world application. It would require the creation of a prototype, to be tested and validated in a real environment. Nonetheless, these results can evaluate separately the controller from the hardware, analysing strengths and weaknesses. Furthermore, this study leaves aside everything that is related to functional safety and reliability, thus calling for another level of complexity and ulterior stringent requirements to follow the standardizations in use, like the ISO 26262.

For what concerns the control unit, the response to the external scenario guarantees sufficient promptness during operations. The Stanley's kinematic law is not the best solution, but it is based on on-time inputs that, apart from its tuning, do not require the offline collection of vehicle parameters. This means that the controller can be installed on every motorcycle and be ready to use. The actual limitation of the controller performance is related to the modelling of the vehicle, in particular the rolling dynamics show inaccuracies for higher values of the roll angle, compromising the overall result of the simulations. That said, it is unlikely that a strong motorcycle lean is needed on a real road and, before even reaching high lean angles, the rider can regain control and apply other commands to reestablish safe conditions. Therefore, this kind of system cannot be used as the equivalent of a lane-keeper for prolonged autonomous manoeuvres, but it can be found more suitable for tempestive, quicker operations, in assistance to the rider. Even a small stroke of the actuator permits the motorcycle to sensibly change its trajectory, and this intervention is certainly actuated with more rapidity than the human response only.

The components of the hydraulic circuit are adequately sized for the duty that are meant to sustain during operations. Thanks to the applied coefficients, pump and actuator can work with a wide margin before reaching their limit, though the load observed during the trials is far from being challenging, and, as a consequence, the pressure level occurring inside the circuit remains low. The problems rise with the possible behaviour of a real pump, for what concerns the generation of flow rate. In particular, the speed command, sent to the electrical motor, is often too low to avoid that most of the flow rate gets lost in leakages. For this reason, the component efficiency becomes too poor, slowing the actuator performances. The obvious solution raises the operating velocity of the pump, forcing it to work at higher efficiency, at the cost of draining much more power from the supply unit.

Appendix

In this section are reported the values of the parameters encountered inside the **Methodology** chapter, for the design of the entire system.

Table 4.1: *vehicle general parameters.*

m	motorcycle mass + 75 kg driver	[kg]	275
l	wheelbase	[m]	1.4
F/R	weight distribution Front/Rear	[%]	55/45
a	CG-front wheel distance	[m]	0.63
b	CG-rear wheel distance	[m]	0.77
h	CG height	[m]	0.5
h_{hinge}	triple clamp height	[m]	0.95
J_z	yaw moment of inertia [10]	[kgm^2]	22000
ε	caster angle	[deg]	22
a_n	nominal normal trail	[m]	0.085

Table 4.2: *wheels parameters.*

R_{0f}	120/70 R17 front wheel radius	[m]	0.299
R_{0r}	180/55 R17 rear wheel radius	[m]	0.315
k_t	tire vertical stiffness	[N/mm]	180
k_{tf}	front wheel twisting stiffness	[m/rad]	0.035
J_{wf}	front wheel rotational moment of inertia	[kgm^2]	0.634
J_{wr}	rear wheel rotational moment of inertia	[kgm^2]	1.037

Table 4.3: *longitudinal dynamics parameters.*

f_0	rolling linear coefficient	[-]	0.02
K	rolling quadratic coefficient	[s^2/m^2]	$8e^{-6}$
S	motorcycle frontal equivalent area	[m^2]	0.9
C_x	aerodynamic drag coefficient	[-]	0.5
C_z	aerodynamic downforce coefficient	[-]	0.1
m_e	apparent mass	[kg]	289

Table 4.4: *rolling and steering dynamics parameters.*

$J_{f\delta}$	steering system rotational moment of inertia	[kgm^2]	0.103
J_{xf}	front assembly moment of inertia around the leaning axis	[kgm^2]	4
J_x	motorcycle moment of inertia around the leaning axis	[kgm^2]	118
$k_{f\delta}$	steering system rotational stiffness [12]	[Nm/rad]	3.2

Table 4.5: *additional parameters.*

g	gravity acceleration	[m/s^2]	9.81
ρ	air density	[kg/m^3]	1.225

References

[1] Cossalter V.: Motorcycle Dynamics, Lulu, 2006.

[2] Pacejka H. B.: Tyre and Vehicle Dynamics, Butterworth-Heinemann, 2006, Oxford.

[3] Bartolozzi M., Savino G., Pierini M.: Novel high fidelity tyre model for motorcycles to be characterised by quasi-static manoeuvres – Rationale and numerical validation, Vehicle System Dynamics, Taylor & Amp., 2021.

[4] Bartolozzi M.: Motorcycle steering torque estimation using a simplified front assembly model: experimental validation and manoeuvrability implications, Vehicle System Dynamics, Informa UK Limited, 2023.

[5] Fajans J.: Steering in bicycles and motorcycles, Americal Journal of Physics, Vol. 68, N. 7, Berkeley, 2000.

[6] Ministero delle Infrastrutture e dei Trasporti, Norme Funzionali e Geometriche per la Costruzione delle Strade, DM 05/11/01.

[7] Altare G., Rundo M.: Computational Fluid Dynamics Analysis of Gerotor Lubricating Pumps at High-Speed: Geometric Features Influencing the Filling Capability, Journal of Fluids Engineering, 2016.

[8] Passigato F., Eisele A., Wisselmann D., Gordner A., Diermeyer F.: Analysis of the Phenomena Causing Weave and Wobble in Two-Wheelers, Advances in Mechanical Systems Dynamics, 2020.

[9] Piantini S., Giorgetti A., Baldanzini N., Monti C., Pierini M.: Design of a Motorcycle Steering Damper for a Safer Ride, Machines, 2020.

[10] Bartolozzi M., Berzi L., Meli E., Savino G.: Similarities in steering control between cars and motorcycles: application to a low-complexity simulator, UNIPI, 2022.

[11] Genta G., Morello L.: The Automotive Chassis, Volume 1: Components Design, Springer, 2009.

[12] Limebeer D. J. N., Sharp R. S.: On steering wobble oscillations of motorcycles, Proceedings of the Institution of Mechanical Engineers, Part C: Journal of Mechanical Engineering Science, SAGE Publications, 2004.